Interannual Variability of the Pacific Water Boundary Current in the Beaufort Sea

by

Eric T. Brugler
B.S., United States Naval Academy (2011)

Submitted to the Department of Mechanical Engineering
in partial fulfillment of the requirements for the degree
of Master of Science in Mechanical Engineering
at the
MASSACHUSETTS INSTITUTE OF TECHNOLOGY
and the
WOODS HOLE OCEANOGRAPHIC INSTITUTION
September 2013

Author.....
Department of Mechanical Engineering
& Department of Applied Ocean Science and Engineering
August 9, 2013

Certified by.....
Dr. Robert S. Pickart
Senior Scientist, Woods Hole Oceanographic Institution
Thesis Supervisor

Reader.....
Dr. Pierre F.J. Lermusiaux
Associate Professor, Massachusetts Institute of Technology

Accepted by...
Dr. Henrik Schmidt
Chair, Joint Committee for Applied Ocean Science and Engineering
Massachusetts Institute of Technology

Accepted by.....
Professor David E. Hardt
Chair, Committee on Graduate Students – Mechanical Engineering
Massachusetts Institute of Technology

Interannual Variability of the Pacific Water Boundary Current in the Beaufort Sea

by

Eric T. Brugler

Submitted to the Department of Mechanical Engineering
& Department of Applied Ocean Science and Engineering
Massachusetts Institute of Technology and Woods Hole Oceanographic Institution
on August 09, 2013, in partial fulfillment of the
requirements for the degree of
Master of Science

Abstract

Between 2002 and 2011 a single mooring was maintained in the core of the Pacific Water boundary current in the Alaskan Beaufort Sea near 152°W. Using velocity and hydrographic data from six year-long deployments during this time period, we examine the interannual variability of the current. It is found that the volume, heat, and freshwater transport have all decreased drastically over the decade, by more than 80%. The most striking changes have occurred during the summer months. Using a combination of weather station data, atmospheric reanalysis fields, and concurrent shipboard and mooring data from the Chukchi Sea, we investigate the physical drivers responsible for these changes. It is demonstrated that an increase in summertime easterly winds along the Beaufort slope is the primary reason for the drop in transport. The intensification of the local winds has in turn been driven by a strengthening of the summer Beaufort High in conjunction with a deepening of the summer Aleutian Low. Since the fluxes of mass, heat, and freshwater through Bering Strait have increased over the same time period, this raises the question as to the fate of the Pacific water during recent years and its impacts. We present evidence that more heat has been fluxed directly into the interior basin from Barrow Canyon rather than entering the Beaufort shelfbreak jet, and this is responsible for a significant portion of the increased ice melt in the Pacific sector of the Arctic Ocean.

Thesis Supervisor: Dr. Robert S. Pickart
Title: Senior Scientist

Acknowledgments

Although the list could go on for awhile I will briefly mention some people who were instrumental to my thesis and time at MIT/WHOI.

First, I would like to give a special thanks to my advisor, Bob Pickart. When I entered the Joint Program, I was looking to work with an Arctic physical oceanographer, but getting to know Bob made me realize that I got so much more. Although the time we had together was short, his guidance, mentorship and friendship are such that they will last a lifetime. I am also grateful to Bob for giving me the opportunity to do research at sea, those experiences were unforgettable.

I was fortunate to get to know some other people who work closely with Bob who not only became good friends, but accelerated my research as well. Some of them include Wilken von-Appen, Carolina Nobre, Ben Harden, Femke de Jong, Dana Mastropole, Donglai Gong, Jeremy Kasper, Frank Bahr, Dan Torres, Jim Ryder, John Kemp and Terry McKee. I would like to give a special thanks to Wilken, his technical help and friendship were crucial to my first year at WHOI. Also, Carolina deserves a special thanks for the huge amount of programming help she gave and also for the friendship we developed.

Thank you to everyone who traveled to Norway and especially to Kjetil and Selina Våge for hosting us during our stay. I could not think of a better place to complete a thesis!

Thank you Dr. (MK1) Steve Jayne for the help along the way as well as all the great times in Woods Hole. I would also like to send a thanks to the housemates at 168 Auburn St., Nick, Alex, Connor and Steph all made the year at MIT quite enjoyable.

Thank you to Kelly Knorr, your love and support has and will continue to be a

sustaining portion of my life.

My mom, dad and brothers (Chirs, Scott) are always there to support me and I am blessed to have such a great family.

It would be a shame not to mention the true cornerstone in my life, which is my faith in God. Thank You for sustaining me always and re-calibrating me when I need it most.

I would like to thank Kent Moore for his help with the reanalysis data and the willingness in which he did so. I would also like to thank Tom Weingartner and Hank Statscewich from the University of Alaska, Fairbanks for providing and assisting me with the Barrow Canyon mooring data collected as part of the Bureau of Ocean Energy Management study OCS 2012-079. Also I would like to acknowledge Steve Roberts for his assistance and hard work with the satellite and sea surface temperature data.

The majority of the data for this project was funded by grant # ARC-0856244 from the Office of Polar Programs of the National Science Foundation. My time at WHOI was funded by the United States Navy and the WHOI Academic Programs Office.

Contents

Chapter 1

Introduction

In the western Arctic Ocean, Pacific-origin water is transported in a narrow shelf-break jet at the edge of the Chukchi and Beaufort Seas. In the mean this jet (also known as the western Arctic boundary current) flows eastward toward the Canadian Arctic Archipelago (Figure 1-1) (Pickart, 2004; Mathis et al., 2007; Spall et al., 2008; Nikolopoulos et al., 2009; Pickart et al., 2009a; von Appen and Pickart, 2012). The source of the boundary current is the Pacific water that has entered the Arctic Ocean via Bering Strait, with an annual mean transport of 0.8 Sverdrups (1 Sv $== 10^6$ m^3 s^{-1}) (Woodgate et al., 2005). Despite the opposing northerly winds prevalent in the region (Overland and Roach, 1987), the flow through Bering Strait is northward due to the sea-level gradient between the Pacific and Atlantic Oceans (Aagaard et al., 2006). After entering the Chukchi Sea the water is steered by the topography of the shelf, which divides the throughflow into three main northward-directed branches (Figure 1-1) (Weingartner et al., 2005a). Upon reaching the edge of the Chukchi shelf some of the water is channeled eastward and makes its way around Pt. Barrow, Alaska, continuing along the Beaufort shelf edge (Figure 1-1) (Pickart, 2004; Nikolopoulos et al., 2009).

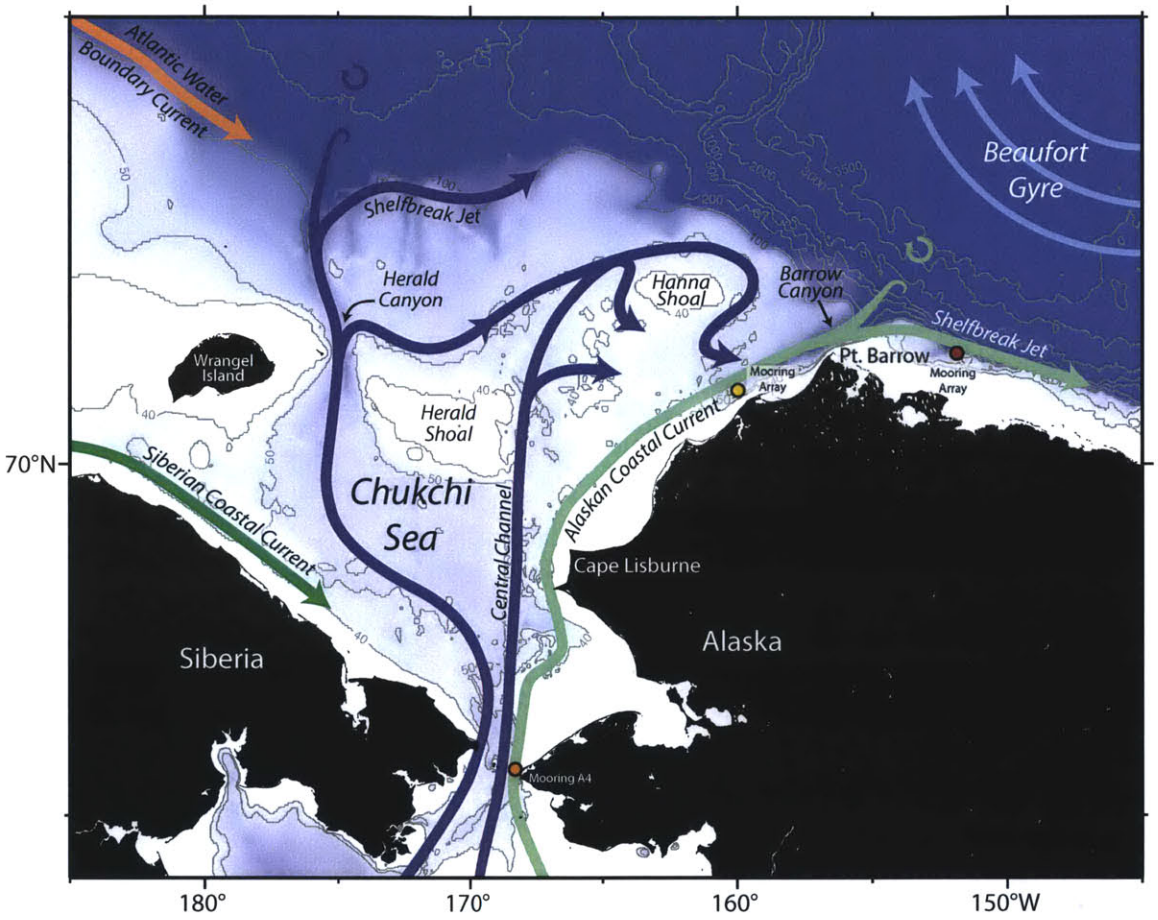

Figure 1-1: Schematic showing the major currents in the Chukchi and Beaufort Seas and the geographical place names for the region. The location of the Beaufort slope mooring array is indicated by the red circle, while the location of the Barrow Canyon mooring array is indicated by the yellow circle. Bering Strait mooring A4 is indicated by the orange circle.

Based on mooring measurements across the Alaskan Beaufort shelf and slope, the shelfbreak jet is only 10-15 km wide east of Pt. Barrow and carries less than 20% of the Pacific water that enters the Arctic through Bering Strait (Nikolopoulos et al., 2009). Farther down the slope Atlantic water also flows eastward as part of the large-scale Arctic cyclonic boundary current system (Rudels et al., 1994; Woodgate et al., 2001; Karcher et al., 2007; Aksenov et al., 2011). There is a clear seasonality of the Pacific water component of the current (Nikolopoulos et al., 2009; von Appen and Pickart, 2012; Spall et al., 2008). In summertime the flow is surface-intensified and advects two types of Pacific summer water masses (von Appen and Pickart, 2012). From early fall through winter the flow is bottom-intensified and the predominant water mass transported by the current is remnant winter water (Nikolopoulos et al., 2009). Finally, during spring and early summer, newly-ventilated Pacific winter water is advected in a bottom-intensified jet (Spall et al., 2008). While these seasonal configurations seem to occur each year, the variation in timing and spatial distribution of the different water masses from year to year is presently unknown.

Along the north slope of Alaska the prevailing winds are from the east and thus oppose the shelfbreak jet. Much of the variability of the current is wind-driven (Nikolopoulos et al., 2009; Pickart et al., 2009a; Schulze and Pickart, 2012). Enhanced easterly winds can reverse the shelfbreak jet to the west and induce upwelling (Pickart et al., 2011, 2013b,a), while strong westerly winds accelerate the jet to the east and cause downwelling (R. Pickart, pers. comm., 2013). The winds in the region are dictated to a large degree by two atmospheric centers of action: the Aleutian Low to the south, and the Beaufort High to the north (Pickart et al., 2013a). Strong Aleutian low pressure systems can extend far enough north to influence the western Arctic boundary current, and fluctuations in the Beaufort High can do the same (Mathis et al., 2012; Watanabe, 2011). Interestingly, there has been an increase in the

strength of the summertime Beaufort High in the last decade, (Moore, 2012), while there is still debate as to the interannual variability of the Aleutian Low (McCabe et al., 2001; Mesquita et al., 2010).

Pacific water is known to play a vital role in the Arctic Ocean for various reasons. The cold winter water helps maintain the halocline (Aagaard et al., 1981) and is also the main source nutrients that drive primary production in the region (Sambrotto et al., 1984; Hansell et al., 1993; Hill and Cota, 2005; Hill et al., 2005). The summer water provides freshwater to the Beaufort Gyre and carries heat into western Arctic that can contribute to ice melt. For example, Woodgate et al. (2010) demonstrated that the heat flux through Bering Strait had the potential to account for one third of the massive sea ice retreat that occurred in 2007. However, in order to accurately determine how the Pacific water impacts the Arctic system, we must understand the behavior and variability of the shelfbreak current, since this represents the interface between the shelf and the Arctic Ocean interior.

Exchange across the Beaufort shelfbreak occurs in two ways: through hydrodynamic instability of the boundary current (Spall et al., 2008; von Appen and Pickart, 2012), and, as noted above, via wind-forcing. The shelfbreak jet is both baroclinically and barotropically unstable and is known to spawn eddies that transport Pacific water offshore. Such eddies are found throughout the interior Canada Basin (Pluedemann et al., 1999). Wind-driven upwelling is common and occurs in all seasons and under varying ice conditions (Schulze and Pickart, 2012). Pickart et al. (2013a) showed that a single strong storm can result in a substantial off-shelf flux of heat and freshwater, and a significant on-shelf transport of nutrients. The salt, nutrients, and zooplankton brought to the shelves via upwelling are thought to play a vital role in the productivity and state of the local ecosystem (Pickart et al., 2013a). The wind-driven exchange is also thought to release a significant amount of CO_2 to the

atmosphere (Mathis et al., 2012).

The western Arctic system has experienced drastic changes over the last few decades, and it is vital to determine how the Pacific water has impacted, or even dictated, these changes. Since the shelfbreak current is the major conduit by which Pacific water exits the Chukchi shelf, it is in turn important for us to understand its long-term behavior and changes. During the western Arctic Shelf-Basin Interactions (SBI) experiment, which took place from August 2002 to September 2004, an array of moorings was deployed across the Beaufort shelfbreak and slope. The array was located at 152°W and consisted of 8 moorings that spanned 40 km from the outer shelf to the mid-slope. The data from this array established the existence of the Pacific water shelfbreak jet and provided a wealth of information about the structure, seasonality, mesoscale variability, and dynamics of the current. However, since the SBI field program was only two years in duration, it was unable to provide meaningful information on the interannual variability of the current.

One of the results that emerged from the SBI mooring study is that the core of the Pacific water boundary current is generally trapped to the shelfbreak, and the transport of the full jet is therefore strongly correlated to the velocity at that location. As such, the shelfbreak mooring was deployed again, as part of several subsequent field programs, to obtain a longer timeseries of the current. At this point there have been 7 year-long deployments from 2002-2012, which allows for an investigation of the interannual variability of the flow. The main goal of this thesis is to quantify the variability of the Beaufort shelfbreak jet over the last decade, and to investigate the physical drivers responsible for these changes. The approach is to analyze the hydrographic and transport changes of current and then provide insights as to the underlying causes. To provide background for the present analysis, we begin with a brief review of the circulation in the Chukchi and Beaufort Seas and, in particular, the

Beaufort shelfbreak jet. Next we describe the large-scale atmospheric context of the study area, focusing on the time period of the mooring measurements. This is followed by an investigation of the local atmospheric forcing, lateral boundary conditions, and sea ice concentration near the mooring site. We find that significant changes have occurred in the western Arctic boundary current over the last 10 years, much of which can be explained by atmospheric forcing. Finally, we end with a discussion of possible implications that such variability can have on the western Arctic region as a whole.

Chapter 2

Data

2.1 Mooring Array Data from 2002-2004

An array of 8 moorings was deployed across the Beaufort shelfbreak and slope near 152°W as part of the Western Arctic Shelf-Basin Interactions (SBI) program from 2002-2004 (Figure 2-1). The array was aligned perpendicular to the local bathymetry, and the moorings were spaced 5-10 km apart. The moorings were named BS1-BS8 (onshore to offshore), although the shoreward-most mooring is not considered in this study. Hydrographic variables on moorings BS2-BS6 were measured using a motorized conductivity-temperature-depth (CTD) profiler known as a Coastal Moored Profiler (CMP). The CMPs provided vertical traces over a nominal depth range of 40-500 m 2-4 times a day with a vertical resolution of 2 m. To measure velocity, upward-facing acoustic Doppler current profilers (ADCPs) were used for moorings BS2 - BS6. The ADCPs provided hourly profiles of velocity with a vertical resolution of 5-10 m. Moorings BS7 and BS8 used McLane moored profilers (MMPs) for measuring the hydrographic variables, and acoustic travel-time current meters (attached to the MMPs) for measuring the velocity. The reader is referred to Spall et al. (2008) and

Nikolopoulos et al. (2009) for a detailed description of the hydrographic and velocity measurements, respectively, including a discussion of the calibration and accuracy of the sensors.

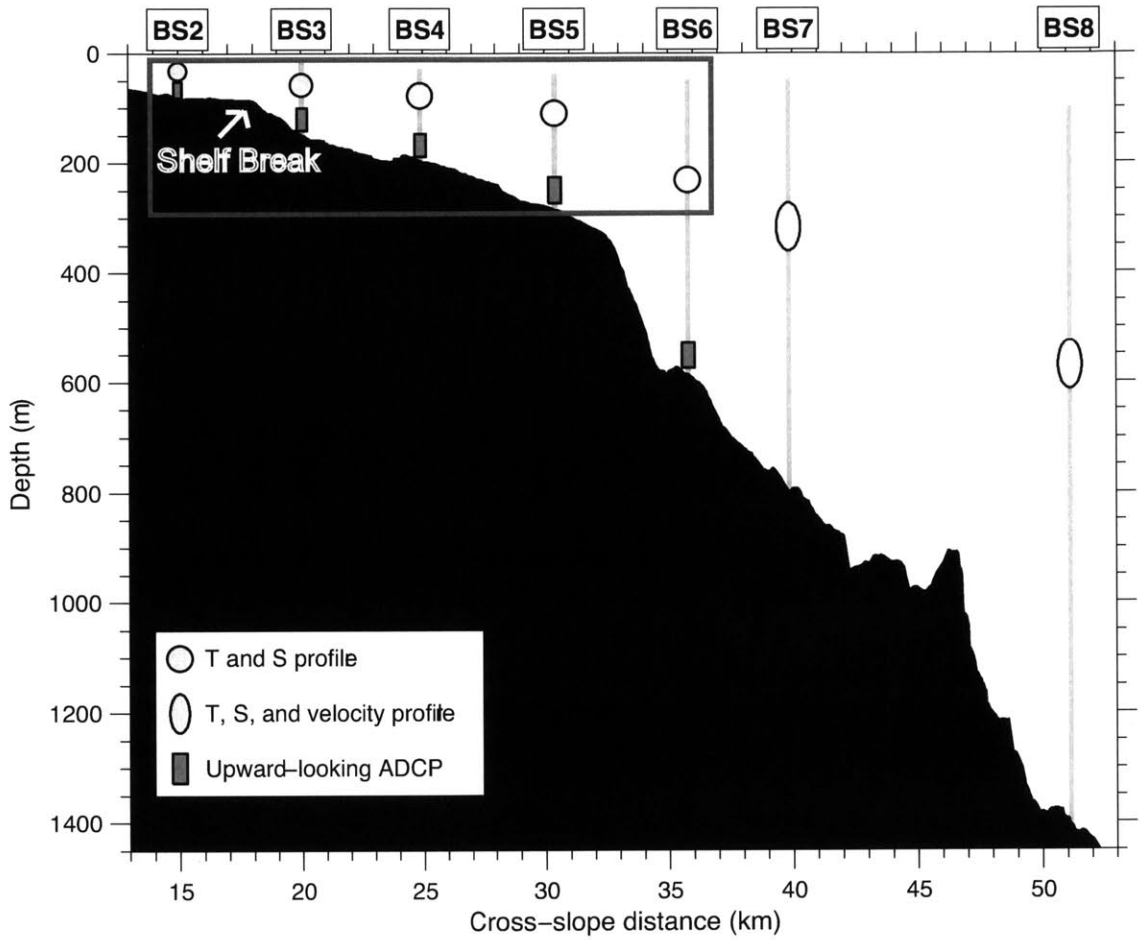

Figure 2-1: The SBI mooring array across the Beaufort shelfbreak and slope near 152°W. The instruments used on each mooring are referenced with the key. The shelfbreak is indicated and is located 70 km offshore from the coastline. The grey box indicates the region considered in this study.

For the present analysis we use data from moorings BS2-BS6, which measured temperature and salinity every 6 hours and velocity hourly. In particular, we employ the same data product used by von Appen and Pickart (2012) who constructed ver-

tical sections of the hydrographic and velocity data at each time step. The sections were gridded using Laplacian-spline interpolation with a grid spacing of 2 km in the horizontal and 10 m in the vertical. Since the present study focuses on the Pacific water masses, the domain is restricted to the upper 300m (Figure 2-1).

2.2 Mooring Data from 2005-2011

A year after the conclusion of the SBI program, a single mooring was re-deployed in the Beaufort shelfbreak current as part of a series of three separate field programs. The mooring in question was BS3, located just offshore of the shelfbreak in 147 m of water. (From this point forward, BS3 will be referred to as the shelfbreak mooring.) The rationale for this was provided by Nikolopoulos et al. (2009) who determined that the vertically integrated velocity from the shelfbreak mooring alone was a good proxy for the transport of the full boundary current. To date the shelfbreak mooring has been deployed seven times between August 2002 and October 2012, with each deployment lasting for about one year. From hereon the deployments will be referred to by their start and end dates: 2002-3, 2003-4, 2005-6, 2008-9, 2009-10 and 2010-11 (the most recent deployment is not used because the data were still being processed at the time of the analysis). Subsequent to the SBI program, the hydrographic data at the shelfbreak mooring were obtained using a CMP, and the velocity data collected using one or two upward-facing ADCPs. Each deployment varied slightly in length, start date, end date, data coverage, vertical resolution, and instrumentation. Table 2.1 provides general information regarding each deployment. A detailed description of the instrument configuration and data processing for each individual deployment is given in Appendix A.

Table 2.1: Shelfbreak Mooring Deployments

Deployment	Location	Depth (m)	Start Date	End Date
2002-2003	71° 23.69' N 152° 5.88' W	147	01-Aug-2002	28-Sep-2003
2003-2004	71° 23.69' N 152° 2.81' W	147	06-Oct-2003	11-Sep-2004
2005-2006	71° 23.73' N 152° 2.14' W	147	06-Aug-2005	13-Aug-2006
2008-2009	71° 24.09' N 152° 2.82' W	147	13-Aug-2008	29-Jul-2009
2009-2010	71° 23.63' N 152° 3.82' W	147	04-Aug-2009	15-Sep-2010
2010-2011	71° 23.65' N 152° 2.81' W	147	16-Sep-2010	11-Oct-2011

2.3 Meteorological Timeseries

Wind data used in the study come from the metrological station located in Barrow, Alaska, which is approximately 150 km to the west of the Beaufort slope mooring site (Figure 1-1). It has been demonstrated previously that the wind record at this location is a good proxy for the winds near 152°W (Nikolopoulos et al., 2009; Pickart et al., 2011). The data were acquired from the National Climate Data Center of the National Oceanic and Atmospheric Administration (NOAA) and subject to a set of routines to remove bad values and interpolate small gaps of less than 6 hours (see Pickart et al. (2013a) for details). Nikolopoulos et al. (2009) determined that alongcoast winds (105°T) are most strongly correlated to the flow of the Beaufort shelfbreak jet. Consequently, we used the alongcoast component of the wind velocity in this study, where positive refers to westerly winds and negative to easterly winds.

2.4 Atmospheric Reanalysis Fields

Reanalysis fields are used to study the large-scale meteorological context over the time period of our mooring records. We employ the high-resolution data set known as the North American Regional Reanalysis (NARR, Mesinger (2006)). The space and time resolution of the NARR product is 0.25° and 3 hourly, respectively. The NARR prod-

uct utilizes newer data assimilation and modeling advances that have been developed subsequent to the original National Centers for Environmental Prediction (NCEP) global reanalysis product. The present study uses the NARR sea level pressure data and 10 m winds for the region shown in Figure 5-1. The NARR data are validated against the Barrow wind timeseries in Appendix C of this thesis.

2.5 Sea-ice Concentration Data

The sea-ice concentration data used in the study are a blended product combining Advanced Very High Resolution Radiometer (AVHRR) data and the Advanced Microwave Scanning Radiometer-Earth Observing System (AMSR-E) data. The record extends from 2002-2011, which is the timeframe that the AMSR-E obtained measurements onboard the National Aeronautics and Space Administration's (NASA) Aqua satellite. NOAA constructed this product in real-time following Grumbine (1996) and then later adjusted and corrected it following Cavalieri et al. (1999). The accuracy of the sea ice concentration is estimated to be $\pm 10\%$ (Cavalieri et al., 1991). The AVHRR-AMSR product is provided once per day at a spatial resolution of 0.25° (Reynolds et al., 2007).

2.6 Satellite Imagery

Satellite-derived sea surface temperature (SST) and visible imagery used in the study were based on data collected from the high-resolution Moderate Resolution Imaging Spectroradiometer (MODIS) sensor onboard NASA's polar orbiting satellites Aqua, Terra. MODIS visible imagery was obtained from `http://lance-modis.eosdis.nasa.gov/imagery/subsets/?mosaic=Arctic` and MODIS SST imagery was retrieved

from http://oceancolor.gsfc.nasa.gov/cgi/browse.pl?sen=am. The images are composites of sea surface temperature and visible imagery and have a spatial resolution of 250 m.

2.7 Shipboard Hydrographic and Velocity Data

Shipboard data obtained from the Chukchi Sea in 2011 are used in the thesis. In July 2011 the United States Coast Guard Cutter (USCGC) Healy occupied a transect across the Chukchi Sea continental slope to the west of Barrow Canyon. Expendable CTDs (XCTDs) were dropped approximately every 5 km while the ship steamed at 10 knots, and the vessel-mounted ADCP collected data continuously during the transect. The accuracy of the XCTD is taken to be 0.02°C for temperature, 0.04 for salinity, and 1 m for depth (see also Kadko et al. (2008)). The vessel-mounted ADCP data from Healy's Ocean Surveyor 150 KHz instrument were collected using the University of Hawaii's UHDAS software and subsequently processed using the CODAS3 software package (see http://currents.soest.hawaii.edu). Following this the velocities were de-tided using the Oregon State University model (http://volkov.oce.orst.edu/tides; Padman and Erofeeva (2004)). The accuracy of the final de-tided velocities is estimated to be ± 2 cm/s.

Chapter 3

Methods

3.1 Shelfbreak Mooring Transport Proxy

The SBI mooring array located at 152°W measured the Pacific Arctic boundary current for two consecutive years, 2002-2004. Using the full suite of hydrographic and velocity data, Nikolopoulos et al. (2009) demonstrated that the current was trapped to the shelfbreak throughout the year. Therefore, a single mooring placed at this location should be able to capture the dominant transport signal of the Pacific water, which is generally confined to the upper 150 m of the water column. Nikolopoulos et al. (2009) showed this by comparing the vertically integrated alongstream velocity at the shelfbreak mooring to the Pacific water transport calculated from the full SBI mooring array. It was found that these two time series were highly correlated (r=0.87), indicating that the dominant variability of the current is due to fluctuations in transport rather than meandering. Figure 3-1 shows the mean structure of the current from August 2002 to mid-September 2003. The black vertical line indicates the location of the shelfbreak mooring and the solid circles represent the gridded velocity measurements. Using the data from the first year we constructed a proxy for the vol-

ume transport of the full current using only the shelfbreak mooring measurements.[1] This is subsequently used in the thesis to analyze the interannual variability of the current.

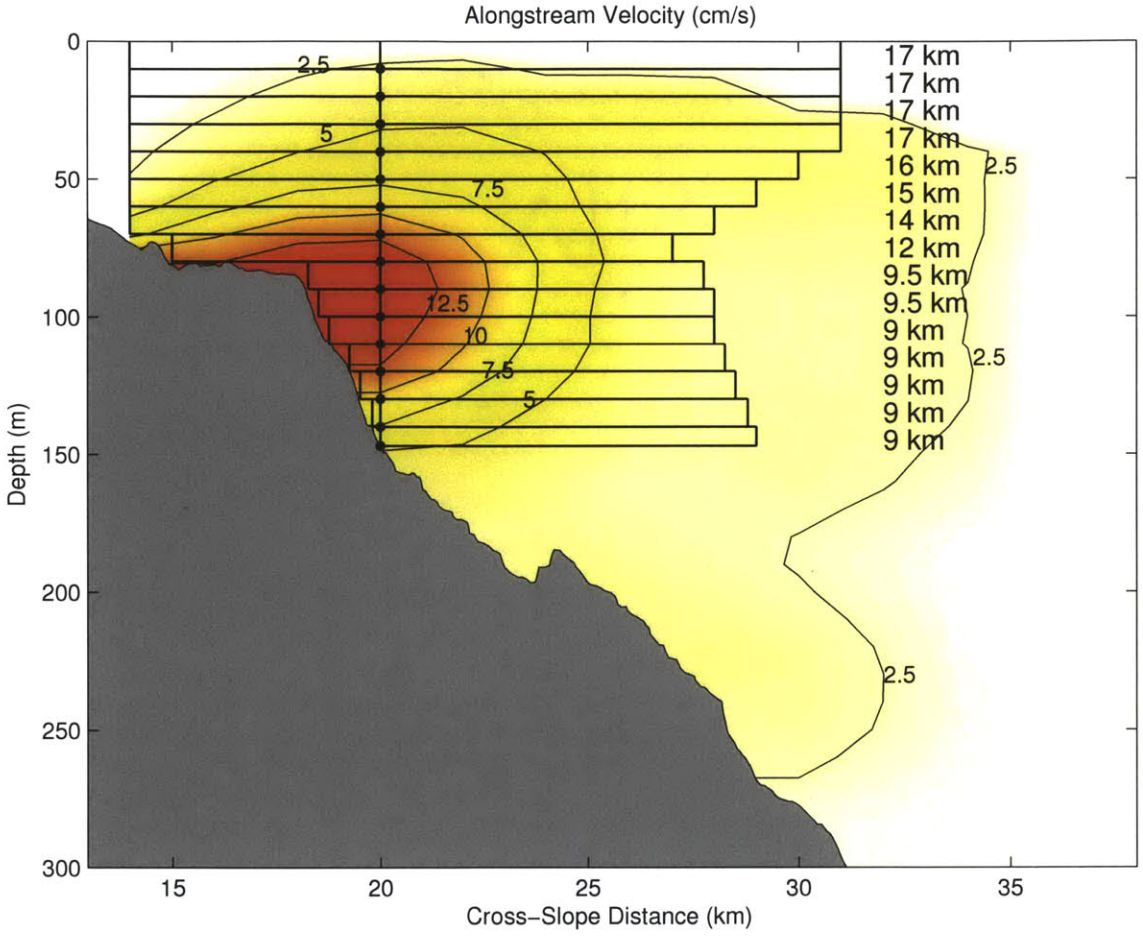

Figure 3-1: Mean alongstream velocity (cm/s) for the time period August 2002 to September 2003. The vertical line with dots represents the shelfbreak mooring and gridded velocity measurements. The boxes represent the calculated width of the current at each velocity grid point.

The first step in devising the proxy was to choose a width for the current. A depth-varying width was employed for each 10 m bin. Two metrics were considered in the

[1]The second year of data were not used to construct the proxy because of a data gap in the upper portion of the water column at the shelfbreak mooring.

choice of the widths. The first criterion was to minimize the root mean square (rms) difference between the full SBI array transport and the shelfbreak mooring proxy transport, and the second criterion was to minimize the difference in the record-length mean of the two transports. For each bin we chose the width that best met these two criteria jointly. Figure 3-1 shows the resulting widths for the current. It is important to note that in this study, transport measurements are restricted to the upper 147 meters of the water column because the shelfbreak mooring only measured to this depth. However, Figure 3-2 demonstrates that, in the mean, most of the Pacific-origin water resided above this depth. In particular note that the cold Pacific layer extends only slightly deeper than the mooring. Using the full array data it was determined that the upper 150 m annually accounted for 91% of the volume transport, 97% of the heat transport, and 98% of the freshwater transport of Pacific water.

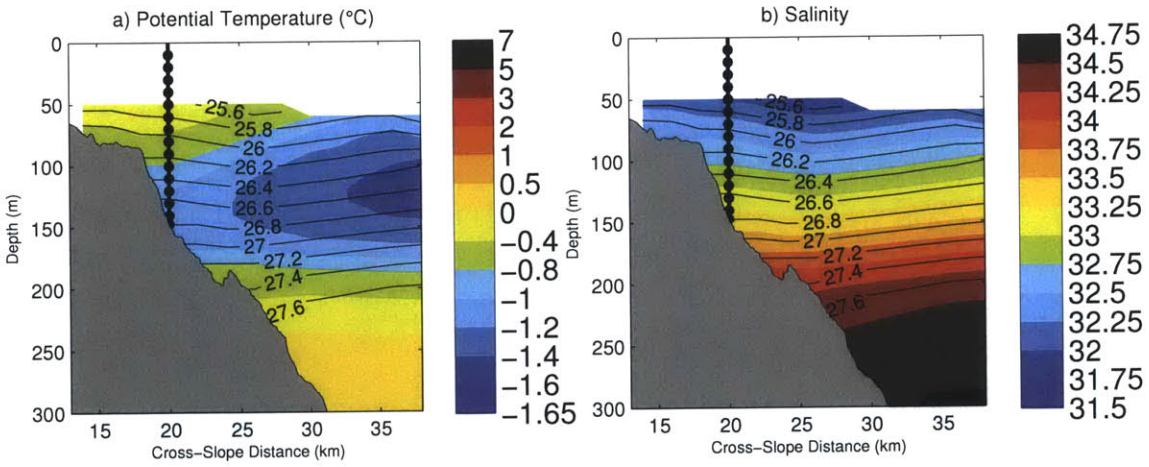

Figure 3-2: Vertical sections of (a) mean potential temperature (color) and potential density (contours, kg/m^3) and (b) mean salinity (color) and potential density (contours) for the year of August 2002 to July 2003.

The transport proxy was further refined to account for two different types of current behavior that resulted in systematic discrepancies between the full transport

and the estimate from the single mooring. During summer the Pacific water jet, which can be thought of as the eastward extension of the Alaskan Coastal Current (ACC), is surface-intensified and, as such, is not as strongly constrained by the bottom topography. Consequently there are times when the jet meanders a bit offshore of the shelfbreak. In these instances the proxy underestimates the true transport. In the fall and winter months, during upwelling events, the flow in the vicinity of the shelfbreak (i.e. the core of the jet) does not reverse as readily as the seaward part of the current. At these times the proxy overestimates the transport of the actual jet. Fortunately, by considering the full SBI array data, we were able to establish objective procedures to mitigate each of these scenarios and increase the accuracy of the proxy. These procedures are described in detail in Appendix B. We note, however, that the use of these adjustments resulted in only small quantitative differences.

The resulting proxy transport timeseries for year 1, after applying the depth-varying width and incorporating the corrections for the summer ACC and the upwelling events, is compared with the full transport of the Pacific water in Figure 3-3. One sees that the agreement is excellent (r=.92). The year-long mean full transport is 0.114 Sv, while that of the proxy is 0.123 Sv. The rms difference between the two timeseries is 0.20 Sv, with the proxy slightly underestimating the true variability of the current (the range of the transport is between -1.7 and 2.3 Sv).

3.2 Gridding the Shelfbreak Mooring Data

For certain parts of the analysis, the mooring hydrographic and velocity data were interpolated onto a regular depth/time grid. First the velocity data were rotated into a coordinate frame dictated by the direction of the depth-averaged flow and the principal axis variance ellipses, following Nikolopoulos et al. (2009). The positive

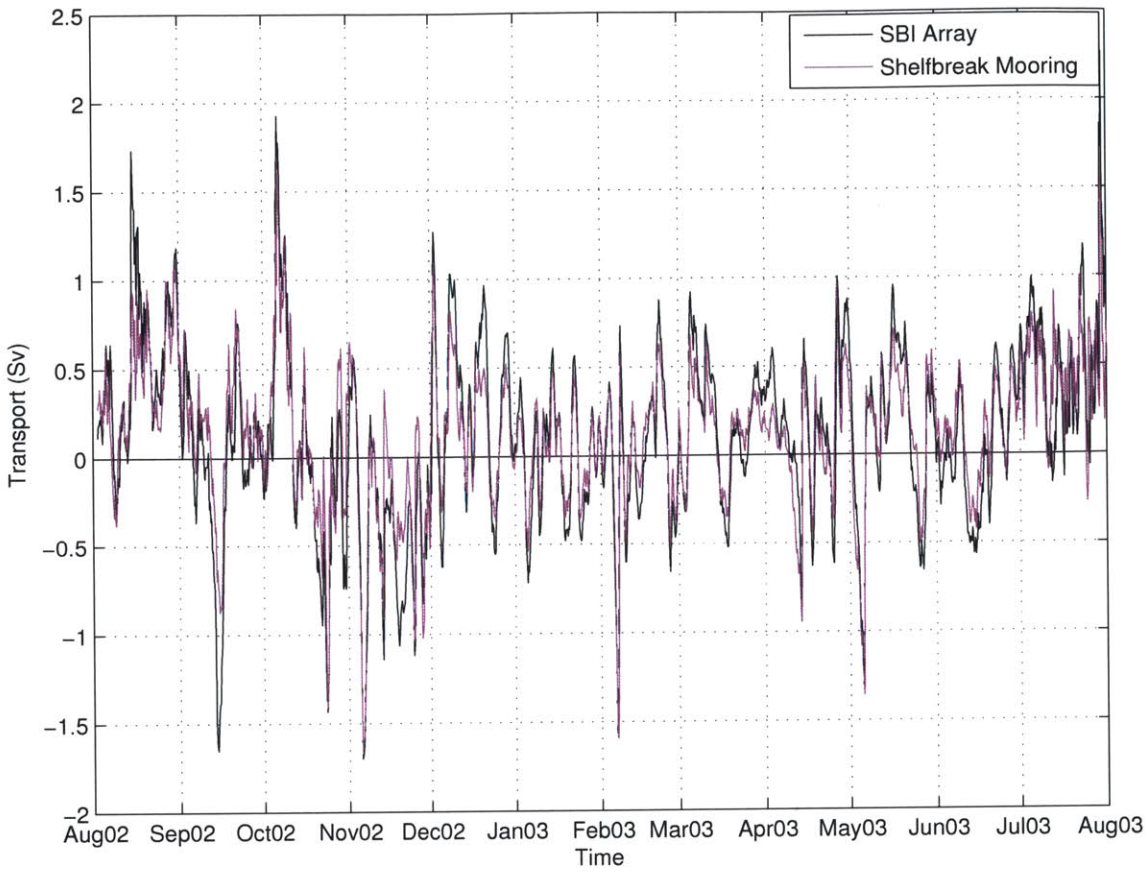

Figure 3-3: Timeseries of daily transport calculated for the SBI array (black) and the shelfbreak mooring proxy (purple). Correlation between the two timeseries is r=.92.

x (alongstream) direction is 120°T, which is nearly parallel to the local bathymetry, and the positive y direction (cross-stream) is 30°T. These are slightly different (by 5°) than the directions determined by Nikolopoulos et al. (2009) who used only the first year of data. The velocities were then low passed using a second order Butterworth filter with a cut-off frequency of 1/(36h). This effectively removed both the tidal (semi-diurnal and diurnal) and inertial signals, which were small to begin with (see Pickart et al. 2013b).

Following this, both the hydrographic (potential temperature, salinity, potential

density) and velocity data were gridded using a 2-D Laplacian-spline interpolation scheme with a vertical spacing of 10 m and temporal grid spacing of 3 hours. This procedure not only formulated the data onto a standard depth-time grid, but it filled data gaps as well. The velocity grid extened from 10–150 m, while the hydrographic grid extended from 50–130 m (since the CMP sampled a smaller part of the water column). Other interpolation methods were attempted as well, but they all produced similar results. As such, the results presented below are not sensitive to the gridding procedure employed.

3.3 Transport Calculations

3.3.1 Volume Transport

The volume flux of the Pacific Water shelfbreak jet at each point in time is given by Equation 3.1, where $v(x, y)$ is the alongstream velocity and A is the cross-sectional area of the current. The timeseries of volume flux was constructed by multiplying the alongstream velocity at each bin by the height of the vertical grid cell (10 m) and the width of the current at that depth (see Figure 3-1), then summing. The height of the deepest bin was truncated by 3 m due to the fact that the mooring was located at 147 m depth. We also consider the volume flux of the specific Pacific-origin water masses (i.e. summer and winter waters, see next chapter). To do this it was necessary to extrapolate the hydrographic variables upward to the surface and downward to bottom, which was done using constant extrapolation. The volume flux timeseries for each water mass was then constructed by identifying which grid cells contained the water mass in question for each time step, and summing accordingly. Importantly, the sum of the volume flux for the five different Pacific water masses

(defined in the next chapter) equals the flux of the full shelfbreak jet calculated using the velocity data alone. A final transport calculation was to determine the flux of each individual water mass only when it was present. For example, a given summer water mass might only be advected by the current for a relatively short time during the year, and it is of interest to know how strong the flux was over this period.

$$Q = \int_A v(x,z)dA, \tag{3.1}$$

3.3.2 Heat Transport

The transport of heat is given by Equation 3.2, where ρ is the in-situ density, θ is the potential temperature, and C_p is the specific heat of seawater. To obtain a true heat flux, the volume transport across the section must be identically zero (e.g. Schauer and Beszczynska-Moeller (2009)), which of course is not the case for the shelfbreak jet. Following earlier studies in the Pacific Arctic (e.g. Woodgate et al. (2010)), we compute the heat flux relative to a reference temperature $\theta_o = -1.91$ °C. This is the freezing point for the mean Atlantic water in the Arctic Ocean; consequently, it reflects the amount of heat available to melt sea-ice (e.g. von Appen and Pickart (2012)).

$$H = \int_A (v(x,z)(\rho)(\theta - \theta_o)(C_p))dA \tag{3.2}$$

Again the hydrographic variables were constantly extrapolated from the uppermost bin to the surface and from the deepest bin to the bottom. Since the heat flux is dominated by the summer waters, which are warmest near the surface, the use of constant extrapolation leads to an underestimate of the heat transport. von Appen and Pickart (2012) used shipboard hydrographic and velocity data collected

near 152°W, together with the SBI mooring data, to assess the magnitude of this error. They found that for times when the warmest summer water was present, the heat transport calculated using the array data was 70% of that calculated using the shipboard data. When other water masses were present the heat transport was less biased, but still an underestimate. This should be kept in mind when considering the results presented below.

3.3.3 Freshwater Transport

As was true for heat flux, we are unable to compute a formal freshwater transport because the volume flux across the section is non-zero. Following earlier Arctic studies, we compute the freshwater flux anomaly (hereafter simply called the freshwater flux) relative to a reference salinity of $S_o = 34.8$, which is the mean salinity of the Atlantic water in the Arctic Ocean. This is given by Equation 3.3, where S is the salinity.

$$F = \int_A (v(x,z)(1 - \tfrac{S(x,z)}{S_o}))dA \tag{3.3}$$

To assess the impact of using constant extrapolation of salinity from 50 m to the surface we consider coastal winched profiler data. During the 2005-6 deployment, the shelfbreak mooring contained two moored profilers. The lower profiler was the CMP which profiled from 130 m to 45 m depth. The upper profiler (coastal winched profiler) was located on the mooring's top float at 40 m. The winched profiler is a CTD on a small buoyant sphere connected by line to a winch. The buoyant float released daily and profiled between 40 m to 10 m depth (or deeper if encountering pack ice). The winch then retrieved the CTD back to the top float where the data was downloaded to a logger. CMP data along with the coastal winched profiler data provided hydrographic vertical profiles for the full water column at 2 m resolution.

Salinity data from the upper water column in 2005-6 allows us to assess the impact of constantly extrapolating salinity from 50 m to the surface. We find that the freshwater transport calculated using the constant extrapolation is 83% of that calculated using data from the full water column. Therefore, constantly extrapolating salinity from 50 m to the surface causes a substantial underestimate of the freshwater flux.

Chapter 4

Pacific Water Shelfbreak Current

4.1 Water Mass Constituents

Throughout the course of the year, five distinct water masses are advected by the Western Arctic Boundary Current. Figure 4-1 shows the marked variation in potential temperature at the core of shelfbreak jet. While there is clear seasonality, the exact timing of the water masses within the boundary current varies from year to year. Warm Alaskan Coastal Water (ACW) is present at various times between July and early October (this water mass is also referred to as Eastern Chukchi Summer Water, see Shimada et al. (2001)). The ACW is transported to the Beaufort Sea by the Alaskan Coastal Current (ACC), which emanates from the easternmost branch of Bering Strait inflow[1]. The water is very warm and fresh, with temperatures greater than 2°C and salinities between 30 and 33.5. It is formed as a result of river runoff into the Gulf of Alaska and Bering Sea (Weingartner et al., 2005b). Note in Figure 4-1 the different arrival times and quantities of ACW each year. For example, in 2003

[1]The Beaufort shelfbreak jet can be considered the eastward extension of the ACC during the time period that it advects ACW.

ACW is present for three months of the year, whereas in 2009 it is there for only about a month. Interestingly, in 2008 there is no sign of ACW after mid-August, yet in every other year there are large amounts of ACW present beyond this date.

A second Pacific summer water mass transported by the shelfbreak jet is known variously as Chukchi Summer Water (CSW, von Appen and Pickart (2012)), Summer Bering Sea Water (Steele et al. (2004)), and Western Chukchi Summer Water (Shimada et al. (2001)). Here we refer to it as CSW, and define it to be water with temperatures between $-1°C$ and $2°C$ and salinities between 30 and 33.5. CSW is cooler, saltier, and less stratified than ACW, and is generally found in the Beaufort shelfbreak current in early summer and again in early fall (i.e. bracketing the presence of ACW, von Appen and Pickart (2012)). However, it can be found in the current nearly any time of the year (for instance it was present in February 2006 near 50 meters depth).

Two different types of Pacific winter water are advected by the boundary current. The first type is recently ventilated Winter Water (WW), which is weakly stratified and colder than $-1.6°C$. Its characteristics are close to the water entering Bering Strait during the winter months, formed via convection in the Bering Sea (Muench et al., 1988). It is the coldest water mass found in the Beaufort shelfbreak jet and generally appears in the current in late-winter into spring. However, this varies significantly from year to year (Figure 4-1). Several factors seem to be responsible for this variability, including changes in the Bering Strait inflow, atmospheric forcing, and sea ice cover / polynya activity (Itoh et al., 2012). The second cold Pacific water mass is Remnant Winter Water (RWW), which is winter water that has been modified by a combination of lateral mixing and atmospheric heating after its formation. This is defined as water with temperatures between $-1.6°C$ and $-1°C$ and salinities ranging from 30 to 33.5. RWW can appear in the shelfbreak current in every month of the

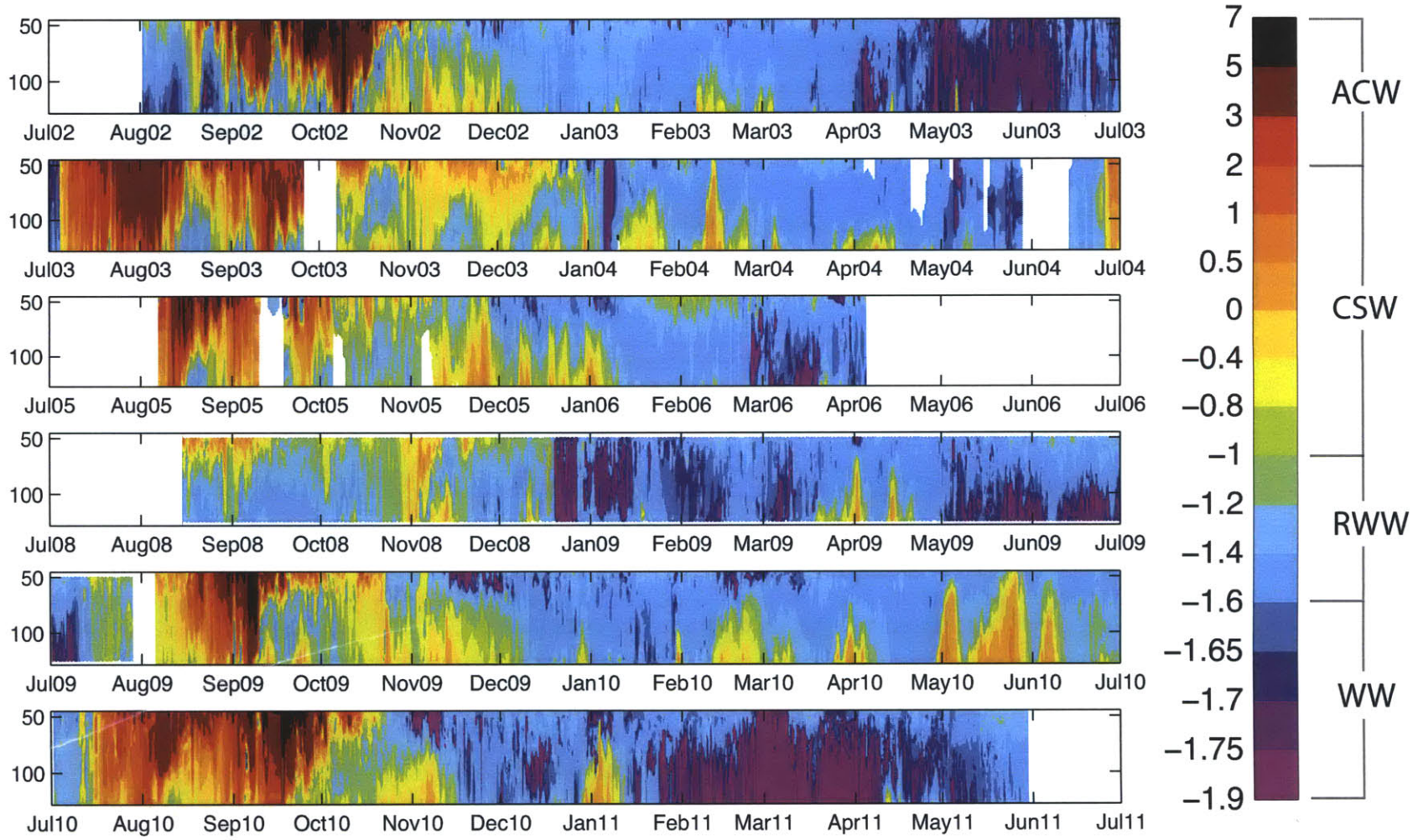

Figure 4-1: Depth/Time plot of potential temperature (°C) at the shelfbreak mooring (in the core of the boundary current) from 45 to 130 m depth.

year, including summer.

The final water mass found in the boundary current is Atlantic Water (AW), which has salinities exceeding 33.5. As noted in Chapter 1, AW is transported eastward along the Beaufort slope by the Arctic-wide cyclonic boundary current system (e.g. Rudels et al. (1994), Woodgate et al. (2001), Karcher et al. (2007), Aksenov et al. (2011)), which is not considered as part of the shelfbreak jet (there is a minimal contribution in transport to the deepest part of the jet, see Nikolopoulos et al. (2009)). However, the frequent easterly winds in the region cause the shelfbreak current to reverse and the Atlantic Water to be upwelled to the vicinity of the shelfbreak. These events can be seen in Figure 4-1 as warm spikes emanating from depth. In this regard AW does influence the shelfbreak current.

Figure 4-2 displays the five water masses in temperature – salinity space and indicates their relative occurrence in the core of the boundary current over the 6-year period of the study. The two types of winter water (RWW and WW) appear most frequently in the current, while CSW is more commonly found than ACW. The high percentage of AW attests to the frequent occurrence of upwelling in the region.

4.2 Mean Structure

Using data from the seven-mooring array during the SBI period we present the cross-stream velocity and hydrographic structure of the Beaufort shelfbreak jet (Figure 4-3, based on the first year of data from 1 August 2002 to 31 July 2003). One sees that the jet is centered near the shelfbreak at approximately 100 m depth. Over the year-long period the average alongstream velocity at the core of the current was roughly 15 cm/s. The mean potential temperature section reveals Pacific summer water near the shelfbreak in the upper 100 m, a layer of Pacific winter water between

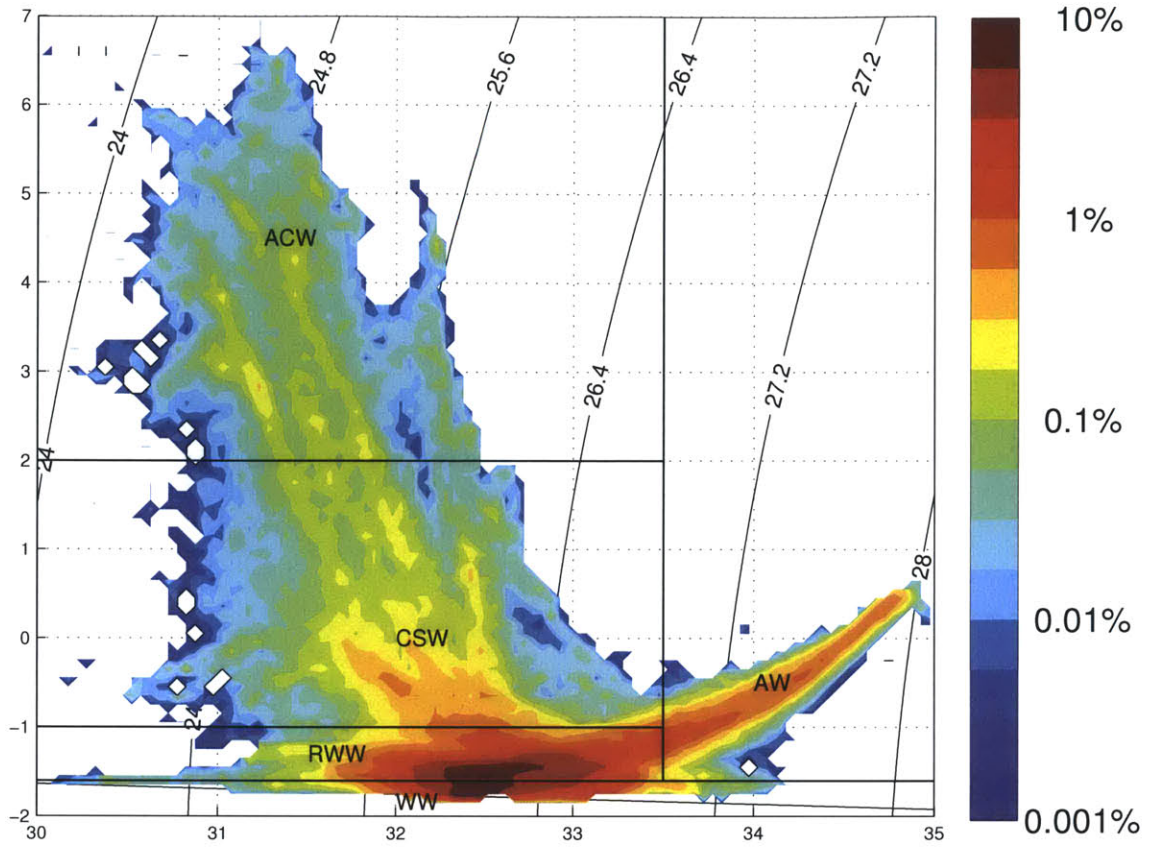

Figure 4-2: Occurrence of water types in temperature – salinity space for the six shelfbreak mooring deployments. Units are percentage of all measurements per 0.1 °C and 0.05 salinity (note the logarithmic scale). The black lines delimit the five water masses. ACW=Alaskan Coastal Water; CSW=Chukchi Summer Water; WW=Winter Water; RWW=Remnant Winter Water; AW=Atlantic Water.

100-150 m, and below this the relatively warm and salty AW. In the mean it is hard to distinguish ACW from CSW because the former is only present a few months of the year and gets averaged out. Similarly, the two winter waters, RWW and WW, are not distinguishable in the year-long average due to the relatively sporadic occurrence of WW.

While the full mooring array was only deployed for two years, the shelfbreak mooring provides a nearly 6-year timeseries of velocity and hydrographic data in the

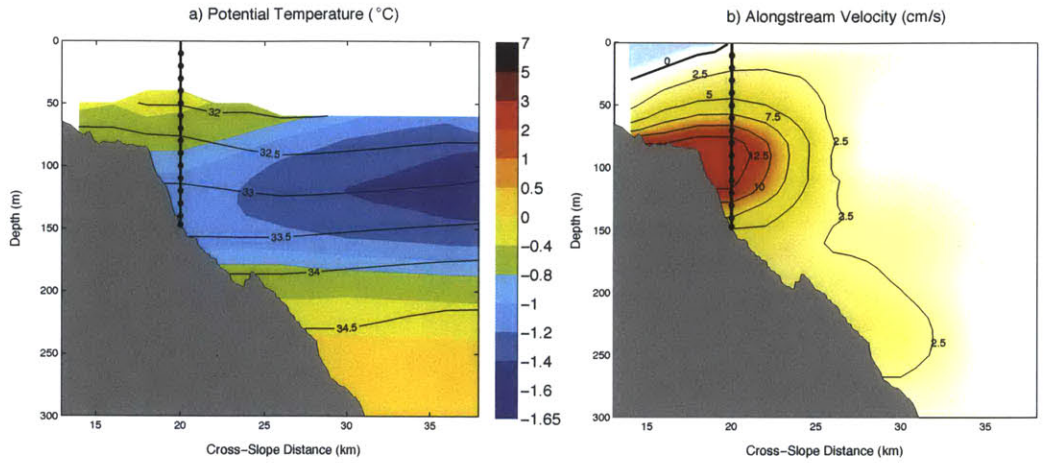

Figure 4-3: Vertical sections of (a) mean potential temperature (color) and salinity (contours) and (b) mean alongstream velocity (cm/s) for the year of August 2002–July 2003.

core of the current. Figure 4-4 shows the mean vertical profiles of these variables for the full deployment. Similar to the SBI cross section, the mean hydrographic profiles for the shelfbreak mooring show relatively warm, fresh Pacific summer water in the core of the current above 100 m, with cooler, saltier Pacific winter waters below this. The mean alongstream velocity profile shows a peak between 80-100 m. As the full array cross section suggests, this is the depth range where the core of the boundary current is trapped to the shelfbreak. Below 100 m, the alongstream velocity decreases to the bottom at 147 m. Note that in the 6-year mean the maximum alongstream velocity just exceeds 10 cm/s, whereas in the SBI cross-section the peak velocity is near 15 cm/s. Furthermore, the average velocity above 20 m is flowing towards the west in the longer-term mean. This suggests that the core of the boundary current has weakened since the SBI period, and the near-surface flow has reversed.

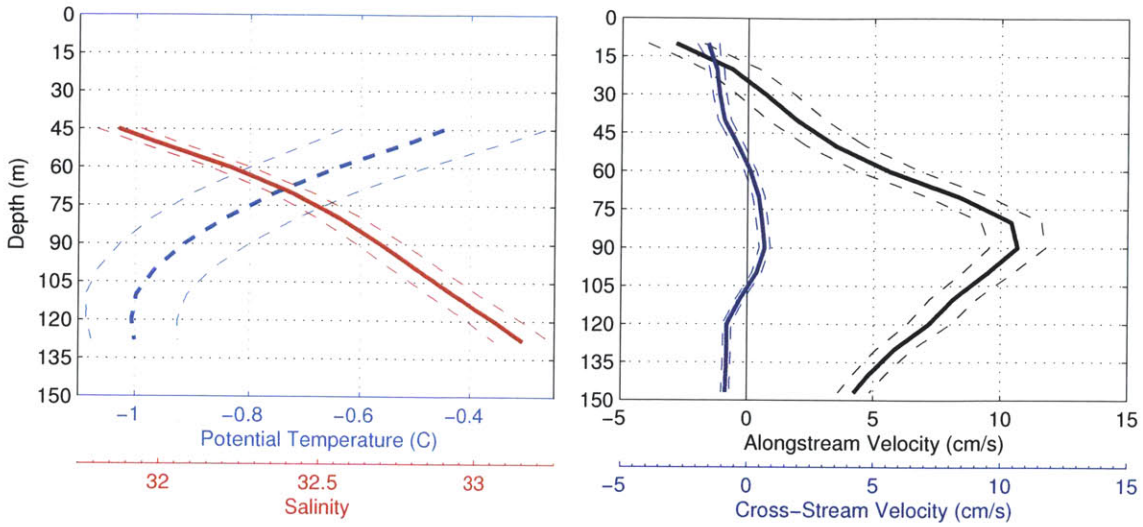

Figure 4-4: Vertical sections of (a) mean potential temperature (color) and salinity (contours) and (b) mean alongstream velocity (cm/s) for the year of August 2002–July 2003. Dashed lines represent the standard error.

4.3 Seasonal Configurations

Nikolopoulos et al. (2009) demonstrated that over the course of a year the boundary current varies both in structure and strength. However, their conclusions were based on only one year of data. Here we use the full 6-year timeseries from the core of the jet to quantify the seasonal variability of the Beaufort shelfbreak current.

4.3.1 Climatological Monthly Mean Volume, Heat and Freshwater Transports

Using the proxy defined in Chapter 3, we constructed climatogical monthly mean timeseries of volume transport (Sv), heat transport (J/s) and freshwater transport (mSv) (Figure 4-5). The data used for these monthly means are specified in Table 4.1. One sees that that there is a pronounced seasonality in all three quantities. The most noticeable feature is the increase in transport during the summer months,

which is largely associated with the appearance of the ACC. The months of June, July, August, and September account for approximately 85% of the yearly volume transport of the boundary current. During the remainder of the year the volume transport is significantly less, and is indistinguishable from zero during three of those months. November and May are both characterized by reversed flow to the west. Interestingly, these two months correspond to the two months of strongest upwelling activity on the Alaskan Beaufort slope (Pickart et al., 2013a). This suggests that wind forcing plays a significant role in the seasonality of the shelfbreak jet. To quantify this we also calculated the climatological monthly transports in the absence of wind (red dashed curves in Figure 4-5). The volume transport of the undisturbed current is eastward throughout the year, although the strengthening of the current in summer is still evident.

Table 4.1: Monthly inputs to the volume, heat and freshwater transport figures. X's denote both velocity and hydrographic data are available and O's represent only velocity data.

Year	Jan	Feb	Mar	Apr	May	Jun	Jul	Aug	Sep	Oct	Nov	Dec
2002								X	X	X	X	X
2003	X	X	X	X	X	X	X	X	X	X	X	X
2004	X	X	X	X	X	X	X	O				
2005								X	X	X	X	
2008								X	X	X	X	X
2009	X	X	X	X	X	X	X	X	X	X	X	X
2010	X	X	X	X	X	X	X	X	X	X	X	X
2011	X	X	X	X	X	O	O	O	O			

The seasonality of the heat and freshwater transport of the current is just as pronounced. In fact, nearly all of the heat transport occurs in the three months of July, August, and September. In the absence of winds the heat flux is greater for every month of the year, with the biggest difference from July to December. Similar to the heat transport, most of the freshwater transport occurs within the months

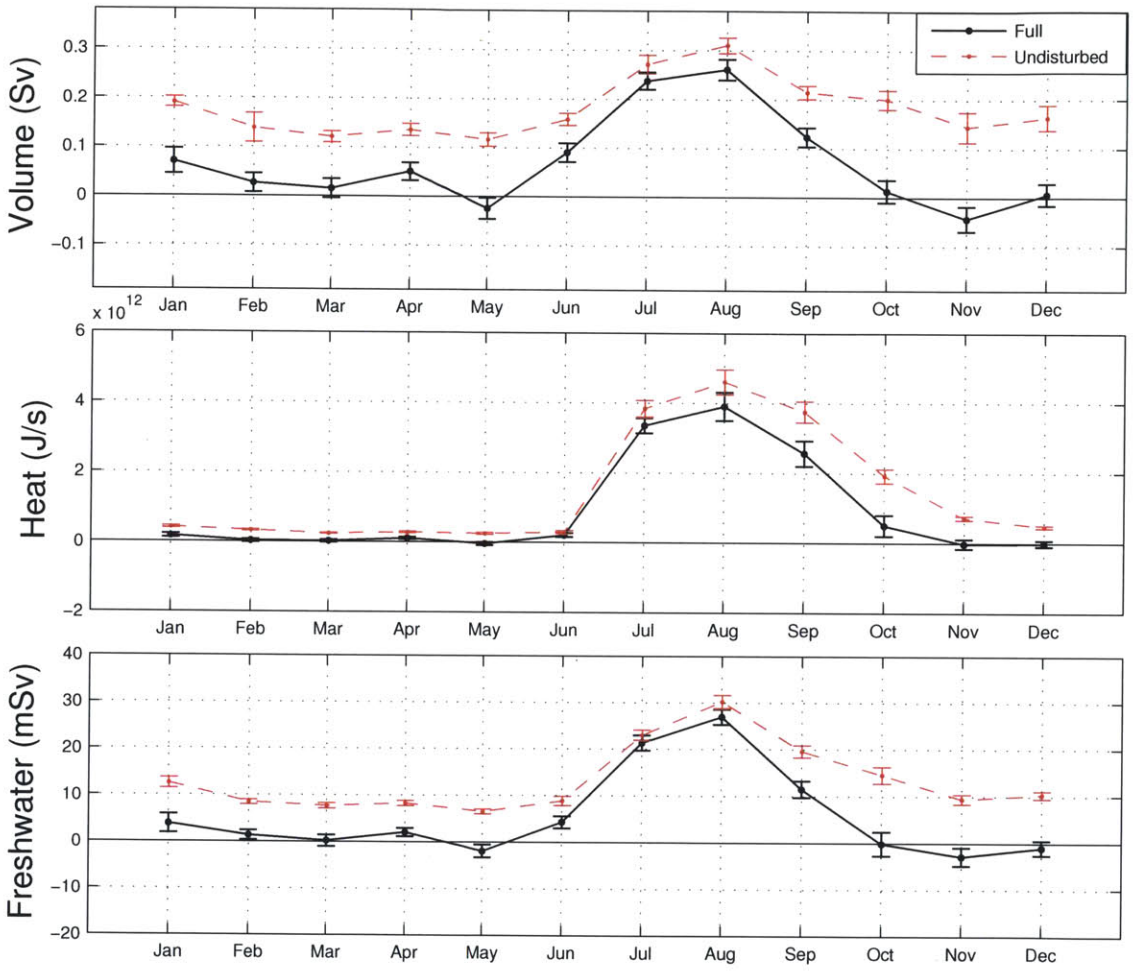

Figure 4-5: Climatological monthly mean volume transport (Sv), heat transport (J/s) and freshwater transport (mSv) of the Western Arctic Boundary Current. Solid black lines represent the full transports, while red dashed lines represent the transport in the absence of atmospheric forcing. The standard errors are marked.

of July, August and September. However, unlike the heat flux, there is a small but significant freshwater flux in June. The nature of the seasonality of the heat and freshwater transports of the boundary current is elaborated on below.

4.3.2 Individual Water Mass Transports

(a) Water Mass Volume Transport

Figure 4-6 shows the climatological mean volume transport broken down into the five water mass components. We only use data for those months in which both hydrographic and velocity data exist (denoted by "X" in Table 4.1). One sees that ACW is the dominant water mass transported by the boundary current during the summer months, accounting for over half of the yearly volume transport. Note that most of this transport occurs in July, August, and September, and, other than a small contribution in October, ACW is absent from the current over the remainder of the year. The volume flux of CSW is also strongest in summer, although it is present in the boundary current nearly year round. However, for seven of these months the transport is not significantly different from zero. As mentioned above, RWW is present in the current every month of the year, with an appreciable amount of transport during the summer months. Outside of summer, RWW is the dominant water mass transported by the boundary current.

The seasonality in volume flux of the newly-ventilated WW is distinct from that of the RWW. It has a maximum in the month of June. However, note that in the absence of winds the WW attains its peak transport in May (followed closely by April and June). This is consistent with the notion that the WW predominantly flushes out of the Chukchi Sea in late-winter and early-spring each year (e.g. Spall et al., 2008). Small amounts of AW are discernible within the boundary current year round,

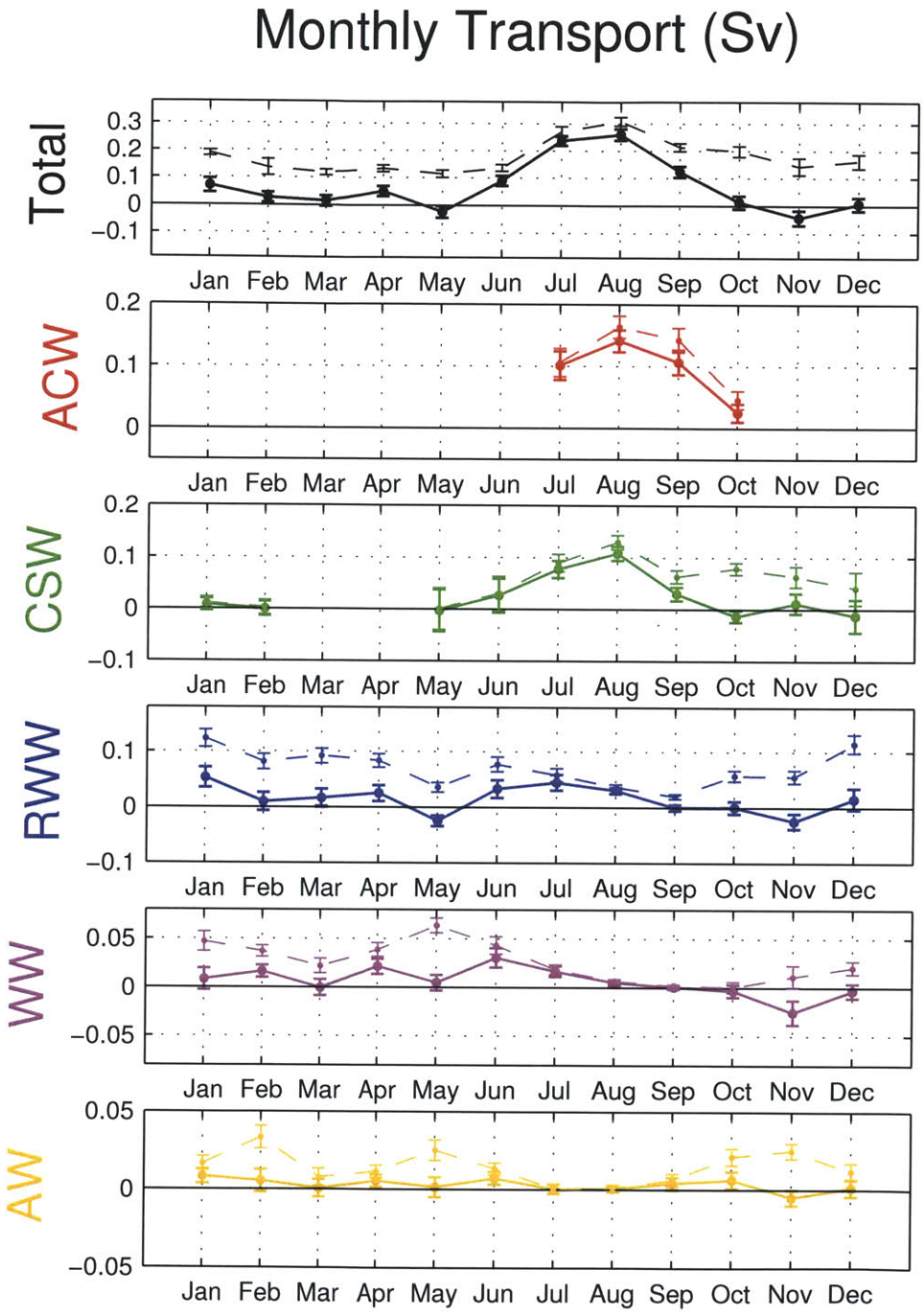

Figure 4-6: Climatological mean volume transport (Sv) for the Pacific Water Boundary Current. Solid lines represent the full transports, while dashed lines represent the transport in the absence of atmospheric forcing. (note that each plot has a different y axis).

although the associated volume transports for the most part are not significantly different than zero. This is not surprising since AW usually appears in the shelfbreak jet as a result of upwelling when the current is reversed to the west. The presence of AW within the core of the boundary current is evidence that upwelling can occur year round, regardless of month.

The annual contributions of volume transport due to each of the water masses are shown in Figure 4-7. Strikingly, even though ACW is only present 1–4 months of the year, in the mean it accounts for the majority of the volume transport. The next biggest contributor is the CSW, followed by the RWW, although their annual values are not statistically different. Very little WW is transported to the east, likely due to the fact that wind forcing often reverses the shelfbreak jet when this water mass is present. Similarly, AW accounts for a very small fraction of the total transport because it is upwelled into the boundary current when the flow is usually westward.

(b) Water Mass Heat Transport

Most of the heat transported by the shelfbreak jet past 152°W is associated with the warm ACW. In particular, this water mass accounts for approximately two-thirds of the heat transport between July and October (Figure 4-8). CSW makes up the most of the remaining heat transport over the same time period, with RWW contributing a very small amount for these months. Annually, ACW and CSW account for nearly all of the heat transport, with minimal contribution from the winter water masses RWW and WW (Figure 4-9). This is not surprising considering the cold temperatures of these waters. Finally, AW contributes very little to the heat transport due to the weak flow (or reversed flow) associated with upwelling events.

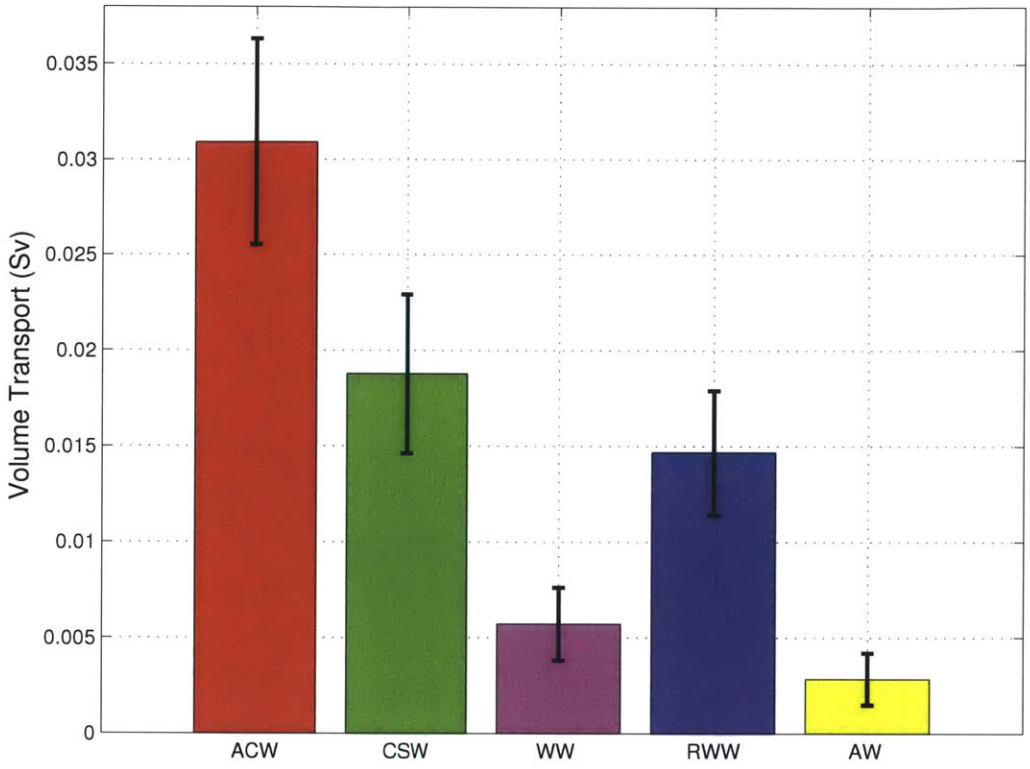

Figure 4-7: Water mass contribution to the overall yearly volume transport (Sv) including the standard error. All of the shelfbreak mooring data are considered in this calculation.

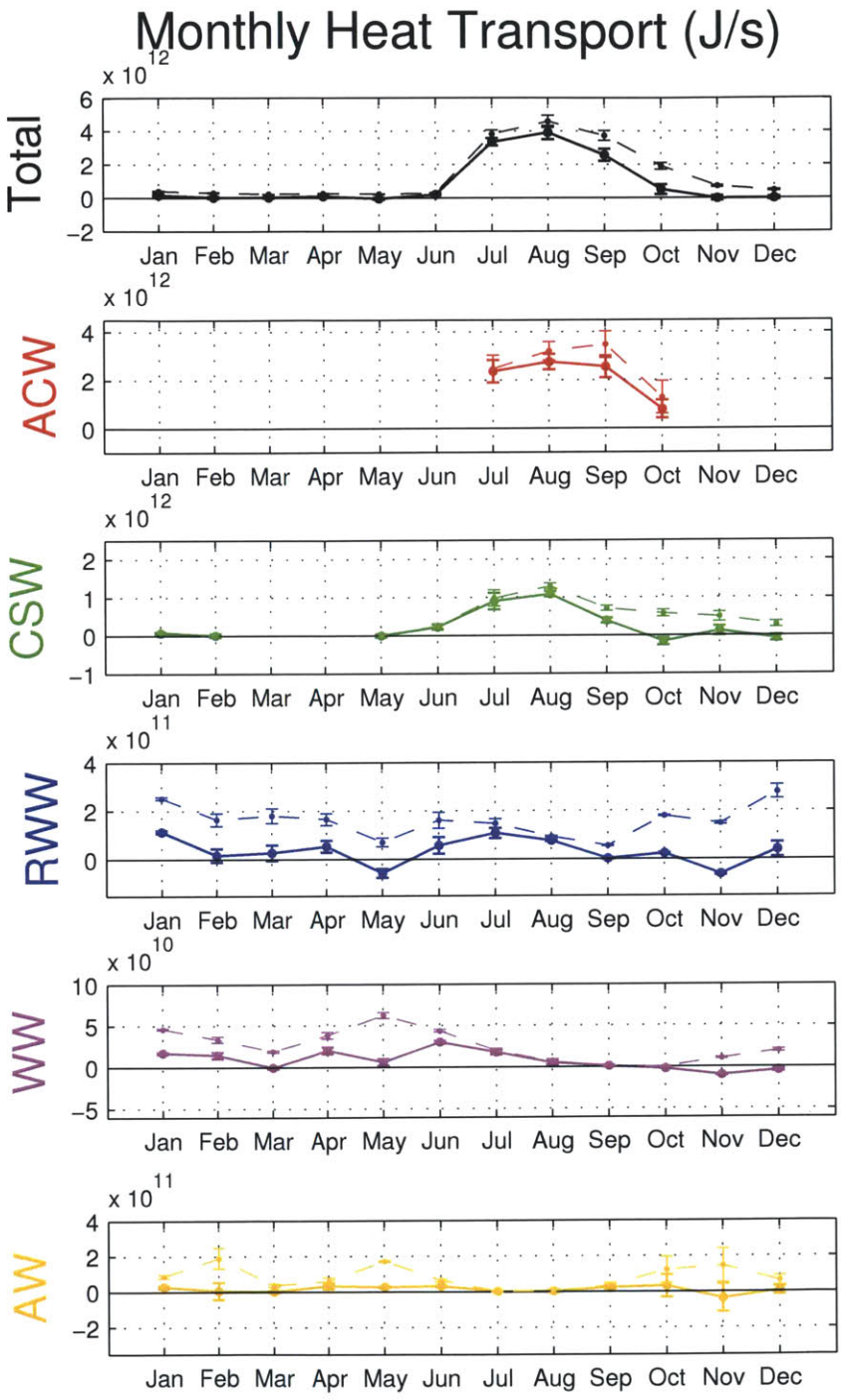

Figure 4-8: Climatological mean heat transport (J/s) for the Western Arctic Boundary Current. Solid lines represent the full transports, while dashed lines represent the transport in the absence of atmospheric forcing. (note that each plot has a different y axis). Standard errors are marked.

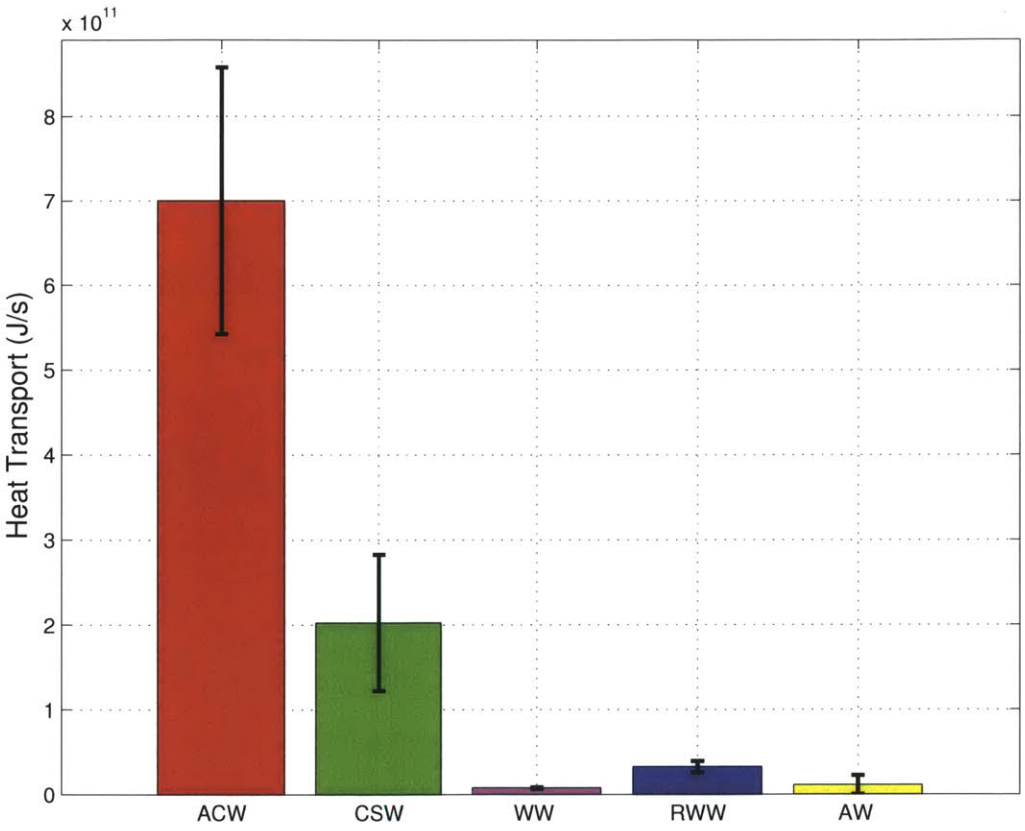

Figure 4-9: Same as Figure 4-7 for heat transport (J/s).

(c) Water Mass Freshwater Transport

As was true for heat flux, ACW and CSW are the dominant contributors to the freshwater transport in the shelfbreak jet. Together, these two summer waters account for about 80% of the freshwater flux during July, August and September (Figure 4-10). RWW provides a fraction of the freshwater transport during several months of the year, while WW contributes to the transport in June but minimally the rest of the year. Not surprisingly, AW, due to its high salinity, contributes very little to the freshwater transport throughout the year. Annually, the biggest fraction of freshwater transport comes from the summer waters, although CSW contributes a larger fraction of this flux than for the heat flux (Figure 4-11). Also, the winter waters transport a non-trivial amount of freshwater (in contrast to their heat flux, which is near zero).

To summarize, the months of June, July, August and September are associated with the highest volume, heat and freshwater transport of the shelfbreak jet in the Alaskan Beaufort Sea. This is largely, but not entirely, a function of wind forcing, which is evident by comparing the flux values for the undisturbed current.

4.4 Interannual Variability

Next we consider the year-to-year variability of the Pacific water boundary current at 152°W. To assess this, we use the five full years of velocity data collected at the shelfbreak mooring site, where the year is defined as the period 1 August to 31 July. The reason for this definition is that it maximizes the data coverage (since the mooring is usually serviced in summer/fall). The years with complete records are 2002-3, 2003-4, 2008-9, 2009-10, 2010-11 (2005-6 has velocity coverage only in the fall since the ADCP failed prematurely).

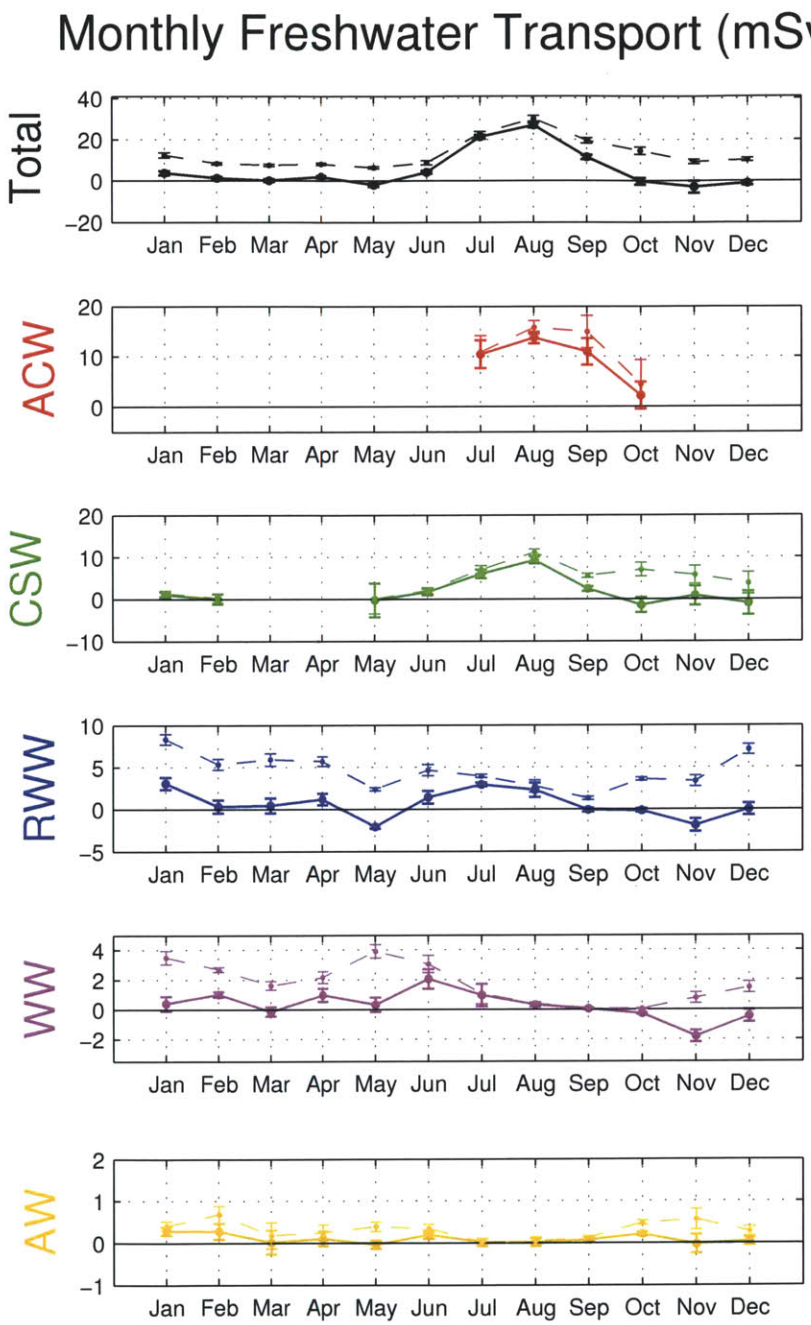

Figure 4-10: Climatological mean freshwater transport (mSv) for the Western Arctic Boundary Current. Solid lines represent the full transports, while dashed lines represent the transport in the absence of atmospheric forcing. (note that each plot has a different y axis). Standard errors are marked.

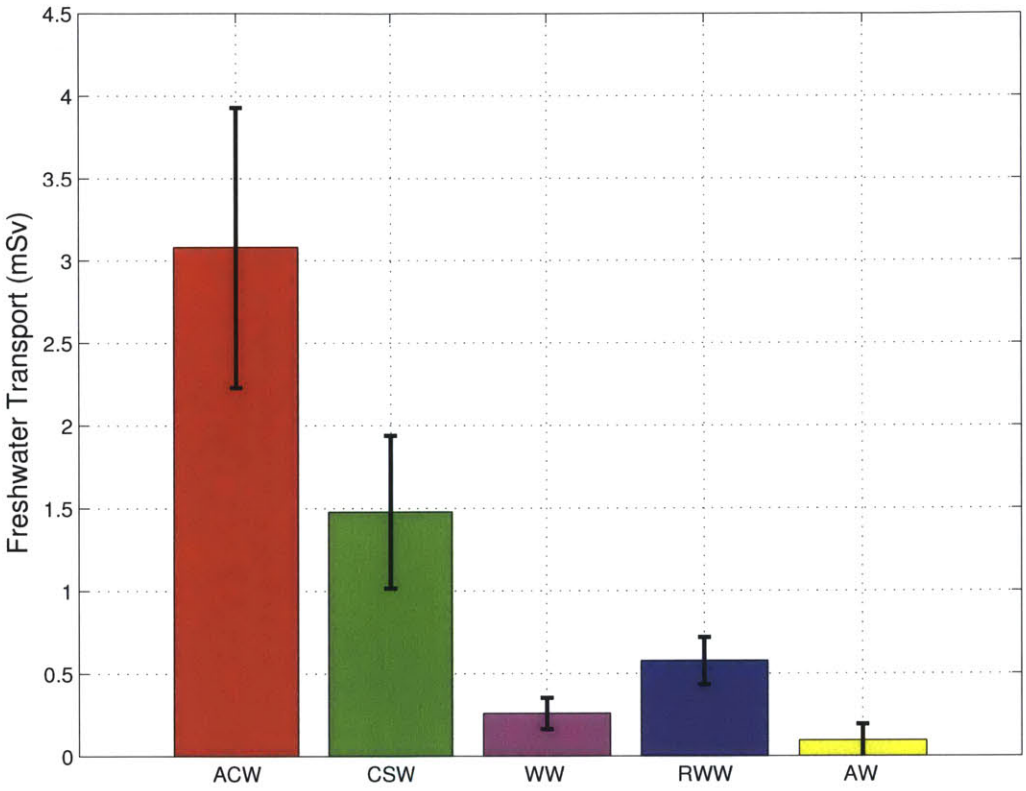

Figure 4-11: Same as Figure 4-7 for freshwater transport (mSv).

4.4.1 Volume Transport

Over the course of the last decade (2002-2011) the volume transport of the Western Arctic Boundary current has decreased dramatically (Figure 4-12). During the first two deployments the transport was roughly 0.11-0.12 Sv, but five years later the transport had dropped to the range of 0.021-0.041 Sv. This represents a reduction of nearly 80%. We note that this transport loss is qualitatively the same if we consider only the first three months of each year, in which case we can include an additional data point (2005-6) whose value is in between the two clusters in Figure 4-12. In other words, the trend is preserved when considering this additional information. Interestingly, in 2009-10 there was a slight "rebound" in transport to just over 0.04 Sv. In the analysis below we will consider two regimes within the decade: the high transport during the first period and the low transport during the later period.

What water masses are responsible for this pronounced reduction in transport? To assess this we considered the four years where there were corresponding hydrographic data over the same time period as the velocity data (see Table 4.1). The volume transports broken into the different water masses are shown in Figure 4-13. While there is considerable year-to-year variability for each water mass, there are clear trends. In particular, there is significantly more summer water transport (ACW and CSW) during the first two years than in the latter two years. In contrast, the changes in winter water transport (RWW and WW) are not as pronounced. Interestingly, there is no eastward flow of WW in two of the years (2003-4 and 2009-10), and the transport of CSW is particularly large in 2003-4. Lastly, AW is either flowing westward (not represented in Figure 4-13) or very weakly eastward throughout the study period.

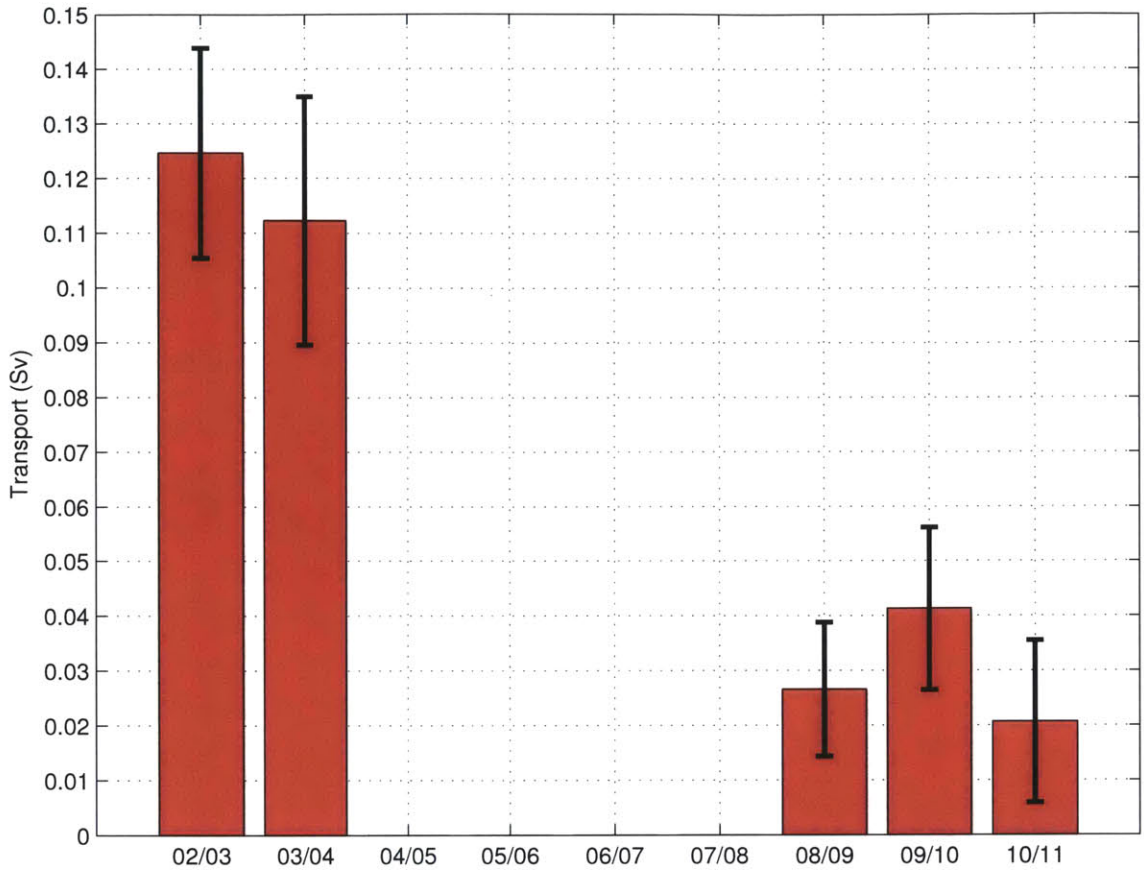

Figure 4-12: Yearly volume transport (Sv) of boundary current measured by the shelfbreak mooring, including the standard error. Years are defined from 01 August to 31 July.

4.4.2 Heat and Freshwater Transport

Since the largest decline in volume transport occurred for the two summer waters, not surprisingly there is also a substantial drop in the heat and freshwater transport of these two water masses from 2002 to 2011 (Figures 4-14 and 4-15). However, a reduction in heat content of the ACW and CSW over this time period (not shown) makes the decrease in heat flux between early and later years even more dramatic. Individually, the ACW heat flux declined by 90%, while the CSW heat flux decreased by 80%. We note that over this same period the heat flux through Bering Strait

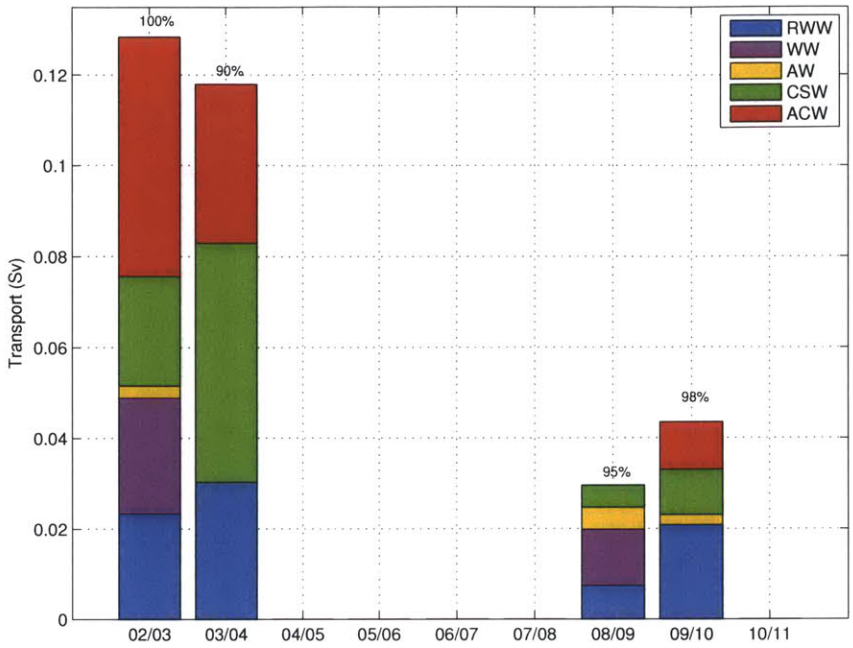

Figure 4-13: Yearly volume transport (Sv) of boundary current measured by the shelfbreak mooring, broken into the five water masses. Years are defined from 01 August to 31 July. Percentage at the top of each bar indicates the amount of the year that both velocity and hydrographic properties were measured simultaneously. Note: 2003-4 and 2009-10 measured negative transports for certain water masses and are not included in the bar graph. By omitting these negative transports, the total transports are not equal to those in Figure 4-12.

has increased, which begs the question, where has this extra heat gone? This is addressed below in Chapter 7. There is a similar discrepancy between the early years and later years for the freshwater transport. Strikingly, while the freshwater transport is dominated by the ACW and CSW in the early years, there is hardly any summer water freshwater flux in 2008-9, and in the following year the RWW contributes to the freshwater flux as much as the two summer water masses.

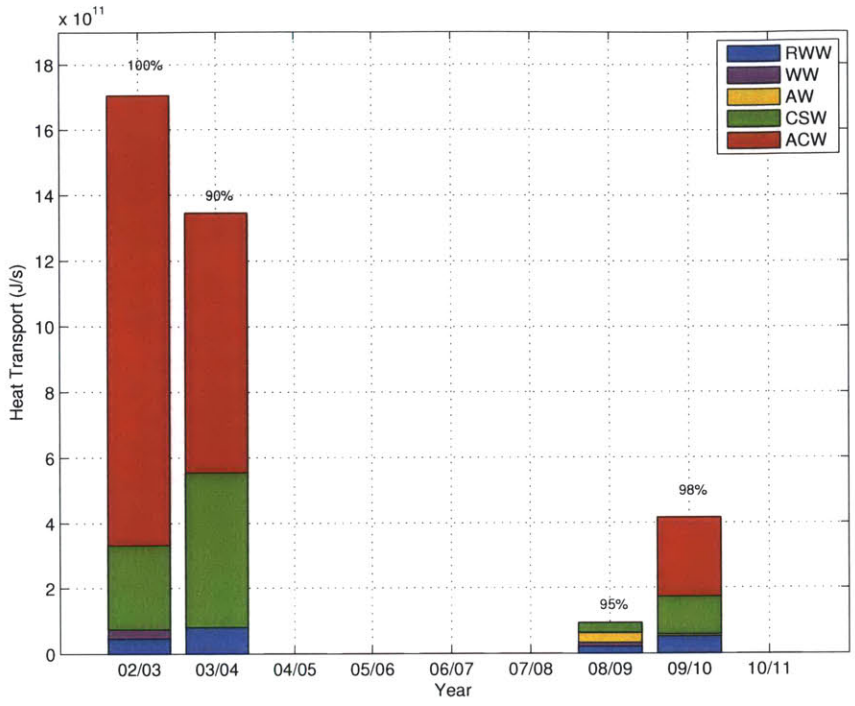

Figure 4-14: Yearly heat transport (J/s) of boundary current measured by the shelf-break mooring broken into the five water masses. Years are defined from 01 August to 31 July. Percentage at the top of each bar indicates the amount of the year that both velocity and hydrographic properties were measured simultaneously.

4.4.3 Partial Year Water Mass Transports

The analysis above considered the transport of the individual water masses when distributed over the course of the full year. We now examine the transports for the time periods only when each water mass was present (please refer to Chapter 3 for description of these calculations). This is done for all realizations of the water mass as well as for the periods when the flow was undisturbed by winds (Figure 4-16). When ACW is present within the boundary current, its transport is significantly greater than for any other water mass (left-hand panels of Figure 4-16). Note that the trends of the two summer water masses is the same as when distributed throughout the year; i.e., there has been a drop in volume flux over the decade. Notably, this trend vanishes

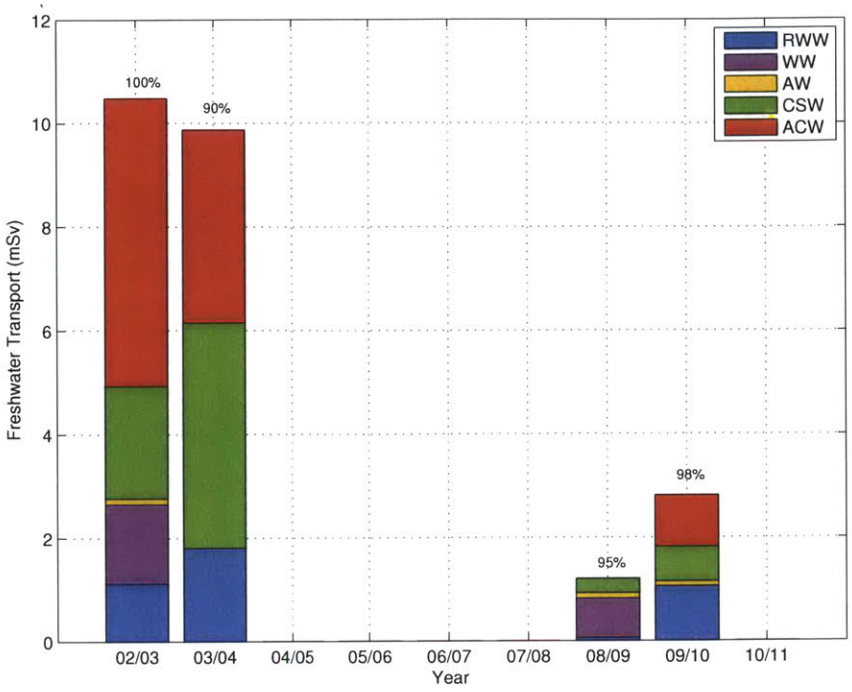

Figure 4-15: Same as Figure 4-14 for freshwater transport (mSv).

for the undisturbed current (right-hand panels of Figure 4-16). This suggests that the decline in summer water transport is largely wind-driven. Interestingly, Figure 4-16 suggests that there has been a decline in transport of winter water of the undisturbed current over the decade (particularly for the WW). This implies a reduction in the formation rate of winter water in the Bering Sea. The undisturbed Atlantic water transport has remained steady during the study period.

4.4.4 Summer Transport

The above results demonstrate that there has been a huge drop in transport of the shelfbreak jet between the early years (2002-3, 2003-4) and the later years (2008-9, 2009-10, 2010-11). Furthermore, the biggest change has occurred for the summer water masses (ACW and CSW). This motivates us to compute the full transport for

the summer months of June, July, and August, which is shown in Figure 4-17. The trend is even more striking in this presentation, as is the rebound year of 2010. This decrease in summer water transport is primarily responsible for the large reduction in heat and freshwater flux of the current. Woodgate et al. (2012) show that there has been an increase in the volume and heat flux through Bering Strait over the past decade, suggesting that the changes in the transport of the shelfbreak jet in the Alaskan Beaufort Sea presented here are not remotely driven. This, together with the above results for the undisturbed flow, points to wind forcing as the key. We now investigate the role of atmospheric forcing in an attempt to explain the signals seen in Figure 4-17.

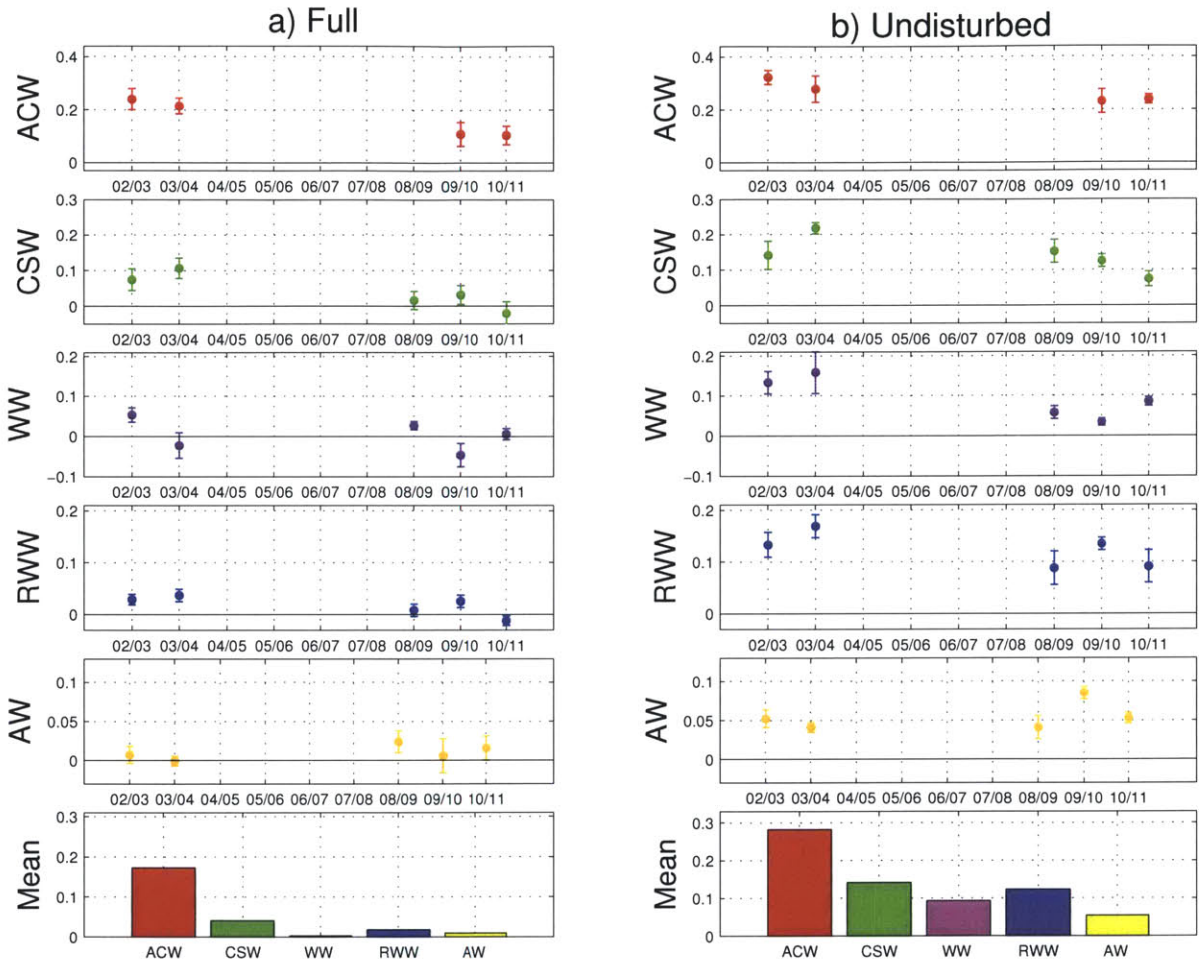

Figure 4-16: Yearly volume transport (Sv) of boundary current for a) the full transport and b) the undisturbed transport. Transport is measured for each water mass only when the water mass is present. The mean over all years is shown as a bar graph in the bottom of each panel. Years are defined from 01 August to 31 July. Standard error is calculated using the integral timescale of the most continuous timeseries for each water mass.

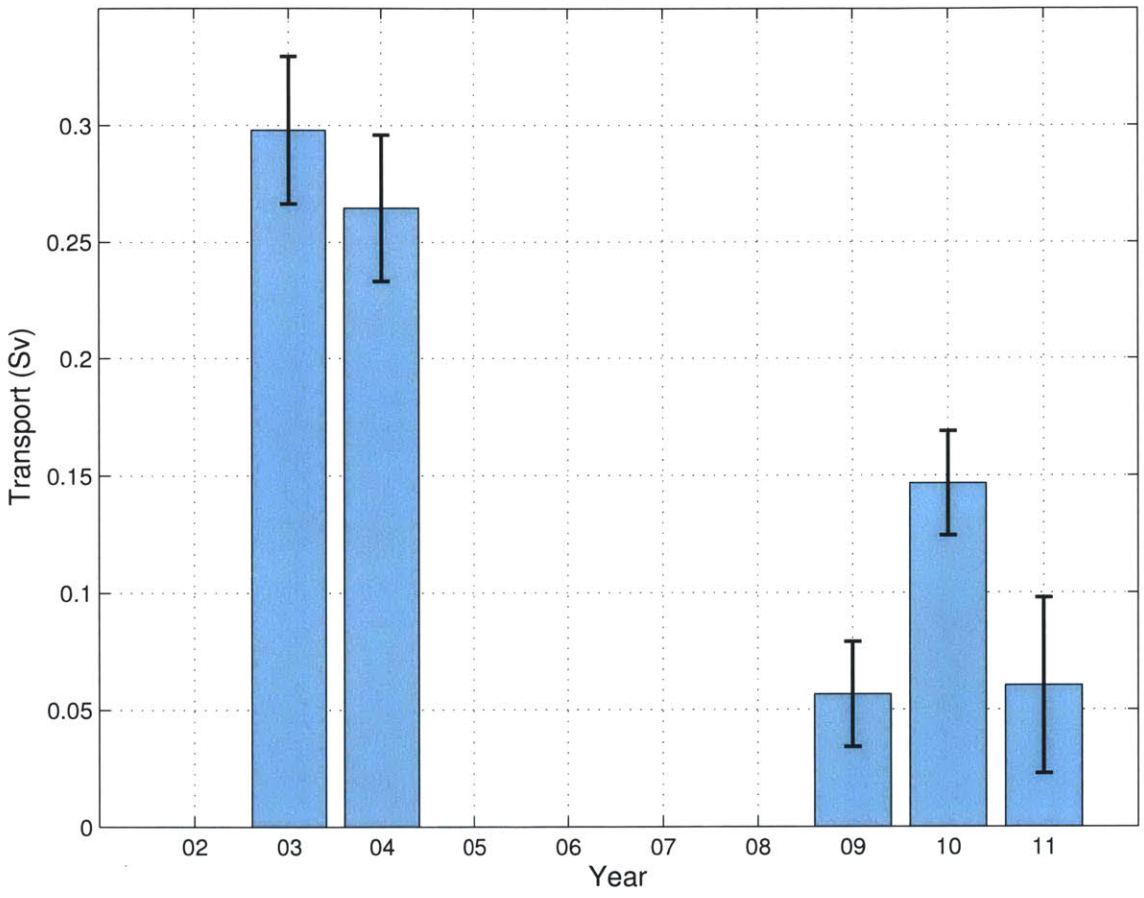

Figure 4-17: Mean summer volume transport (June, July, August) of the boundary current, including the standard error.

Chapter 5

Nature of the Atmospheric Circulation in the Pacific Arctic

5.1 Mean Circulation

Local winds on the Beaufort slope are, to first order, driven by two prevalent atmospheric centers of action: the Beaufort High (BH) and the Aleutian Low (AL). The BH appears as an isolated feature north of Alaska or as a region of high pressure that extends from the East Siberian Sea to the Beaufort Sea. It is primarily a summertime phenomenon and is quasi-stationary. The BH shows up very clearly in the decade-long (2002-2011) mean of sea-level pressure (SLP) using the NARR re-analysis fields (Figure 5-1). The AL is the integrated signal due to low pressure systems that traverse from west to east along the North Pacific storm track (Wilson and Overland, 1986; Pickart et al., 2009b). The systems tend to intensify in the region of the Aleutian Island chain. The AL is evident as well in the decade-long mean of Figure 5-1 as an area of low pressure centered over the island chain extending into the Gulf of Alaska. The BH is characterized by anti-cyclonic circulation, while the AL is characterized

by cyclonic circulation. Together, these two large-scale atmospheric features result in a SLP gradient that leads to easterly winds in the Alaskan Beaufort Sea.

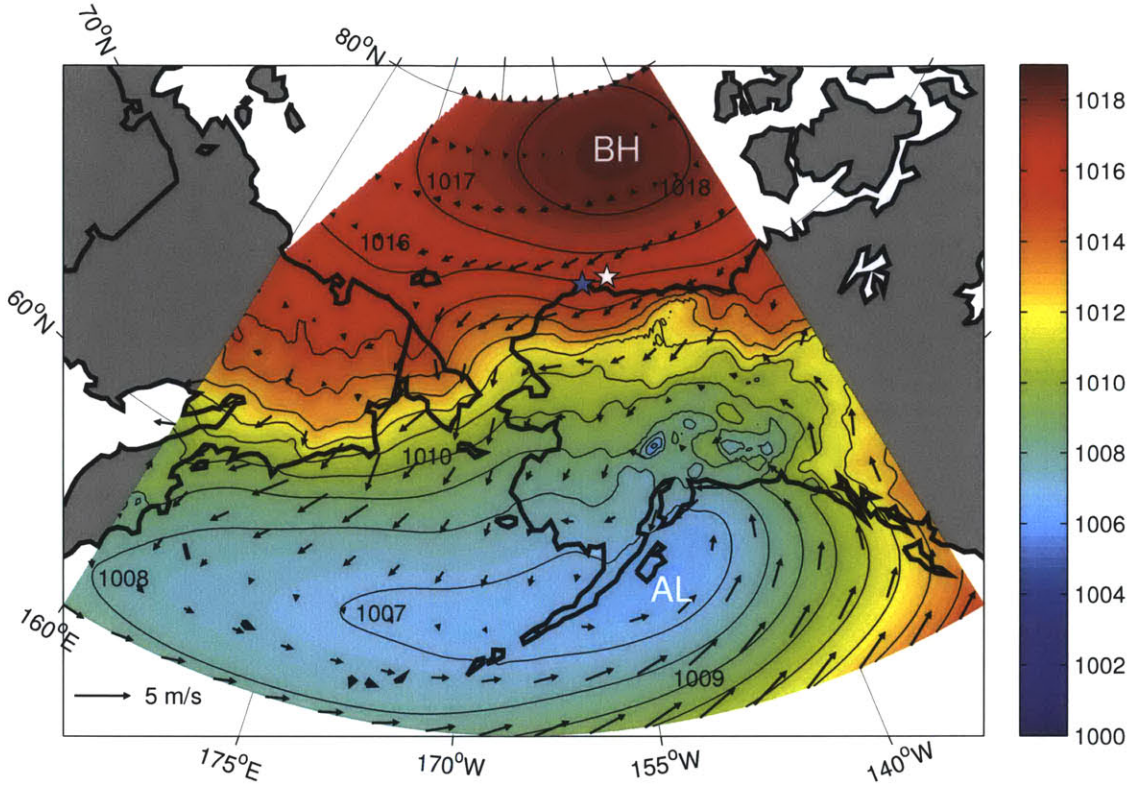

Figure 5-1: Mean sea-level pressure (contours and shading, mb) using the NARR data set for the period 2002-2011. Overlaid are 10 m wind vectors (m/s). The Beaufort High (BH) and Aleutian Low (AL) are labeled accordingly. The white star indicates the location of the shelfbreak mooring and the blue star indicates the location of the Pt. Barrow weather station.

The Pt. Barrow weather station is located roughly 150 km to the west of the shelfbreak mooring site, and, as discussed in Chapter 2, the winds at the weather station are a good proxy for those at the array site. Using these data we find that the most frequent and most intense winds are out of the east to northeast (Figure 5-2). Northerly and southerly winds are rare and when they do occur they are very weak. Westerly winds are possible (although not frequent), and, as Figure 5-2 indicates,

they have the potential to be substantial (shown by the red colors at the tips of each spoke). If strong enough, winds out of the west can accelerate the current to the east and drive downwelling (R. Pickart, pers. comm., 2013).

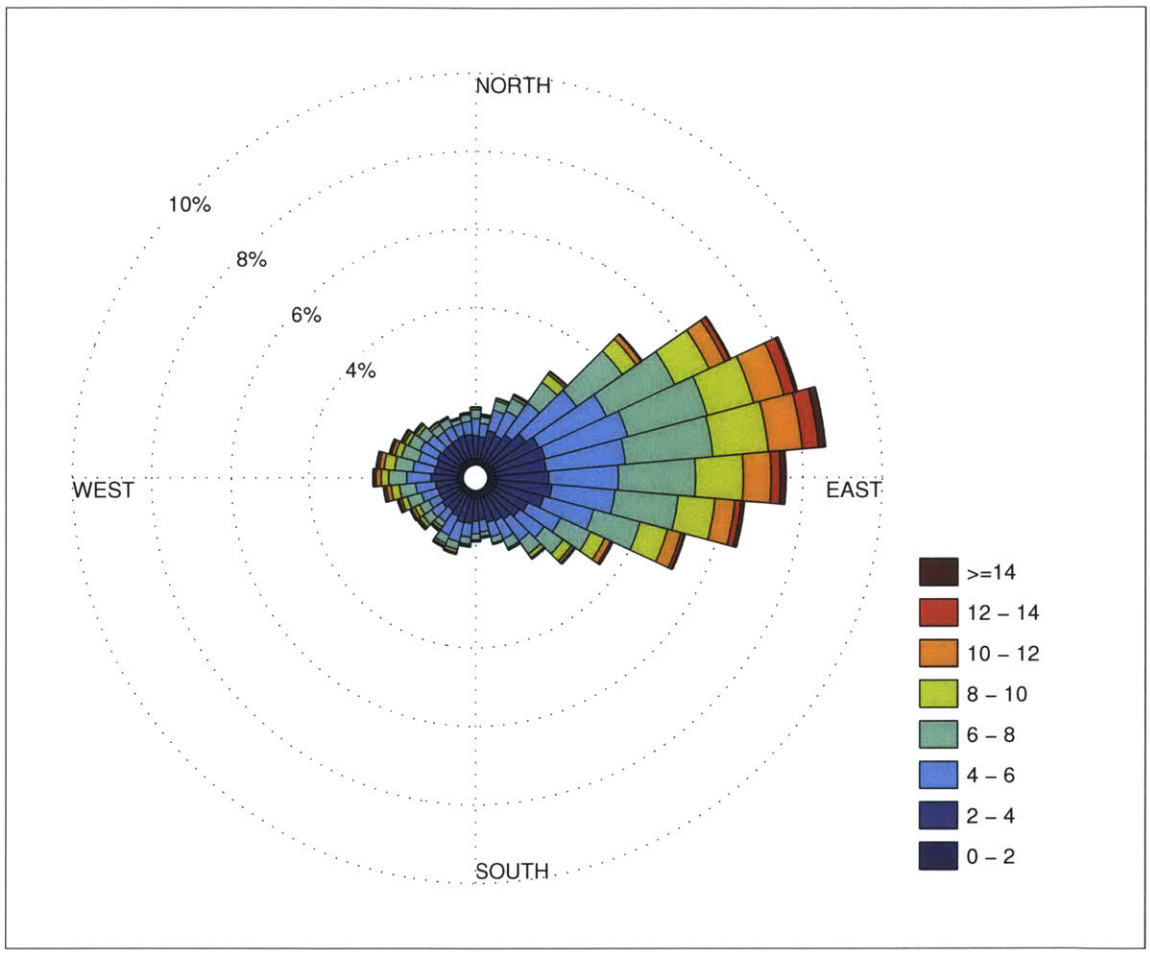

Figure 5-2: Wind rose plot from Pt. Barrow weather station for the decade (2002-2011). Colors represent wind speed, spokes (directional quadrants) are where the winds come from, and percentage contours represent the amount of data that falls into a given direction.

5.2 Seasonal Circulation

Seasonally, the two centers of action vary in both strength and location. During autumn and winter the AL deepens due to the combined effect of more frequent and stronger storms (Figure 5-3). Pickart et al. (2009a) demonstrated that some of these storms are broad enough in extent and track far enough to the north to trigger upwelling events on the north slope of Alaska. These Pacific-born storms occur much less frequently from spring through summer, and, as such, the AL is almost indistinguishable during this time period (Figure 5-4). It should be noted, however, that Aleutian low pressure systems can occur year round and can lead to upwelling on the Beaufort slope regardless of season (Pickart et al., 2013a).

The BH also has marked seasonal variability. In the fall and winter, when the AL is intensified, the BH is part of a ridge of high pressure extending from the East Siberian Sea to the Beaufort Sea (Figure 5-3). Serreze and Barrett (2011) demonstrate that the Siberian high and the Yukon High influence the structure of the BH this time of year. The seasonal composite of Figure 5-3 for the decade 2002-2011 is also consistent with the results of Walsh (1978) who shows that, during winter, there appears to be a large scale high pressure ridge extending from east Asia to northwestern Canada. During the spring and summer, the BH is more of a distinct feature that is confined to the Beaufort Sea region (Figure 5-4).

In light of the seasonality of the two centers of action, it is not surprising that the winds measured at the Pt. Barrow weather station vary significantly throughout the year. Following Pickart et al. (2013a) we computed the climatological monthly mean alongcoast wind for the 70-year Pt. Barrow data set (Figure 5-5). In each month the mean winds are out of the east, and one sees that there are two seasonal peaks. The first occurs during the October/November timeframe, and is a result of the enhanced

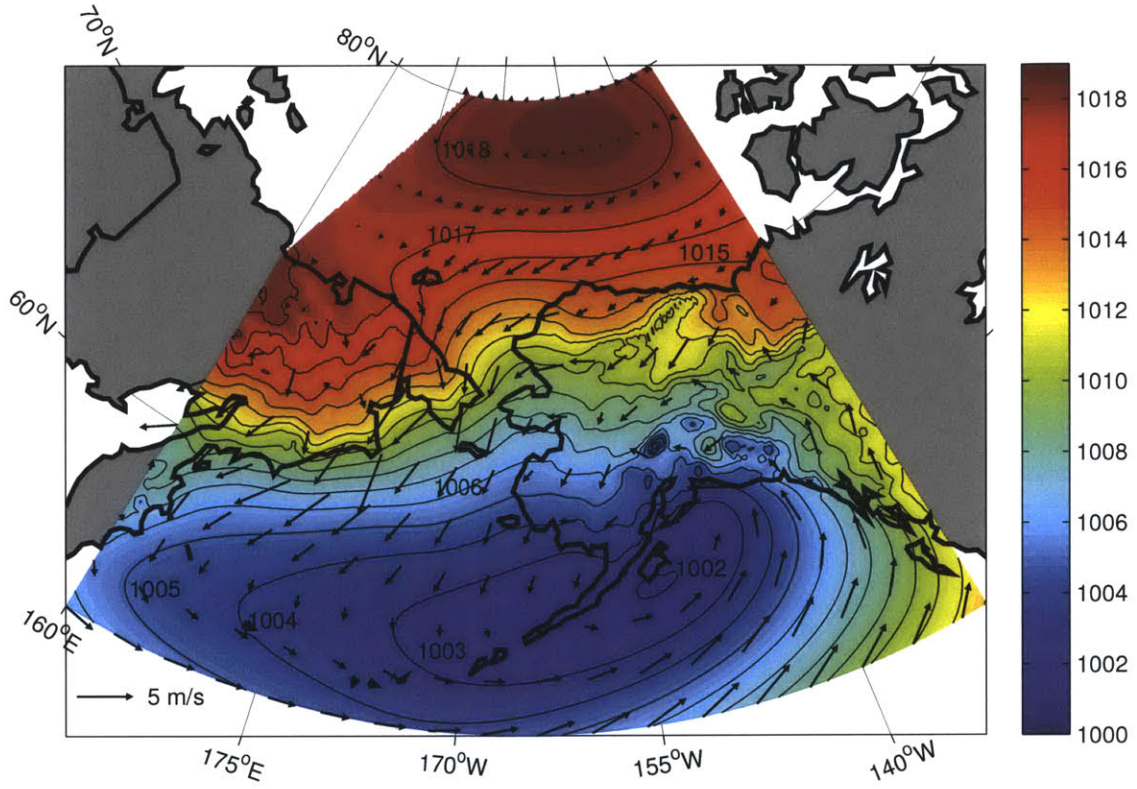

Figure 5-3: Mean September–February sea-level pressure (contours and shading, mb) using the NARR data set for the period 2002-2011. Overlaid are 10m wind vectors (m/s).

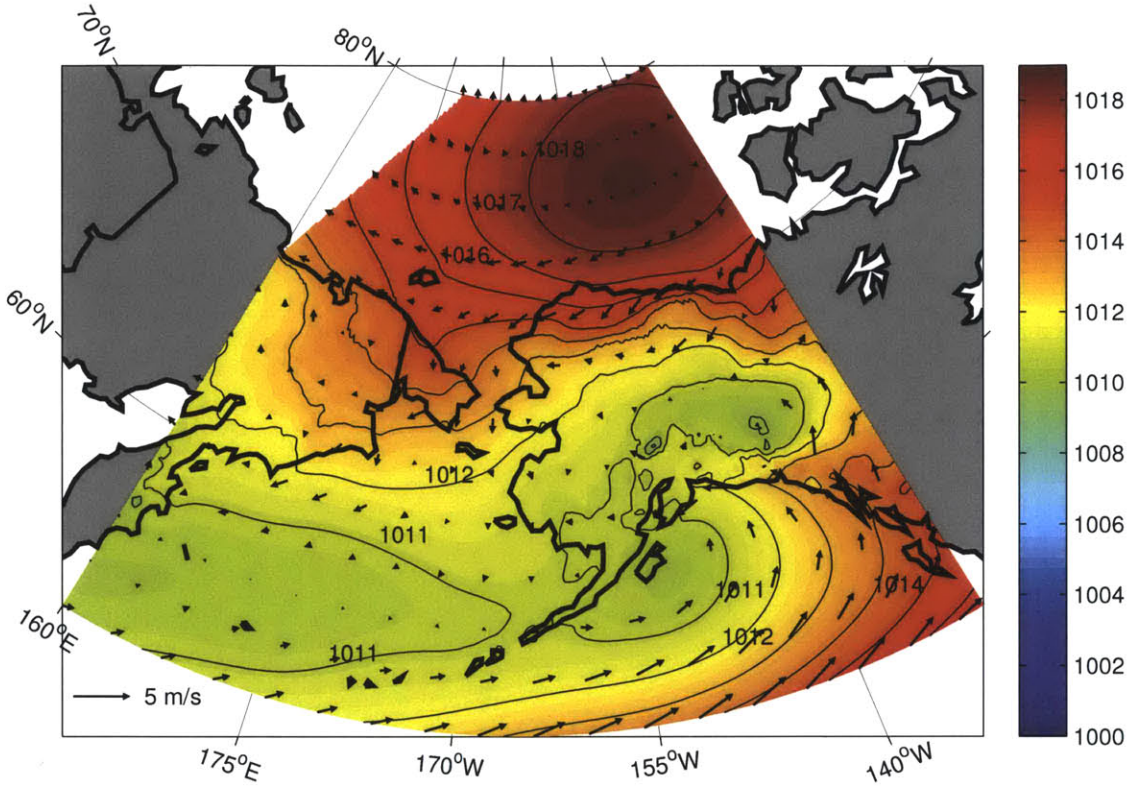

Figure 5-4: Mean March–August sea-level pressure (contours and shading, mb), using the NARR data set for the period 2002-2011. Overlaid are 10m wind vectors (m/s).

SLP gradient between the BH and the deep Aleutian Low. The second peak occurs in May when there is no strong signature of the AL. Pickart et al. (2013a) demonstrate that, even though fewer AL storms exist during that time of year, when they do occur they have a more northward storm track and thus amplify winds on the north slope of Alaska. As seen in Figure 5-5, the weakest easterly winds occur during the summer, specifically in July and August when the Beaufort High is well developed and situated over the southern Beaufort Sea and western Canadian Archipelago (Moore, 2012)

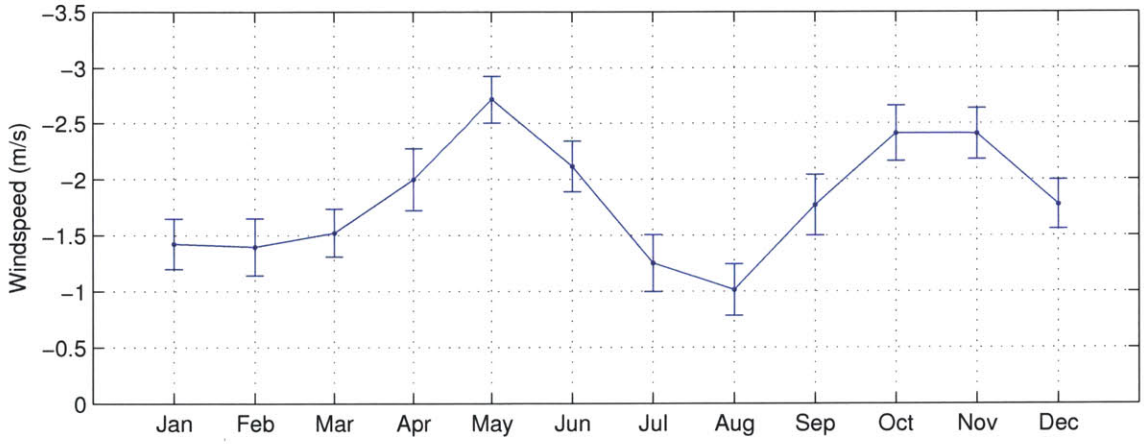

Figure 5-5: Climatological monthly alongcoast (105°T) mean wind speed for the 70-year Pt. Barrow wind record, including the standard error.

5.3 Interannual Variability of the Circulation

Both the AL and BH exhibit a great deal of year-to-year variability. The frequency and intensity of AL storms fluctuate significantly each year and, although McCabe et al. (2001) concludes that storm activity in general is increasing at high latitudes, there is some disagreement regarding trends. For example, due to the large inter-annual variability, Mesquita et al. (2010) argues that trends in storm frequency and intensity are not significant for regions surrounding Alaska. The signature of the sum-

mer BH is also quite variable from year to year. Using the global NCEP reanalysis fields, Moore (2012) analyzed the signature of the summer (June, July, August) BH from 1948 to the present and found that, while there is a great deal of interannual variability, for most of the record there were no noticeable trends. However, since the mid-1990s a statistically significant positive trend has occurred in the strength of the summer BH. The NARR data used here show a similar trend during the decade of our study (2002-2011), and also indicate that, outside of the summer months, the BH has not varied nearly as much.

In light of the results of the previous chapter, where it was demonstrated that most of the interannual change in transport of the Beaufort shelfbreak jet has occurred during the summer months, we focus on the year-to-year atmospheric variability for the months of June, July, August (JJA). Figure 5-6 shows the composite SLP fields for these months over the 10-yr study period. While the SLP for this region displays significant year-to-year variability, there are some clear trends as well. Here we point out some key features in Figure 5-6, which are then revisited later in the thesis when quantifying the effects of the atmospheric forcing on the boundary current.

In the first two years of the decade (2002 and 2003), instead of the typical high pressure over the Beaufort Sea, there was low-pressure in the northern Chukchi Sea which resulted in cyclonic circulation for this region (not shown). For the rest of the decade, however, there was a clear signature of the summer BH, although it varied in strength and location. In summer 2004 and 2005 the BH was strong, although in 2004 it was centered along the northern coast of Alaska which is farther south than usual. The next year, 2006, the BH was quite weak, but the following summer it intensified to the highest pressure of the decade. Wang et al. (2009) shows that during this year the BH played an important role setting up the Dipole Anomaly between the western and eastern Arctic. The winds associated with this SLP difference were believed to

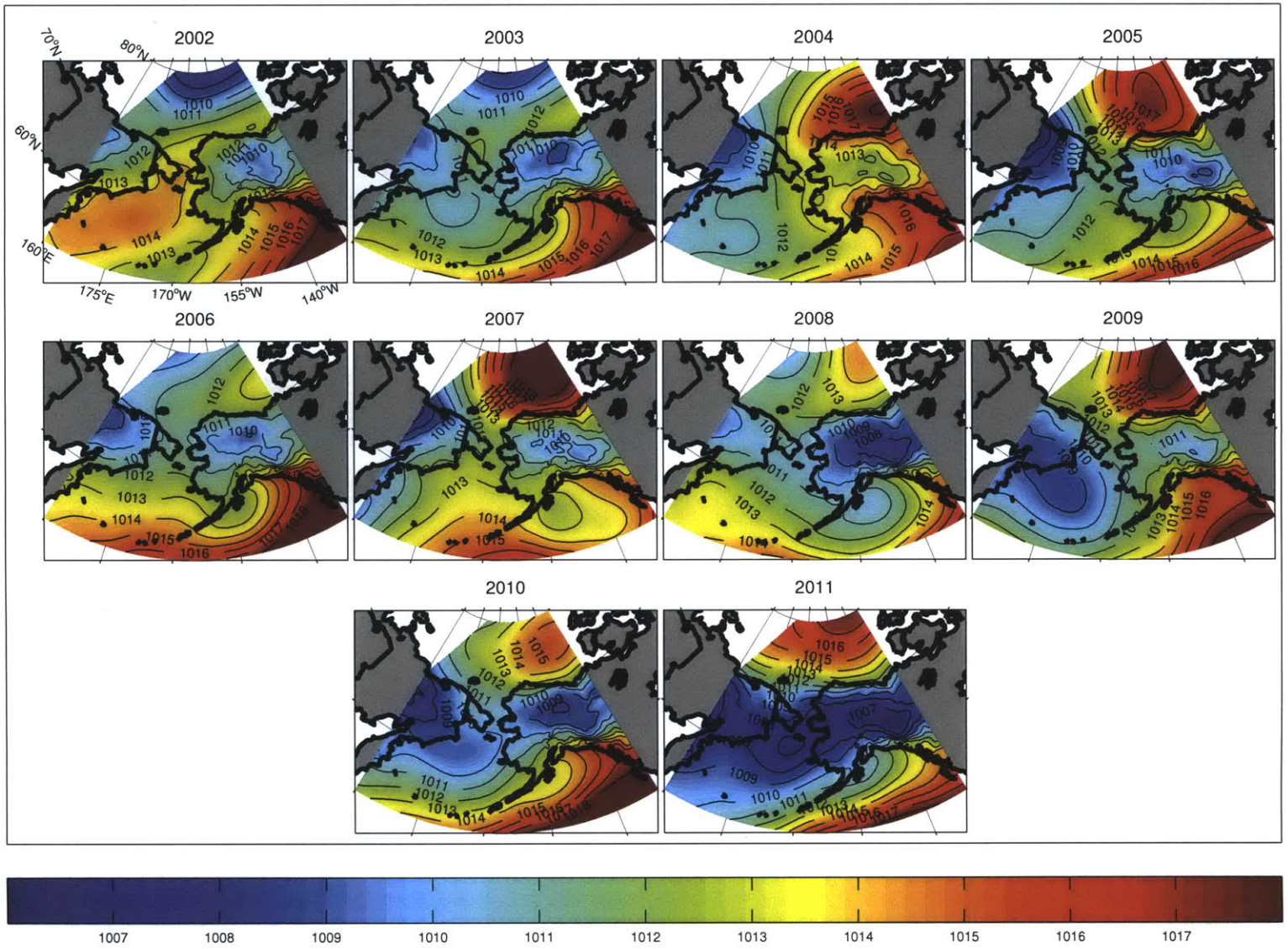

Figure 5-6: Summer (JJA) composite sea-level pressure (mb) from the NARR data set for the period 2002-2011. (Contours and shading, mb).

contribute to the record minimum September sea ice extent in summer 2007 (Wang et al., 2009). Over the following four summers the BH fluctuated in intensity in alternate years, and in the final year (2011) it was positioned farther north than usual. Despite this year-to-year variability, the general trend over the decade was a strengthening of the summer high pressure in this part of the western Arctic.

In general the AL is weak during the summer months, and this decade was no exception (Figure 5-6). However, as will be shown later, this low pressure does impact the local winds along the Beaufort slope during the summer. From Figure 5-6 it is seen that the AL becomes more pronounced over the 10-year period. While traces of the AL are apparent in the first part of the decade (2003,2005,2006), the low pressure becomes much more prevalent during the last four years (2008-2011). In the final summer (2011) the AL is the strongest for the entire decade, and during that year the BH and AL together create a particularly strong SLP gradient over the Chukchi and Beaufort Seas.

Pickart et al. (2013a) have shown previously that the annual easterly wind speeds in the Alaskan Beaufort Sea have increased over the past two decades. Using the Pt. Barrow weather station data we find that the increase for the most recent decade (2002-2011) is largely due to changes in summer winds (Figure 5-7). In particular, the JJA alongcoast winds have strengthened by 5 m/s over this time period. In the next chapter we investigate the consequences of these interannual changes in atmospheric forcing on the Beaufort shelfbreak jet.

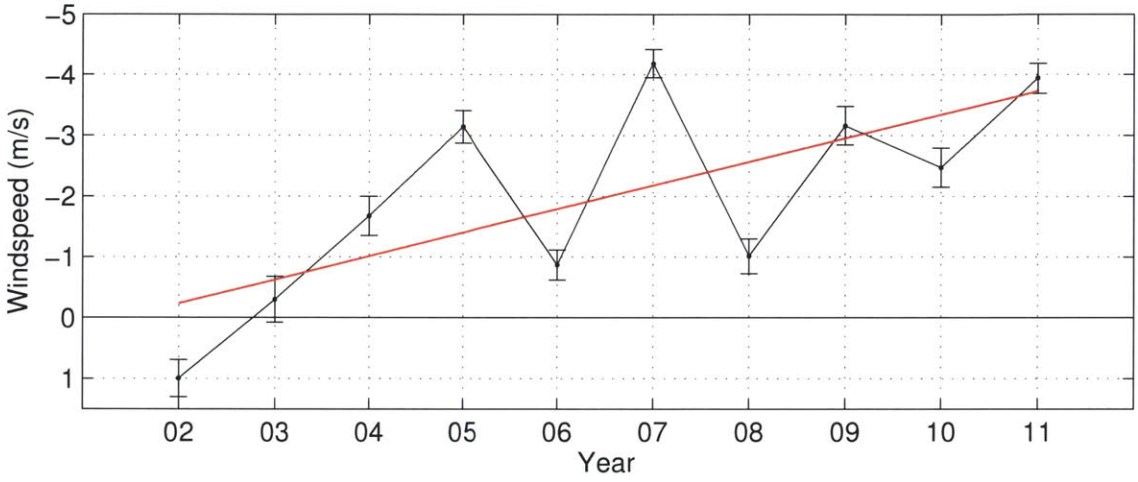

Figure 5-7: Summer (JJA) mean alongcoast wind speed for the decade 2002-2011, including the standard error. The red line indicates the trend in wind speed over the decade.

Chapter 6

Physical Drivers of the Pacific Arctic Boundary Current

Thus far we have shown that the summertime transport in the western Arctic boundary current has drastically diminished over the decade 2002-2011. Furthermore, we have revealed that the summertime atmospheric conditions have changed considerably over the same time period. In this chapter we explore the impact of the atmospheric forcing on the boundary current, and consider the influence of some of the other physical drivers as well.

6.1 Atmospheric Forcing

It has been shown previously that local wind forcing influences the strength of the boundary current near 152°W. In particular, easterly winds can diminish the alongstream flow and readily reverse it, which leads to upwelling and significant shelf-basin exchange (e.g. Nikolopoulos et al. (2009); Pickart et al. (2009a, 2013b). Although not as common, westerly winds can accelerate the current to the east and drive downwelling

(R. Pickart, pers. comm., 2013). The five additional years of transport data and wind data allow us to more thoroughly explore the relationship between the atmospheric forcing and boundary current strength. Overall, every month has similar correlation between current transport and along-coast wind speed, however, the correlation is enhanced during the summer months.

6.1.1 Relationship Between Summer Transport and Wind Speed

When considering the five summers for which complete transport data are available (2003, 2004, 2009, 2010, 2011), the strong relationship between local wind speed and current transport becomes quite evident (Figure 6-1). Summer 2003 is characterized by very weak easterly winds along the Beaufort slope, which are not significantly different than zero. Not surprisingly, the transport during that summer is the highest of all five years. Easterly wind speeds increase in 2004 and the current transport diminishes slightly. In the latter part of the decade the easterly winds increased significantly, in concert with the diminished boundary current transport. As pointed out earlier, the shelfbreak jet "rebounds" in summer 2010 ($\sim$0.15 Sv), which is associated with a corresponding slackening of the easterly winds.

6.1.2 Sea Level Pressure Gradient

The strong correspondence between summertime averaged local wind speed and boundary current transport in Figure 6-1 motivates us to clarify more carefully the nature of the wind. As noted in the previous chapter, it is the gradient in sea level pressure (SLP) between the two centers of action, the Beaufort high (BH) and Aleutian low (AL), that primarily drives the winds along the Beaufort slope. One might wonder

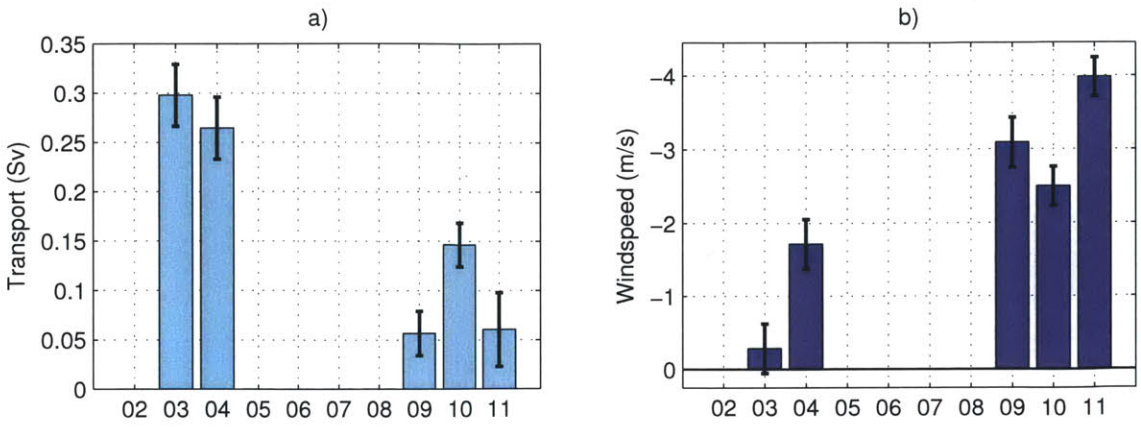

Figure 6-1: a) Mean Volume transport (Sv) of boundary current including the standard error for June, July and August (JJA). b) Mean alongcoast wind speed (105°T) including the standard error for June, July and August.

then to what degree is each center of action contributing to the interannual variability in SLP. Is it mainly the strength of the BH or does the AL play a role? It would be reasonable to assume the former because the summertime signature of the AL is so much weaker in comparison to the fall and winter. To answer this question we calculated the degree to which the BH and AL individually influence the SLP gradient each year as follows.

For each summer the central locations of the BH and AL were identified based on maximum and minimum regions of SLP respectively (pressure values over land were not considered). Summer 2002 is an exceptional case in that there is no signature of the AL in the Bering Sea or Gulf of Alaska. Consequently, for that year the AL was chosen to be in the same location as the decadal mean AL position for June, July and August (JJA). To isolate the effect of the BH, we assumed that the AL has a constant central SLP of 1010.8 mb and is positioned 2300 km away from the center of the BH (based on the decadal mean SLP for JJA) and then used the measured variation in central SLP of the BH. To isolate the role of the AL we assumed that

the BH has a constant central SLP of 1015.2 mb and is similarly positioned 2300 km away from the center of the AL (again based on the decade mean SLP for JJA). Finally, we estimated the actual SLP gradient by taking into account the variation in both centers of action as well as the distance between them.

The results of this calculation are shown in Figure 6-2, along with the measured summertime alongcoast wind speed at Pt. Barrow. Over the decade, both the BH-only SLP gradient and the AL-only SLP gradient increased as a result of the strengthening and deepening of the two centers of action, respectively (Figure 6-2 a,b). Both of these individual components display significant interannual variability as well. Interestingly, however, one sees that the trend in the AL-only value is more in line with the actual SLP gradient trend (compare Figure 6-2a to 6-2c) while the year-to-year variations in the true SLP gradient seem to be explained mainly by changes in the BH-only value. For example, the AL-only component shows little change from 2006 to 2007, yet the actual values for these two years are considerably different.

To quantify this further we compared the magnitude of the trends in Figure 6-2 as well as the de-trended values for the different cases. We find that the decadal increase of the SLP gradient is two-thirds driven by the deepening of the AL and one-third driven by the intensifying of the BH. It should be noted, however, that the local winds throughout the decade do not correspond precisely to the large-scale SLP gradients (compare Figure 6-2c and 6-2d). In actuality, the BH is responsible for approximately 50% of the decadal increase of wind speed measured at Pt. Barrow. In contrast, the de-trended values of SLP gradient reveal that the BH is the principal driver of the year-to-year variability in the actual SLP gradient and local wind speed (Figure 6-3).

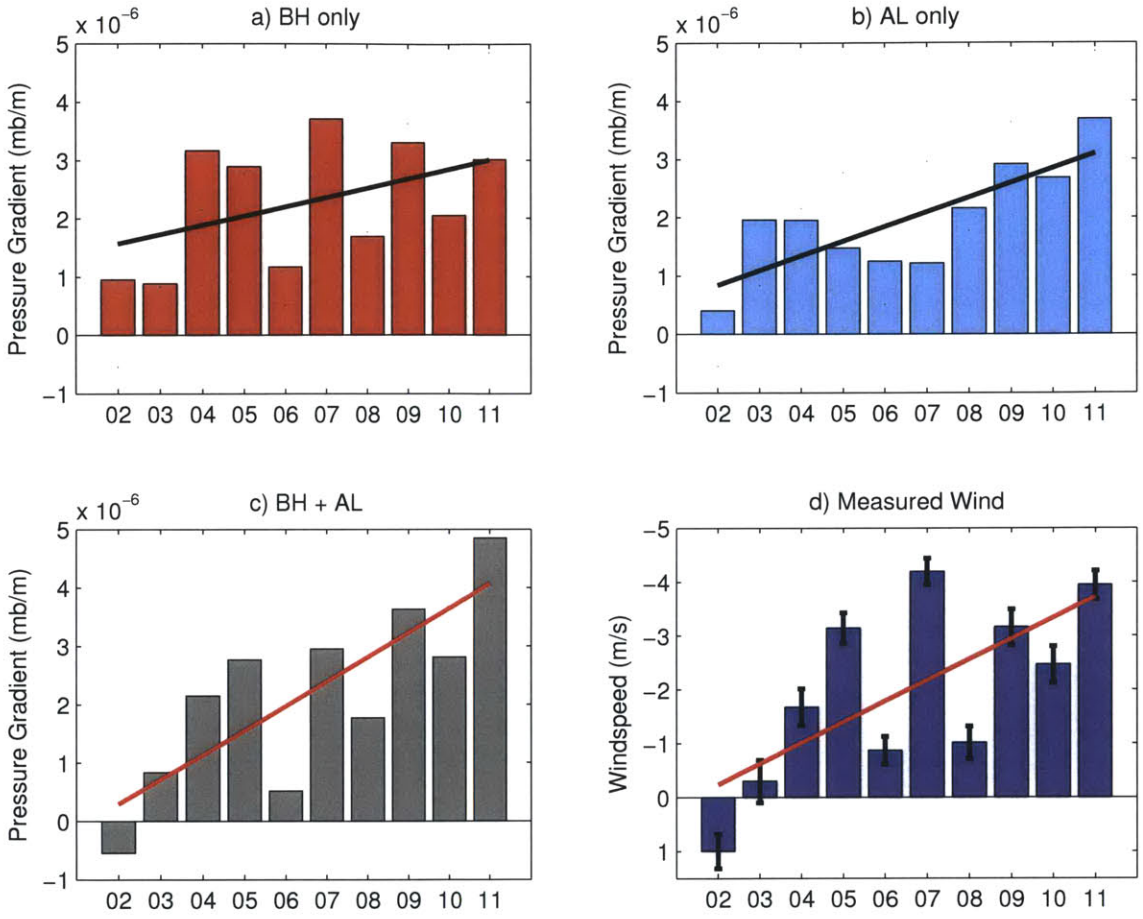

Figure 6-2: Pressure gradient determined from mean SLP for June, July August by a) varying strength of the Beaufort High, b) varying strength of the Aleutian Low and c) varying strength of both the BH and the AL as well as the distance separating them. d) alongcoast (105°T) winds from Pt. Barrow for the decade. Trend lines are included.

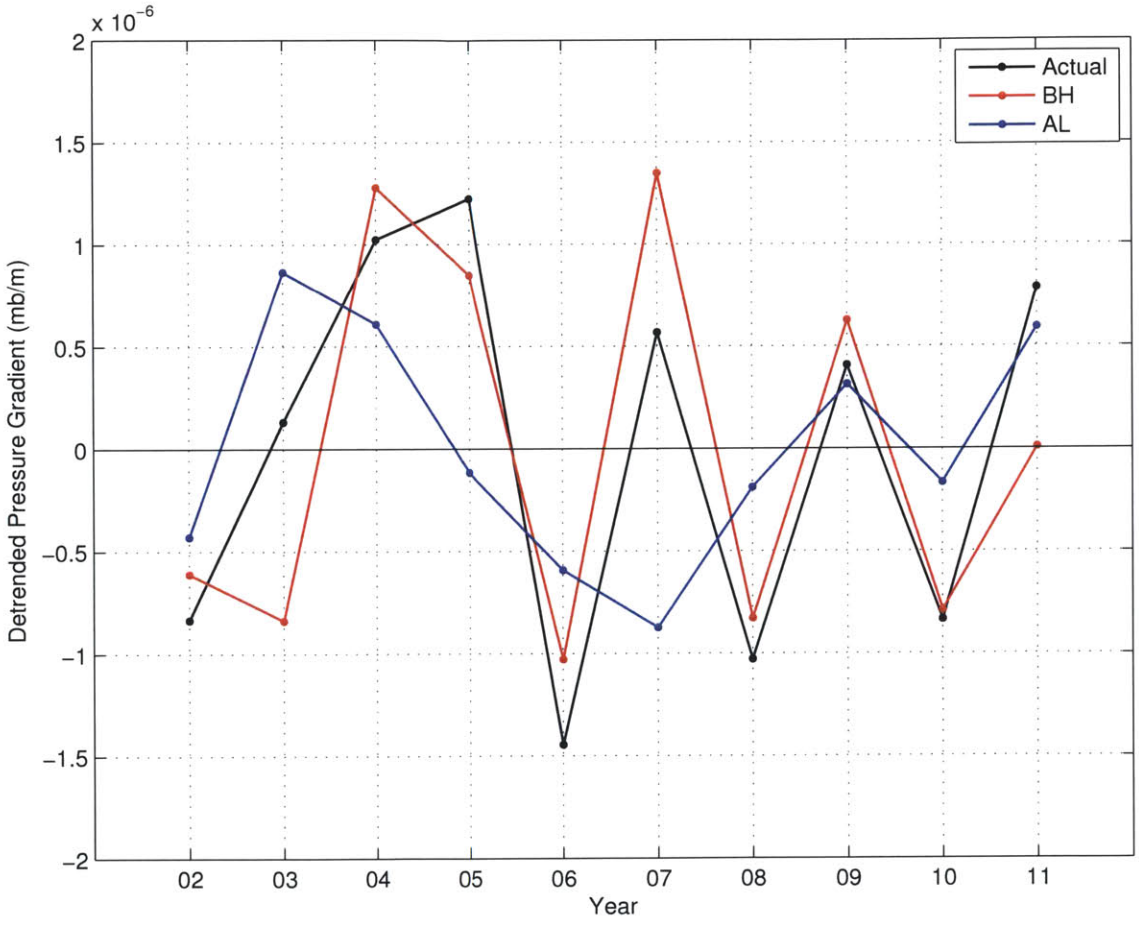

Figure 6-3: Detrended SLP gradient over the Beaufort slope for the decade 2002-2011. The black line is the actual pressure gradient, the red line is the pressure gradient with a varying BH, and the blue line is the pressure gradient with a varying AL.

6.1.3 Large-Scale Atmospheric Context

The above results indicate that both the BH and AL play an important role in forming the SLP gradient over the Beaufort slope. We now highlight two examples that nicely demonstrate this: the summers of 2004 and 2010. To do so we consider the SLP anomaly fields, where the SLP for each summer (for the five years with transport measurements) is subtracted from the decade-long average. These maps are shown in Figure 6-4. In summer 2004 recall that the eastward transport of the boundary current was strong (Figure 6-1), yet the BH was strong (Figure 5-6) which should imply stronger easterly winds that would retard the boundary current. The anomaly map for that year indicates, however, that the spatial extent of high pressure was anomalously broad and extended into the Bering Sea and Gulf of Alaska. For this reason the AL signature was weak and contributed little to the SLP gradient. Recall as well that 2010 was the rebound year when the boundary current transport increased despite a well-developed BH and AL (Figure 5-6) which should decrease the boundary current transport. Again the anomaly maps reveal the cause. One sees that, compared to the bracketing years of 2009 and 2011, the BH and AL had moderate values. Hence while the two centers of action did combine to reduce the boundary current transport compared to earlier in the decade, the degree to which this happened was less pronounced in 2010.

6.1.4 Reconstructing the Shelfbreak Current Observations

Given the strong impact of the local winds on the transport of the shelfbreak jet, we now investigate the degree to which the year-to-year change in transport can be predicted based solely on the winds. To do this we regressed the daily mean alongcoast wind speed versus the daily mean transport of the boundary current for

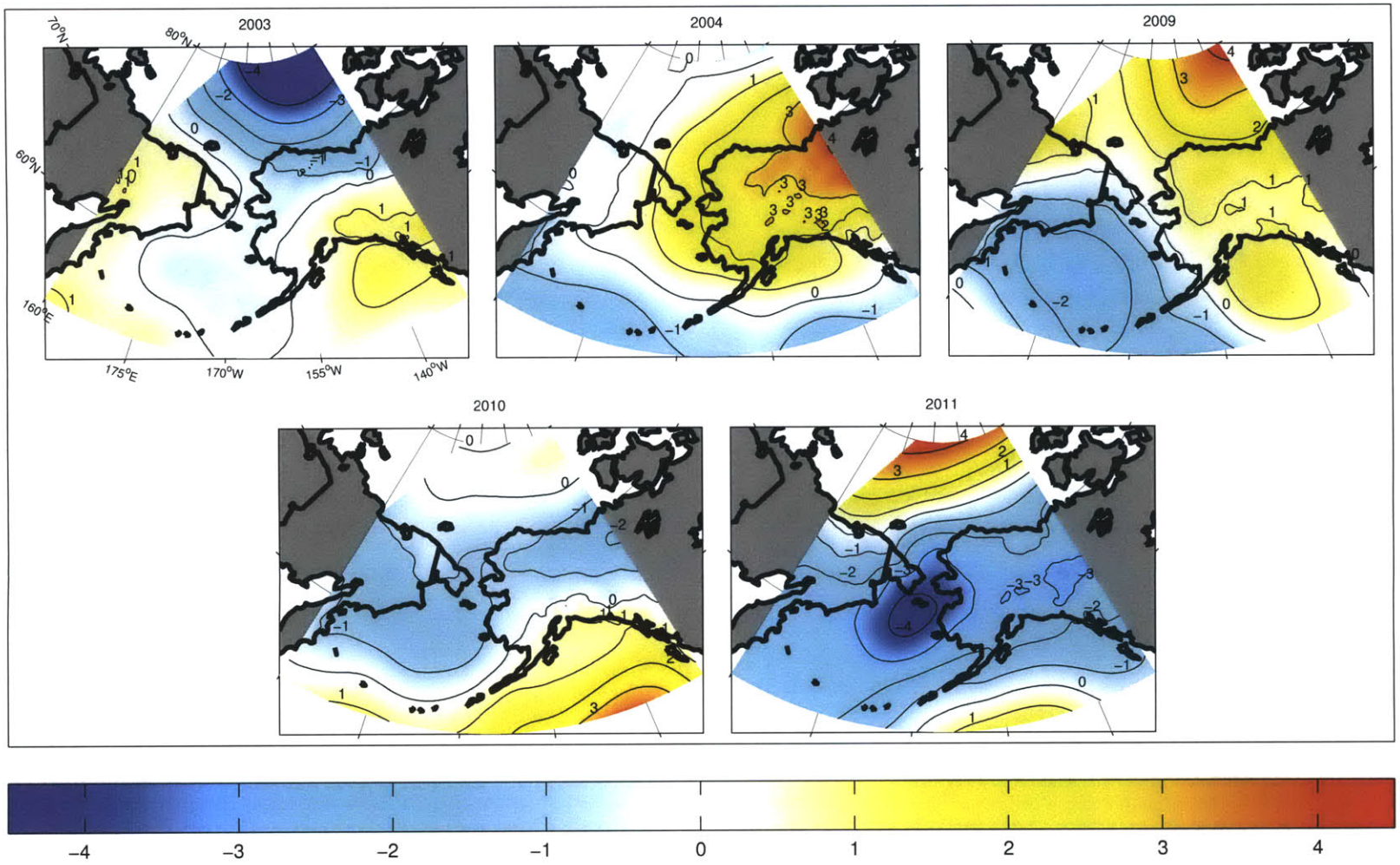

Figure 6-4: Composite anomaly of the sea-level pressure (mb) for June, July and August, versus the decade (2002-2011) mean for these same months.

the combined time period of all five summers (Figure 6-5). The slope of the regression line represents how the current varies with winds, and the y-intercept indicates the transport of the undisturbed current over the five-year period. One sees that, with no wind, the Pacific Arctic boundary current transports 0.27 ± 0.08 Sv to the east, which is about one-third of the long-term transport through Bering Strait (Woodgate et al., 2005). Overall, the predicted summer transport compares well to the measured value for the five years of mooring data (Figure 6-6). One sees that the trend of decreasing transport through the decade is nicely captured, and the qualitative year-to-year variability is reflected in the predicted value as well.

There are, however, significant discrepancies between the transport predicted by the local winds alone versus the measured transport. For example, the reconstructed transport systematically underestimates the high transport in the early part of the decade (2003 and 2004), and overestimates the low transport in the later part of the decade (2009, 2010 and 2011). The primary reason for this is the interannual variability in the strength of the undisturbed current during summer. This was demonstrated by performing individual regressions for each of the five summers and tabulating the y-intercept each year. This reveals that the undisturbed flow was greater in the early part of the decade, and decreased to smaller values in the later years (Figure 6-7).

6.2 Upstream Influences

The fact that the undisturbed flow of the Beaufort shelfbreak jet can change from year-to-year should not come as a surprise. Woodgate et al. (2012) recently showed that the pressure head contribution to the Bering Strait inflow varies on interannual time scales. They demonstrated that in recent years the pressure head term has increased, and is in fact the primary reason for the enhancement in Bering Strait

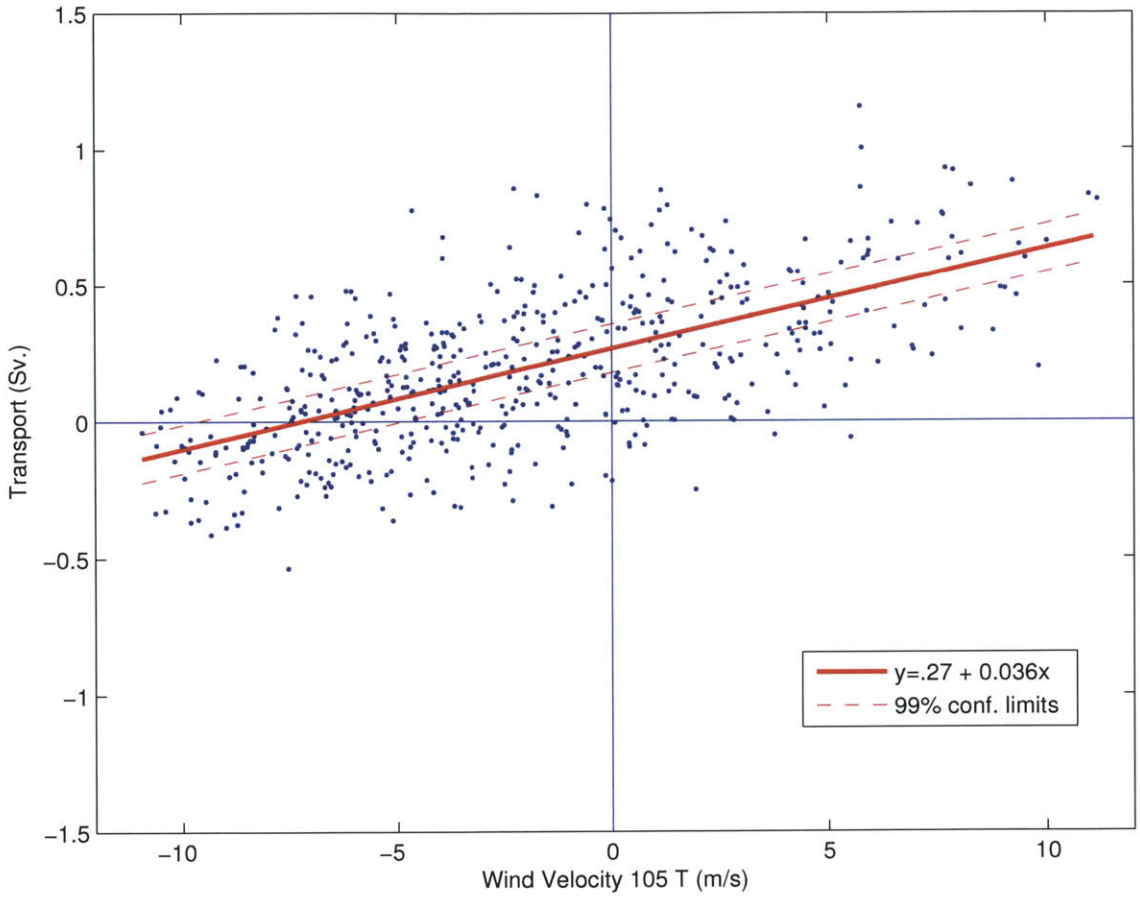

Figure 6-5: Scatter plot of transport (Sv) and the alongcoast (105°T) Pt. Barrow wind speed (m/s). The solid line is the least-square regression line (see legend), and the dashed lines indicate the 99% confidence intervals.

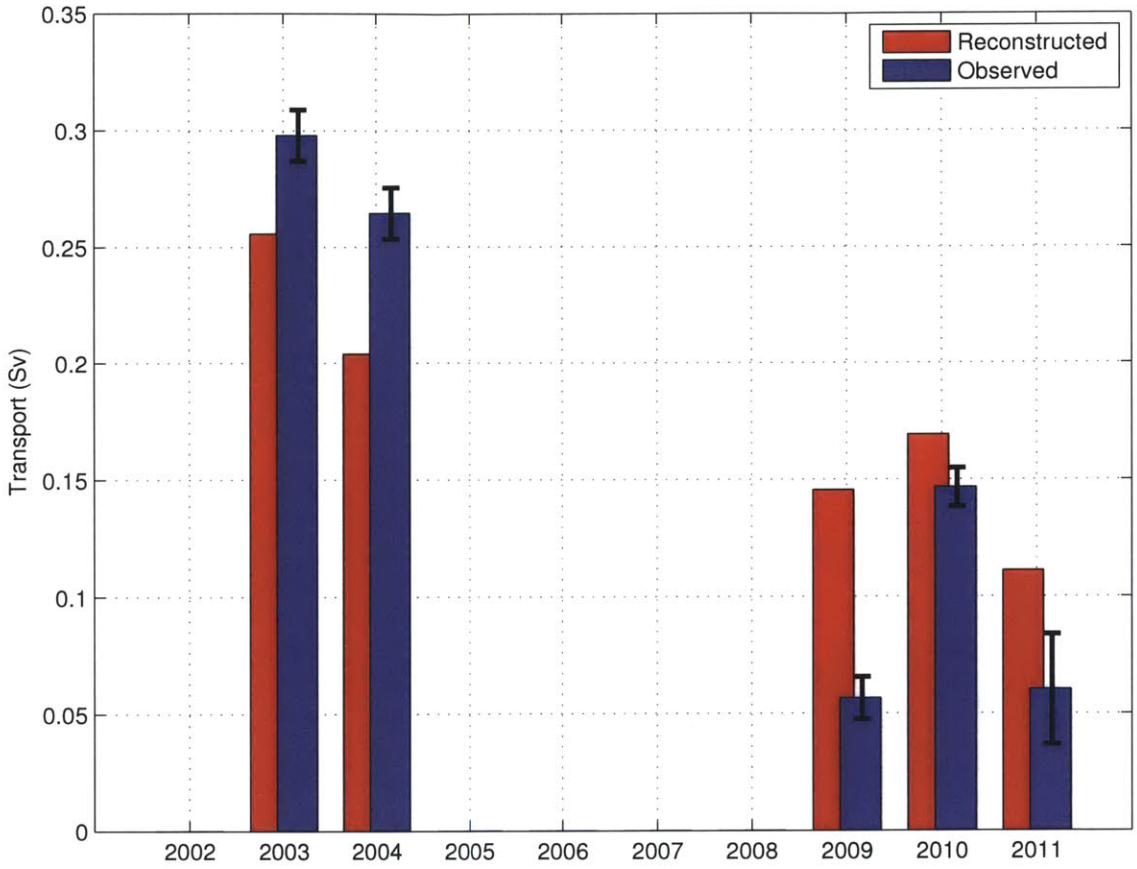

Figure 6-6: Mean volume transport (Sv) of boundary current including the standard error for June, July and August (Blue) and the reconstructed mean volume transport (Sv) for June, July and August based on the relationship of current transport and wind speed (Red).

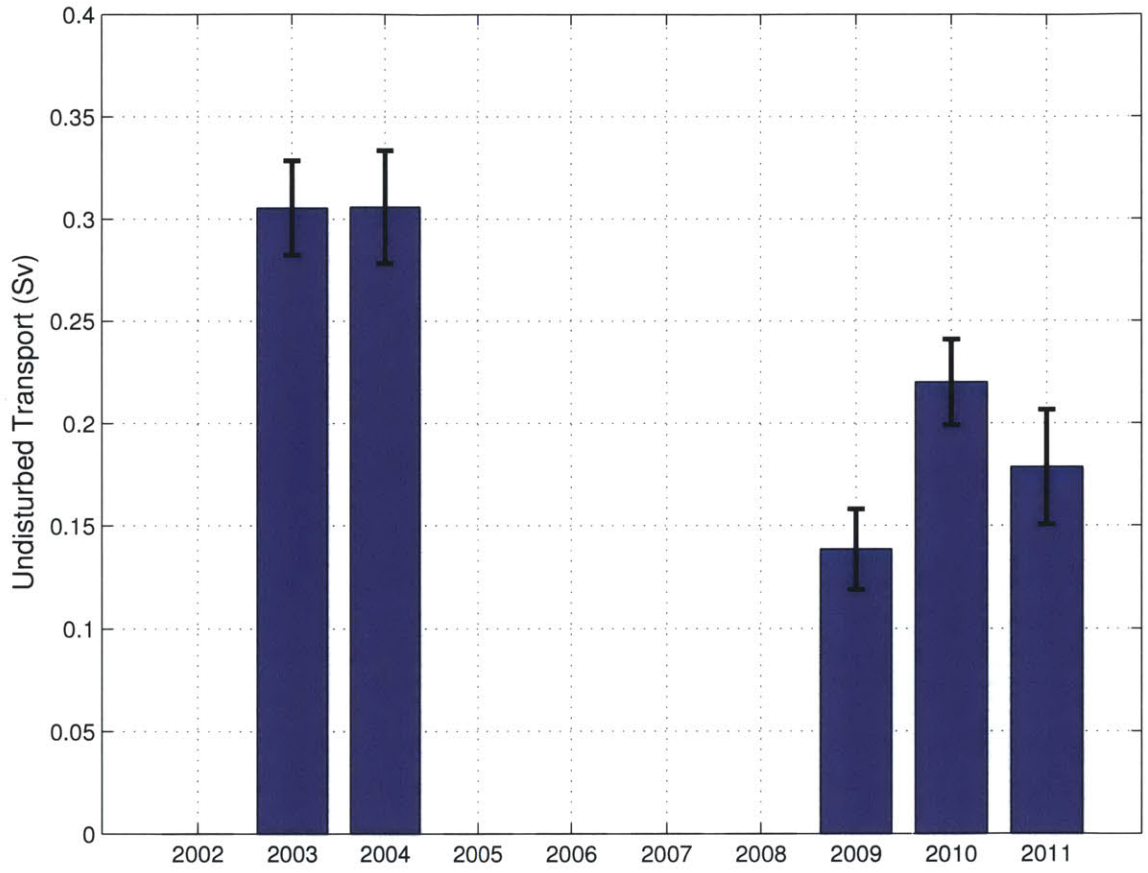

Figure 6-7: Undisturbed transport (Sv) of the boundary current during June, July and August for each year.

transport. It is natural then to wonder if the transport of the undisturbed boundary current on the Beaufort slope has varied in concert to that in Bering Strait over the study period.

To investigate this it is necessary to consider only the flow of summer water through Bering Strait (Woodgate et al.'s (2012) analysis considered the full year). Consequently, we used the eastern-most mooring in the strait, mooring A4, which captures the signal of the near-shore ACC (Woodgate and Aagaard, 2005). Performing the analogous summertime regressions (using the NARR winds), we estimated the undisturbed transport of Pacific summer water through Bering Strait for each of the five years, which is compared to that for the Beaufort shelfbreak jet in Figure 6-8. One sees that during the early part of the decade the agreement is very good, and in 2010 the values are again fairly close (especially in light of the error bars). Recall that 2010 was the rebound year. However, in 2009 and 2011 the undisturbed flow on the Beaufort slope is significantly smaller than that through Bering Strait. We believe the reason that the undisturbed values may not always track each other is because of the large geographical separation between the two sites, and, as such, the undisturbed flow on the Beaufort slope may not always reflect undisturbed flow along the upstream pathway from Bering Strait to Barrow Canyon.

To elucidate this we compared the alongcoast winds on the north slope of Alaska to those in the Chukchi Sea (along the west coast of Alaska) using the NARR data. The Beaufort domain extends from Pt. Barrow eastward to 148°W, while the Chukchi domain extends northward from Bering Strait to Pt. Barrow. We found that in 2003, 2004, and 2010 (i.e. the years when the undisturbed transports were in close agreement) the winds were significantly correlated between the two domains, while in 2009 and 2011 (when the undisturbed transports differed) there was no correlation. Conceptually this makes sense in that when the winds are correlated all along the

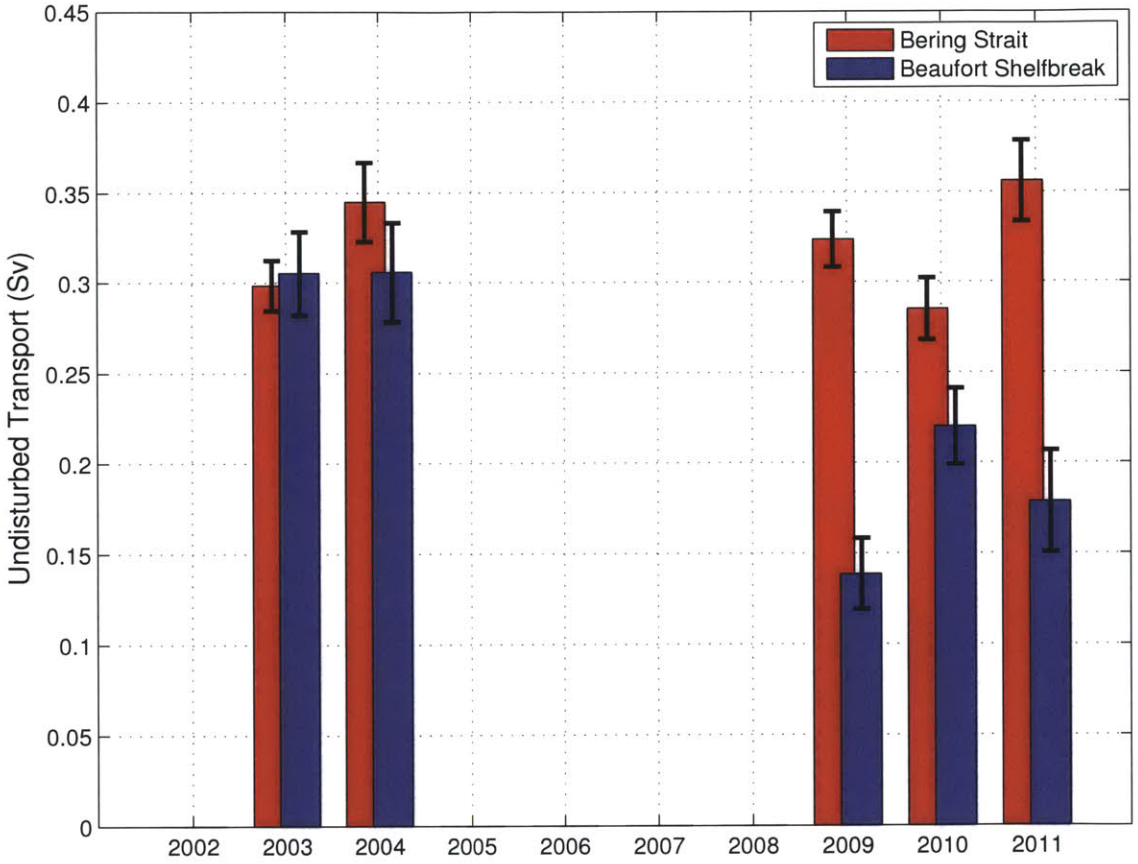

Figure 6-8: Undisturbed transport (Sv) of the Alaskan Coastal Current at Bering Strait (red) and along the Beaufort shelfbreak (blue) for each summer.

pathway from Bering Strait to the Beaufort slope, the transports would be similar at the two locations when the wind slackens. In contrast, for summers when the wind in the Chukchi Sea varies independently from that on the Beaufort slope, the flow entering the Beaufort domain during times of weak local winds was likely subject to wind forcing during some part of its transit through the Chukchi Sea. We note that in 2009 and 2011 – when the undisturbed Beaufort slope transport was weaker than that in Bering Strait – the winds in the Chukchi domain were enhanced out of the north and opposed the northward flow of Pacific water.

6.3 Sea Ice

In light of the pronounced changes in sea ice cover in this part of the Arctic Ocean, it is of interest to determine if this has had any effect on the transport of the Pacific water boundary current. In a study of upwelling on the Beaufort slope, Schulze and Pickart (2012) demonstrated that the water column response to easterly winds was most pronounced when there is partial ice cover. This is due to an increase in stress imparted to the ocean via the freely moving ice keels. Under these conditions the shelfbreak jet was readily reversed and attained its highest speeds to the west. In contrast, the water column has the weakest response when there is complete ice cover. Finally, there is a more moderate response when the area is ice free (Schulze and Pickart, 2012). We now consider the sea ice cover in the vicinity of the shelfbreak mooring. In particular, we compute timeseries of the average sea ice concentration in a 70 km (zonal) by 70 km (meridional) box surrounding the mooring. We define three different sea ice cover regimes following Schulze and Pickart (2012): $\geq$70% concentration is considered full ice, partial ice is taken to be between 10% and 70% concentration, and open water is $\leq$10% concentration.

The timeseries of ice concentration for each year are shown in Figure 6-9, where the boundaries of the three ice regimes defined above are marked. One sees that the sea ice cover in the vicinity of the mooring site is, for the most part, similar for four out of the five years (2003, 2004, 2009, and 2011). In these years, full ice conditions exist during June, then the concentration rapidly lessens during July and reaches the open water state near the beginning of August (Figure 6-9). The seasonal evolution of the ice field is noticeably different in 2010. During that year, full ice conditions persist until late July, and open water does not occur until mid-August.

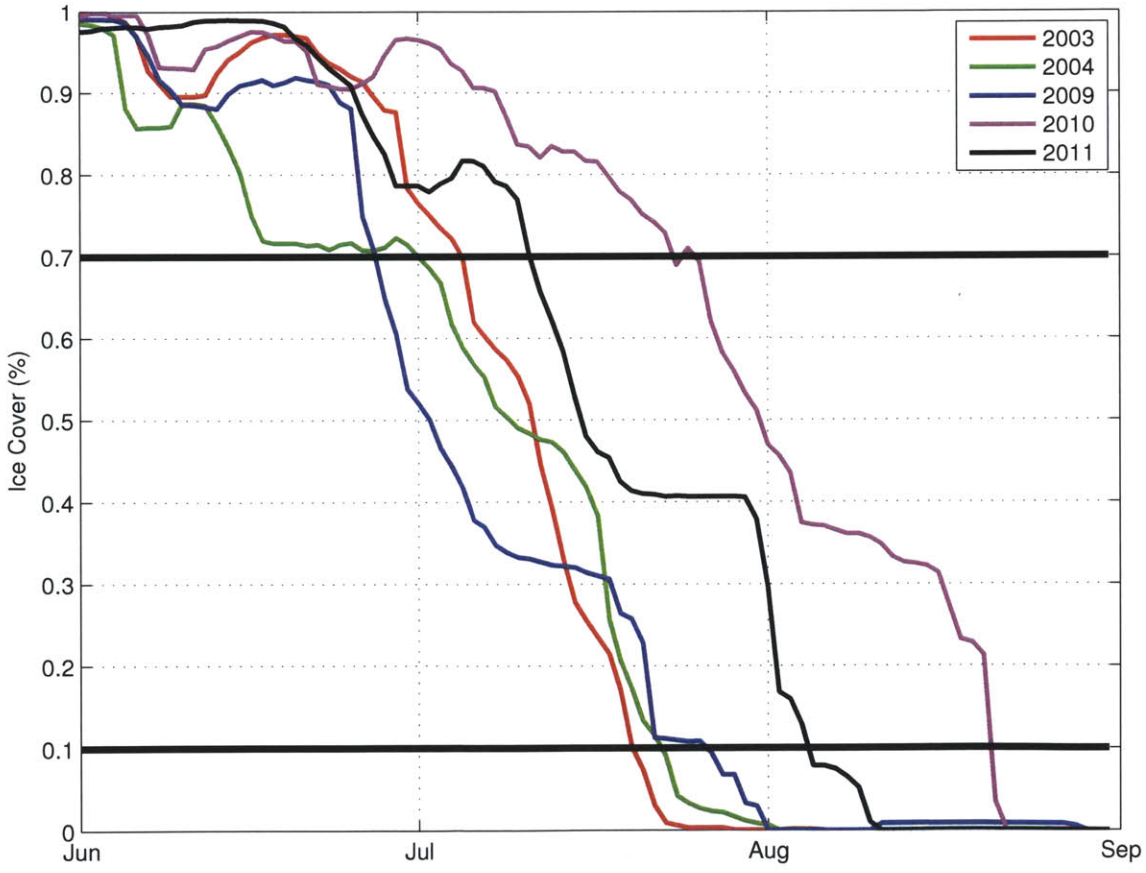

Figure 6-9: Percentage of ice cover in the vicinity of the shelfbreak mooring site for the months June, July and August. Colors denote each of the five years considered. The thick black lines indicate the full ice, partial ice and open water regimes.

It is possible that the prevalence of partial sea ice in July 2009 amplified the effects of the easterly winds. That month was characterized by a mean easterly wind speed of about -5 m/s and was subject to partial ice for 25 days. Instead of seeing the usual rise in transport from June to July associated with the arrival of ACW (Figure 4-5), the alongstream transport for July 2009 was only 0.015 Sv. Overall, however, it is not conclusive whether the ice concentration impacted the transport of the boundary current during the time period of the study. For example, in August 2010 much of the month was characterized by partial ice cover, as opposed to August 2004 during which there was complete open water. Furthermore, there were stronger easterly winds in August 2010. This would suggest that the boundary current would be considerably weaker that month compared to August 2004, but this was not the case; the monthly mean transports were comparable in the two years.

It is clear from the results presented above that wind forcing is the dominant factor driving variations in the summertime transport of the Pacific Arctic boundary current. Since the presence/absence of ice strongly modulates the transmission of stress from the atmosphere to the ocean, one would think that sea ice also plays a key role. However, this is not evident from our analysis, although one needs to keep in mind that, to first order, the seasonal evolution of sea ice concentration in the vicinity of the mooring was similar throughout our study period. It is likely that the influence of sea-ice will be amplified in the future as the ice cover continues to decline, which will presumably lead to more year-to-year variability as well.

Chapter 7

Implications of a Diminished Pacific Water Boundary Current

Between 2001 and 2011 there has been a 50% increase in the volume transport through Bering Strait, and, as a result, there has also been an increase in the heat and freshwater entering the Arctic from the Pacific (Woodgate et al., 2012). Over this same time period, however, the transport of the western Arctic boundary current has decreased markedly, with the most dramatic changes occurring during the summer months. In the previous chapters we have shown that the atmospheric forcing in summer has been the main driver of this change – in particular, an intensification of the Beaufort High (BH) and a deepening of the Aleutian Low (AL). These centers of action lead to easterly winds in the Alaskan Beaufort Sea that oppose the boundary current and make it difficult for Pacific water to progress eastward along the Beaufort shelfbreak.

Previous modeling studies have addressed the impact of the wind on the pathways of Pacific water in the western Arctic. Using a barotropic model, Winsor and Chapman (2004) illustrate that strong northeasterly and easterly winds reverse the flow along the Beaufort shelfbreak. Under this wind regime, the Pacific water exits the

Chukchi Sea in a more northward direction and enters the Canada Basin. Watanabe (2011) used a numerical model in combination with satellite data to examine the shelf-basin exchange in the western Arctic region. They argued that, during summer 2007, the shelfbreak jet was nonexistent due to the enhanced easterly winds, and hence no Pacific Water entered the Alaskan Beaufort Sea. Instead, the majority of the Pacific water veered westward from Barrow Canyon and much of it entered the Canada Basin as a result of Ekman transport.

In terms of atmospheric forcing, summer 2007 is similar to the final three years of our study (2009, 2010 and 2011) in that there are strong easterly winds along the Beaufort slope. While the Beaufort shelfbreak jet was present in those years, its transport was largely diminished. This raises the question as to the fate of the Pacific summer water in the later part of the decade and what the implications are for the western Arctic system. In this chapter we explore the potential impacts of the diminished boundary current, with particular focus on heat flux.

7.1 Summer Heat and Freshwater Transports

In Chapter 4 we computed the heat and freshwater fluxes of the shelfbreak jet at 152°W for each year, where the year was defined as the period from 1 August to 31 July (this definition was used to maximize the data coverage). It was demonstrated that the two Pacific summer water masses, ACW and CSW, accounted for more than 90% of the heat and freshwater flux for a given year. Here we consider the months of June, July, August, and September to capture the full signal of summer water in a given calendar year (the previous definition split the summer into two different years). We include the month of September because a significant amount of heat is transported by the boundary current during that month. Unfortunately this means

that we now only have three realizations, 2003, 2009, and 2010, as opposed to the five realizations investigated in the previous chapter when just the months of June, July, and August were considered. However, importantly, there is still at least one realization in the two extreme states of the boundary current, i.e. early in the decade when the transport was strong, and later in the decade when the transport was weak.

The Aug-Sep heat and freshwater fluxes are shown in Figure 7-1. As expected, the amount of heat and freshwater fluxed past 152°W is significantly greater when the boundary current is fully developed (2003) versus when it is weakened by easterly winds (2009, 2010). We calculate the amount of 1 m thick sea ice that can be melted by a given amount of heat using Equation 7.1, where H represents the ice thickness in meters, ρ_i is the density of ice (920 kg m^{-3}), L_f is the latent heat flux of melting (3.34×10^5 J kg^{-1}), and Q is the heat flux (W m^{-2}).

$$dH/dt = Q/(\rho_i \times L_f) \tag{7.1}$$

We find that the cumulative amount of heat advected past the mooring in 2003 has the potential to melt up to 168,000 km^2 of 1 m thick ice, while the average value for 2009-10 is 51,000 km^2. This difference of more than 100,000 km^2 represents an area roughly one-third the size of the Beaufort shelf. With regard to the freshwater, the fully developed boundary current in summer 2003 transported a total of 300 km^3 of freshwater past 152°W, while the average of the latter two years was roughly 70 km^3. This discrepancy (230 km^3) is comparable to the average year-to-year change in the freshwater content of the Beaufort Gyre during the last decade (175 km^3, see Pickart et al. (2013b)). These results demonstrate that a substantial amount of heat and freshwater – enough to influence ice melt as well as freshwater accumulation in the basin– has been diverted away from the Beaufort slope in recent years and has

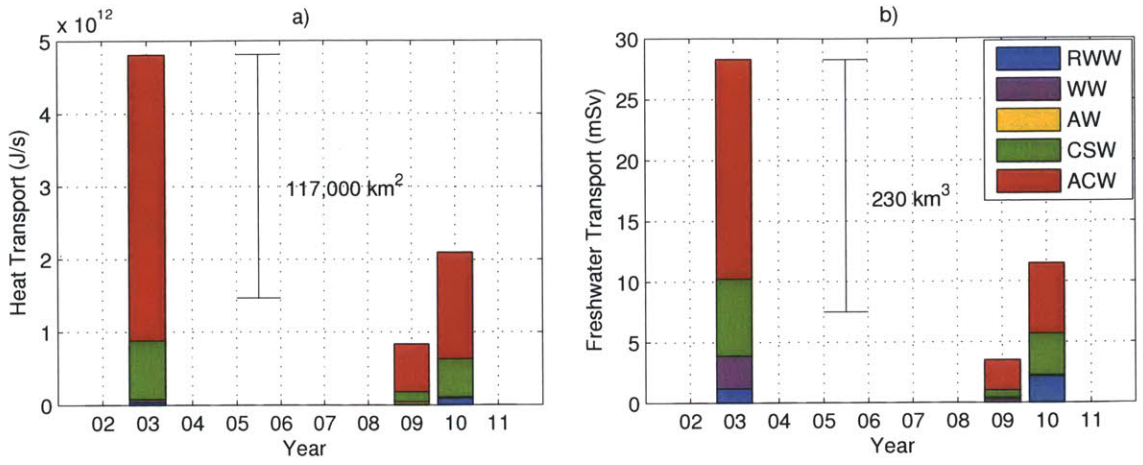

Figure 7-1: a) Heat transport of the boundary current measured by the shelfbreak mooring, broken into five water masses, for months June, July, August and September. The black line indicates the difference in potential 1 m thick ice melt for the given amount of heat advected past the mooring during the four months between 2003 and the average of 2009 and 2010. b) Freshwater transport of the boundary current measured by the shelfbreak mooring, broken into five water masses, for months June, July, August and September. The black line indicates the difference in freshwater transported past the mooring between 2003 and the average of 2009 and 2010.

gone somewhere else. The question is, where?

7.2 Sea Ice in the Pacific Arctic

A number of studies in recent years have addressed the role of Pacific water on sea ice melt in the western Arctic Ocean. Shimada et al. (2006) argues that there is a recently developed feedback loop where the combination of reduced ice stress and anticyclonic wind forcing (associated with the BH) direct the warm Pacific summer water into the Canada basin causing significant changes in sea ice cover for the region. Using an ice-ocean numerical model, Steele et al. (2010) investigated the different causes of sea ice melt in the Pacific sector, defined as the region encompassing the Chukchi, Beaufort, Laptev and East Siberian Seas as well as the adjacent deep basin. They concluded

that basal melt of sea ice (via the ocean) in the Pacific region contributes about two-thirds of the total volume melt, but is geographically constrained to the marginal ice zone. The surface melt (via the atmosphere) contributes one-third of volume melt but occurs over a much broader area of the ice pack. Steele et al. (2010) further considered the portion of basal melt due to local atmospheric heating of the water (adjacent to the ice) versus that due to remote advection by ocean currents. They concluded that the dynamical oceanic contribution accounts for about two-thirds of the basal melt. Therefore, it is clear that Pacific water inflow plays a significant role in melting sea ice in the Pacific sector. We now investigate if the diversion of warm Pacific water from the boundary current in recent years has created a noticeable difference in the pattern of sea ice melt in the region.

7.2.1 Distributions of Sea Ice Melt and Formation

(a) Ice melt

Returning to the five study years considered in the previous chapter, we present the late September sea ice concentration fields for 2003, 2004, 2009, 2010 and 2011 in Figure 7-2. These fields represent the cumulative affect over the summer of both atmosphere-forced and ocean-induced sea ice melt. Typically, the ice begins to retreat in earnest in the Chukchi Sea in mid-May and early-June. Steele et al. (2010) shows that most of the sea ice melt during early summer is top melt associated with a warming atmosphere. By July, much of the Chukchi Sea is ice-free and there is noticeable sea ice retreat along the Russian and northern Alaskan coast for all years. As the summer progresses, the ice edge eventually recedes into the interior basin. Figure 7-2 reveals that there was a significant difference in the extent and character of the ice melt in the later years (2009, 2010, 2011) versus the earlier years (2003

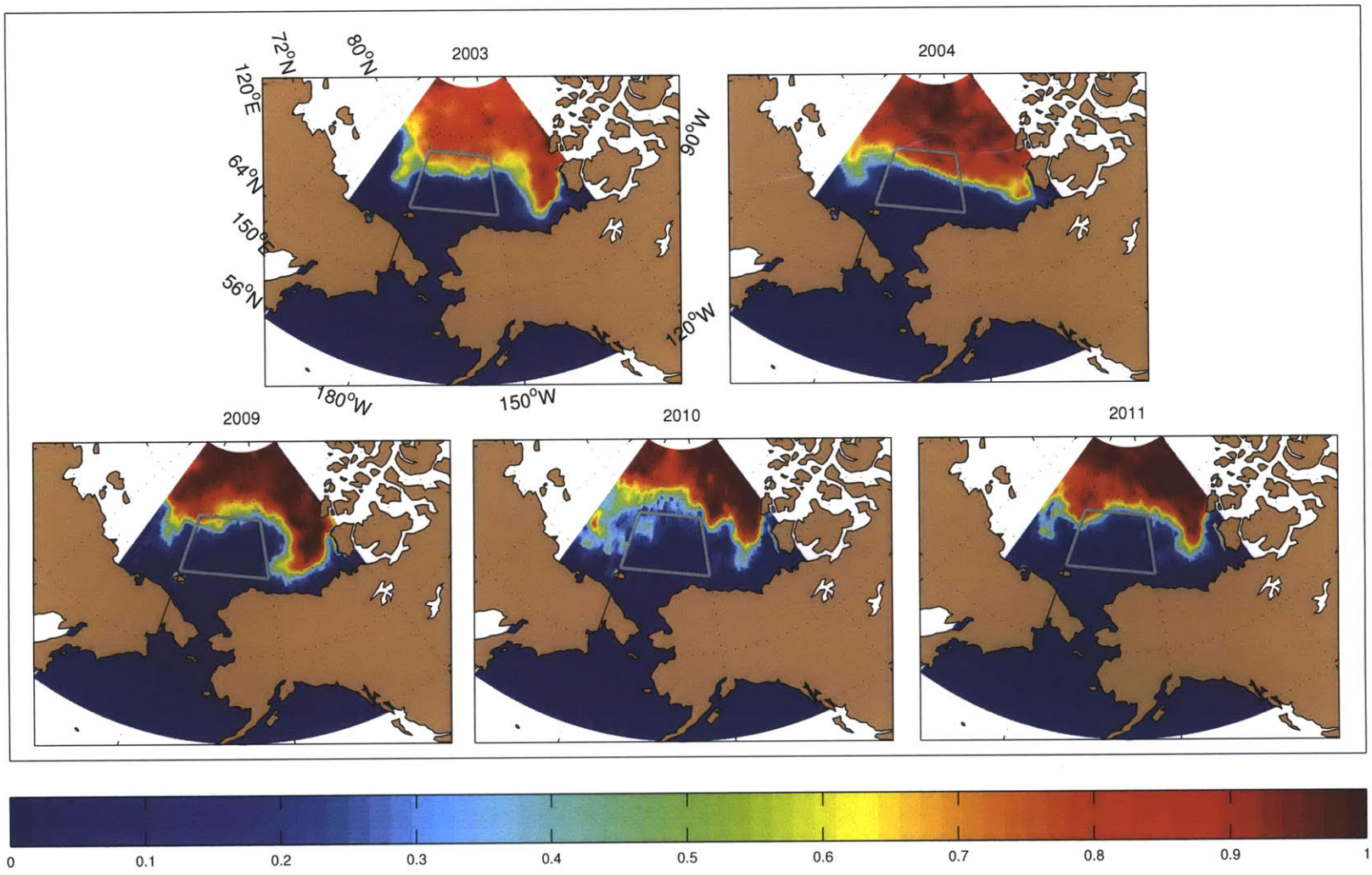

Figure 7-2: Mean sea ice concentration in the Pacific sector of the Arctic Ocean from 15 September to 31 September. The grey box is the region used to determine differences in ice melt in the text.

and 2004). In particular, not only was the ice edge farther offshore in the Canada Basin in the later years, but there was a distinct "bite" of open water protruding into the basin. Here we consider the amount of ice in the region north of the Chukchi and Beaufort shelf breaks to 78°N. This area was chosen because it captures the area where the largest interannual changes occur. Furthermore, this area encompasses a likely destination for Pacific water if it does not make it into the boundary current, but instead gets fluxed from the Chukchi shelf into the Arctic basin. We calculate that in 2003 and 2004 there was approximately 93,984 km^2 and 123,420 km^2 of sea ice, respectively, within the measurement box for late September. This is to be contrasted to the later years when there was 37,443 km^2, 34,024 km^2, and 27,747 km^2 in 2009, 2010, and 2011, respectively. This amounts to a difference of approximately 76,000 km^2 between the early and later years.

Based on the calculations above, the discrepancy in the cumulative amount of heat fluxed past the mooring site for the early years versus the later years ($\sim$100,000km^2) is more than enough to account for the difference in ice melt within the measurement box ($\sim$76,000km^2) over this time period. One might wonder, however, if it is reasonable to assume that the Pacific water influences the basin as far north as 78°N. The model results in Steele et al. (2010) suggest that ocean heat flux warms the Arctic region only within a few hundred kilometers of the northwest Alaskan Coast. However, the basin-scale wind forcing (associated with an intense BH) for summers 2009, 2010 and 2011 is such that warm surface waters would be fluxed north towards the area of significant ice melt. This notion is also in line with the scenario described by Shimada et al. (2006). Interestingly, Steele et al. (2010) does suggest that bottom melt (especially melt associated with ocean heat transport) dominates sea ice melt later in the summer when the atmospheric heating declines. This would be consistent with the rapid ice melt in mid-to-late August for the later years.

(b) Freeze-up

It was also suggested by Steele et al. (2010) that, rather than melting the pack ice, Pacific summer water might delay ice formation in early fall in the region north of the Chukchi Sea. In this scenario no assumptions need to be made about how far north the warm water extends into the basin. To assess this, we consider the sea ice concentration fields for the time period 1 October to 15 November (Figure 7-3). This 6-week period is chosen because, for the years considered, freeze-up generally begins by early October, and mid-November is when the measurement box is completely re-covered with sea ice in 2003. The satellite data set ends on 4 October 2011 and therefore we do not consider that year. Figure 7-3 shows that 2003 and 2004 are quite similar; in particular, there is a substantial re-freezing from October into November. However, in 2009 and 2010 one sees the remnant of the open water bite that formed earlier in those two summers. The difference in ice extent within the measurement box between the early years and late years is approximately 50,000 km^2. Again, the amount of heat that did not enter the Beaufort shelfbreak jet could readily account for this change.

7.3 Pacific Water Exiting the Northeast Chukchi Sea

The above conclusions assumed that all of the heat not entering the Beaufort shelf-break jet east of Pt. Barrow was available either to melt ice in the basin or delay the onset of freeze up. However, it is unclear how much of the Pacific summer water actually made it to Barrow canyon in the latter part of the decade, and, if it did, what was the fate of the water exiting the canyon.

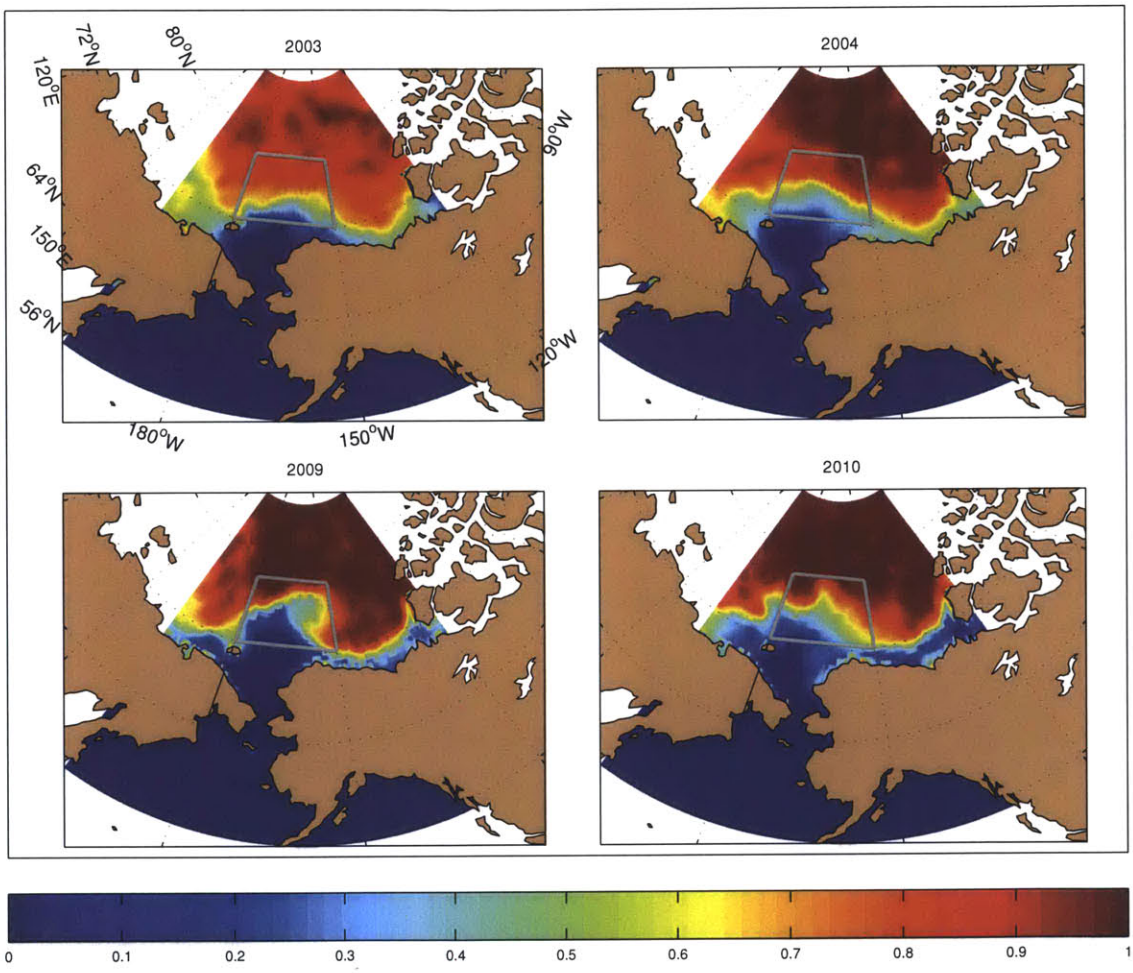

Figure 7-3: Mean sea ice concentration in the Pacific sector of the Arctic Ocean from 1 October to 15 November. The grey box is the region used to determine differences in freeze-up in the text.

Using in-situ hydrographic data, moored measurements, and satellite SST imagery, Okkonen et al. (2009) investigated how different wind regimes impact the summertime flow of Pacific water (i.e. the ACC) within Barrow Canyon. They showed that when the winds are easterly, southeasterly, or southwesterly, the ACC flows northward along the eastern flank of the canyon. However, in the former two cases, if the wind is strong enough, it drives westward flow on the Beaufort shelf that tends to oppose the penetration of the warm summer water to the east. The other case that Okkonen et al. (2009) considered was northeasterly winds. These are approximately aligned with Barrow Canyon, and, consequently, the flow of the ACC on the eastern flank is reversed. In this scenario it is unclear how much warm Pacific water actually enters the canyon; Okkonen et al. (2009) suggest that some portion of the ACC gets diverted to the western side of the canyon.

To assess how the ACC varies within Barrow Canyon for the five years in this study, we constructed wind roses using the Pt. Barrow weather station data (Figure 7-4). There are both moderately northwesterly and southeasterly winds during summer 2003. According to Okkonen et al. (2009), in both cases the ACC within Barrow Canyon would be strong, and, as our observations suggest, a substantial amount of summer water/heat was transported within the shelfbreak jet past 152°W. Summer 2004 is characterized easterly and northeasterly winds, but their magnitudes were considerably weaker than the three later years. Furthermore, summer 2004 had a fair amount of westerly winds. As such, the flow through Barrow Canyon should still be northward and feed the Beaufort shelfbreak jet, which was indeed the case as indicated by our observations at 152°W. As seen in Figure 7-4, the summers of 2009, 2010, and 2011 were all characterized by strong easterly winds, and, as presented above, there was a significant drop in the eastward transport of the Beaufort shelfbreak jet in those years. Also note that the wind speeds were comparatively weaker in 2010, consistent

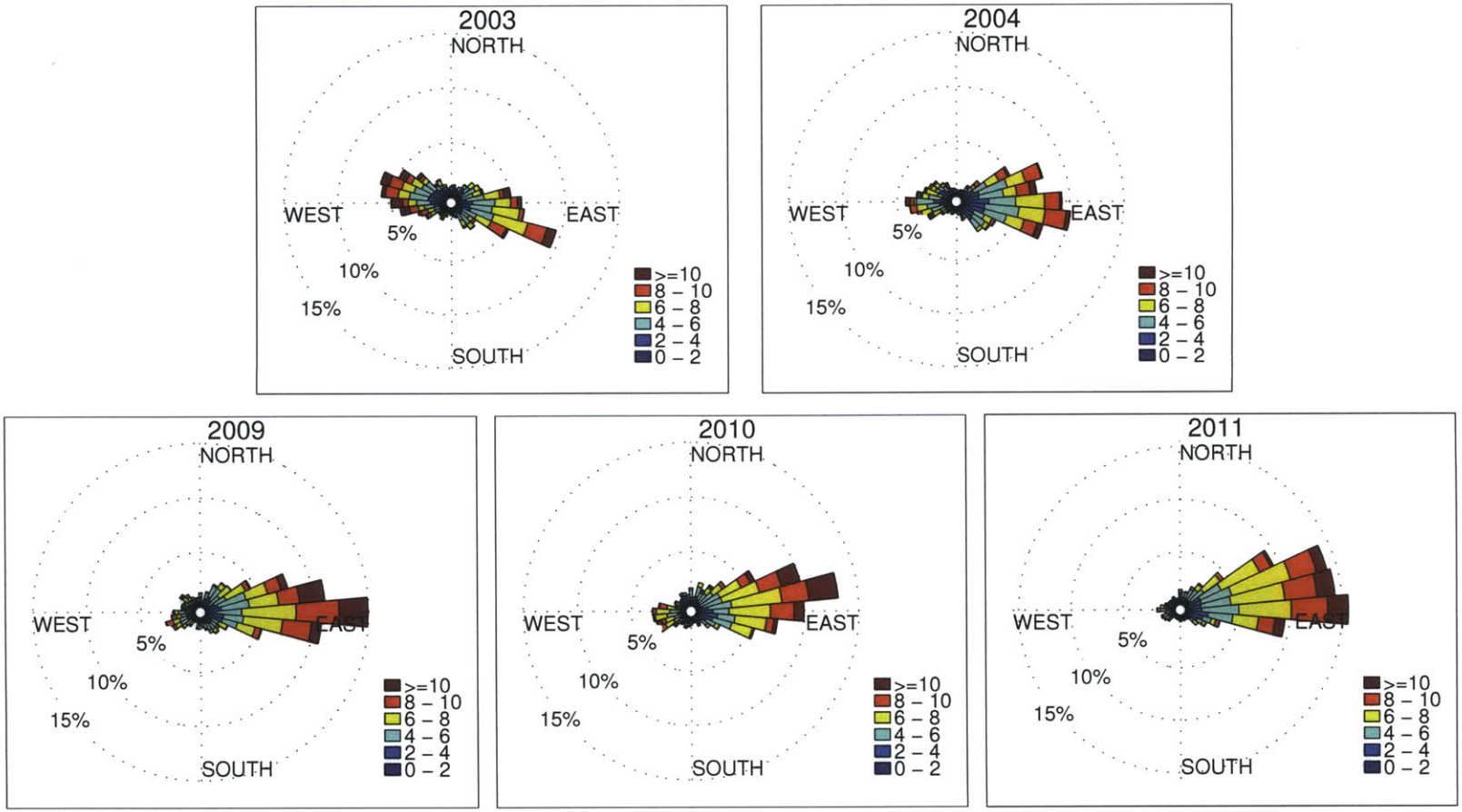

Figure 7-4: Composite wind rose plots for June, July and August from Pt. Barrow weather station. Colors represent wind speed, spokes (directional quadrants) are where the winds come, from and percentage contours represent the amount of data that falls into a given direction.

with the fact that 2010 was the rebound year in boundary current transport.

Due to the strong easterly/northeasterly winds during the latter three summers, it is possible that a portion of the ACC volume and heat flux did not make it to Barrow Canyon, but was instead redirected onto the Chukchi shelf. Therefore, it may not be accurate to assume, as was done above, that all of the water not entering the Beaufort shelfbreak current was fluxed into the Canada Basin. This is now addressed using ancillary data from 2011.

7.3.1 Evidence from a Moored Array

An array of moorings was deployed at the head of the canyon during summer 2011 as part of a BOEM-funded study to investigate the circulation in the northeast Chukchi Sea. One mooring in particular, BC2, was located in the center of the ACC in 50 m of water and included an upward-facing ADCP to measure velocity through the water column. A Microcat located near the bottom of the mooring (48 m) measured temperature and salinity. Unfortunately, the CMP on the shelfbreak mooring at 152°W failed in late-May that year. However, the Microcat at 35 m provides an effective proxy for the temperature of the summer water in the shelfbreak jet. In order to carry out a consistent comparison of the heat flux at the two sites (Barrow Canyon and 152°W), we considered only the velocity measurements at 45 m on each mooring. Because the hydrographic data at 152°W were collected 13 m higher in the water column than in Barrow Canyon, we used the temperature gradient (calculated from previous years) to adjust the temperature at the shelfbreak site. Based on earlier shipboard hydrographic/velocity measurements from the SBI program, it is estimated that the ACC has a width of 20 km at the head of Barrow Canyon, and, as calculated previously in Chapter 3, the width of the shelfbreak jet is 16-18 km. We consider the

time period that summer water was present at each location. In Barrow Canyon the warm water first appeared in early June and lasted until mid-October, while for the Beaufort shelfbreak jet at 152°W it was present from early July to mid-October.

Our calculation reveals that significantly more heat was fluxed northward through the head of Barrow Canyon than was fluxed eastward past 152°W in the Beaufort shelfbreak jet (Figure 7-5). The difference is enough to melt about 52,000 km^2 of sea ice, with a range of 35,000 km^2 – 70,000 km^2. Even with this uncertainty it is clear that a considerable amount of the heat reaching Barrow Canyon in summer 2011 did not enter the Beaufort shelfbreak jet. Where did the heat go? One possibility is that, following the ideas in Okkonen et al. (2009), the ACC was diverted to the western side of Barrow Canyon and exited the canyon as a westward-flowing jet along the edge of the Chukchi shelf. Another possibility is that the summer water was fluxed directly northward into the basin via turbulent processes such as eddy formation. A third possibility is that a jet of warm water emanated from the canyon which was not trapped to the shelf edge. At this point it is impossible to say which of these scenarios is most likely, or if all of them can happen over the course of a summer. However, shipboard and satellite data obtained in summer 2011 during an easterly wind event demonstrates that the third scenario above is a viable mechanism for exporting heat out of Barrow Canyon into the Canada Basin.

7.3.2 Evidence from Satellite and shipboard data

During July 2011 two easterly wind events took place in the vicinity of Barrow Canyon and the Alaskan Beaufort Sea (Figure 7-6). During the first event, which lasted more than two weeks, the USCGC Healy occupied a XCTD/velocity section to the west of the canyon mouth. Figure 7-7 presents a series of four satellite images that nicely

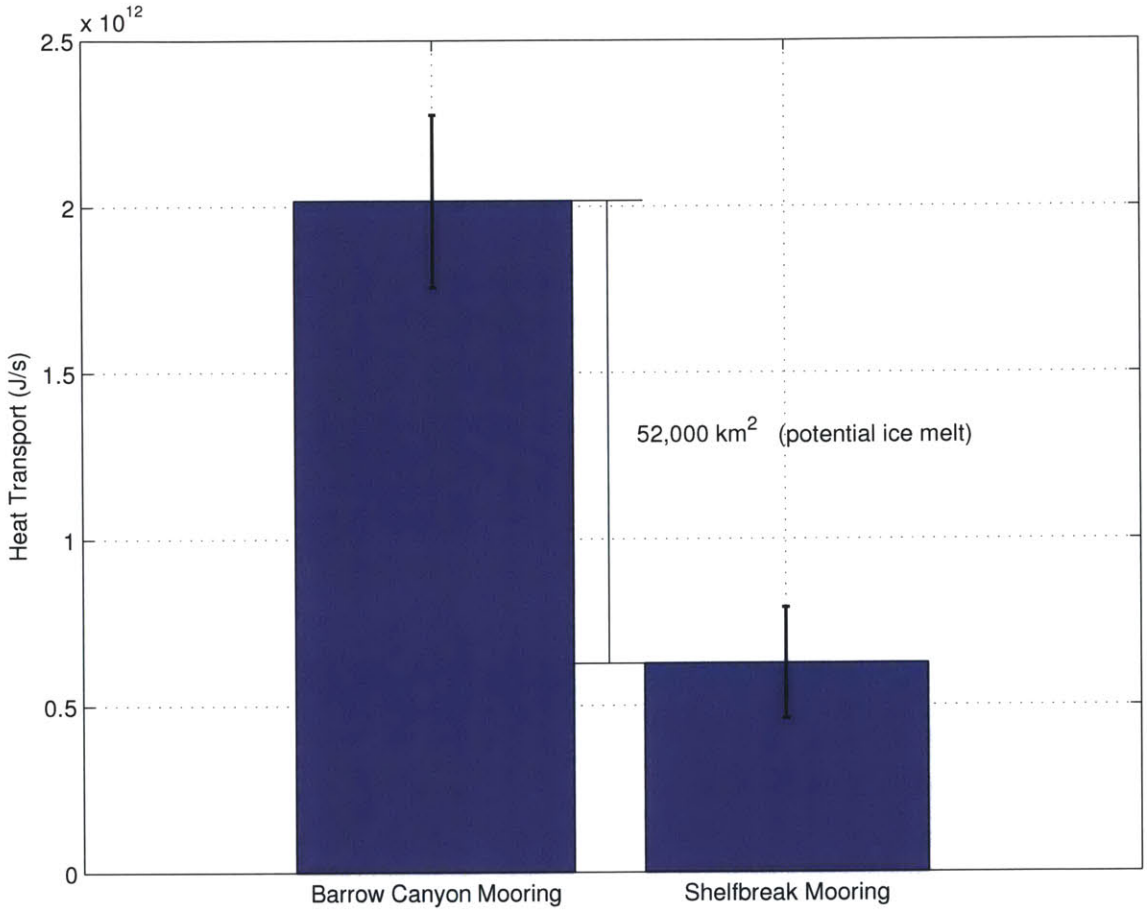

Figure 7-5: Heat transport of the ACC at the head of Barrow Canyon and heat transport of the ACC at the Beaufort shelfbreak for time period between 01 June 2011 and 10 Oct 2011. This represents the full season of summer water passing both locations.

depict the evolution of the sea surface temperature field and sea ice concentration during the latter part of the event. The locations of the Healy XCTD stations are marked in the figure, as well as the two mooring sites (head of Barrow Canyon and Beaufort slope). Despite the presence of clouds in the images, the signals of interest are easily depicted.

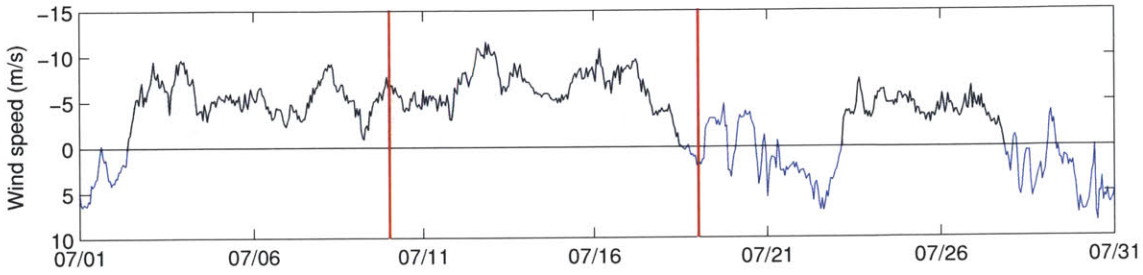

Figure 7-6: Alongcoast wind speed for the month of July, 2011, measured at the Pt. Barrow meteorological station. Shaded winds represent easterly winds which oppose the shelfbreak jet. The red lines mark the time period of the satellite images.

The first satellite image is from 10 July 2011, when the ice edge is near the vicinity of the shelfbreak. One sees the presence of warm surface water (ACW) extending to the tip of Pt. Barrow, a good distance along the canyon. The shelfbreak mooring at 152°W is still covered with sea ice at this time. The next satellite image is four days later on 14 July 2011, at which point the warm water has reached the mouth of the canyon. Note also the tongue of warm water extending westward along the Beaufort shelfbreak past the 152°W mooring site. This is the surface signature of the reversed shelfbreak jet, consistent with the mooring velocity record at 152°W which indicates reversed flow (especially in the upper 50 m) for much of July. It seems likely that the source of the warm water in the jet was Mackenzie River water entrained into the reversed shelfbreak current (although it is not impossible that some of it is Pacific-origin water that had previously passed by the mooring flowing eastward prior to the

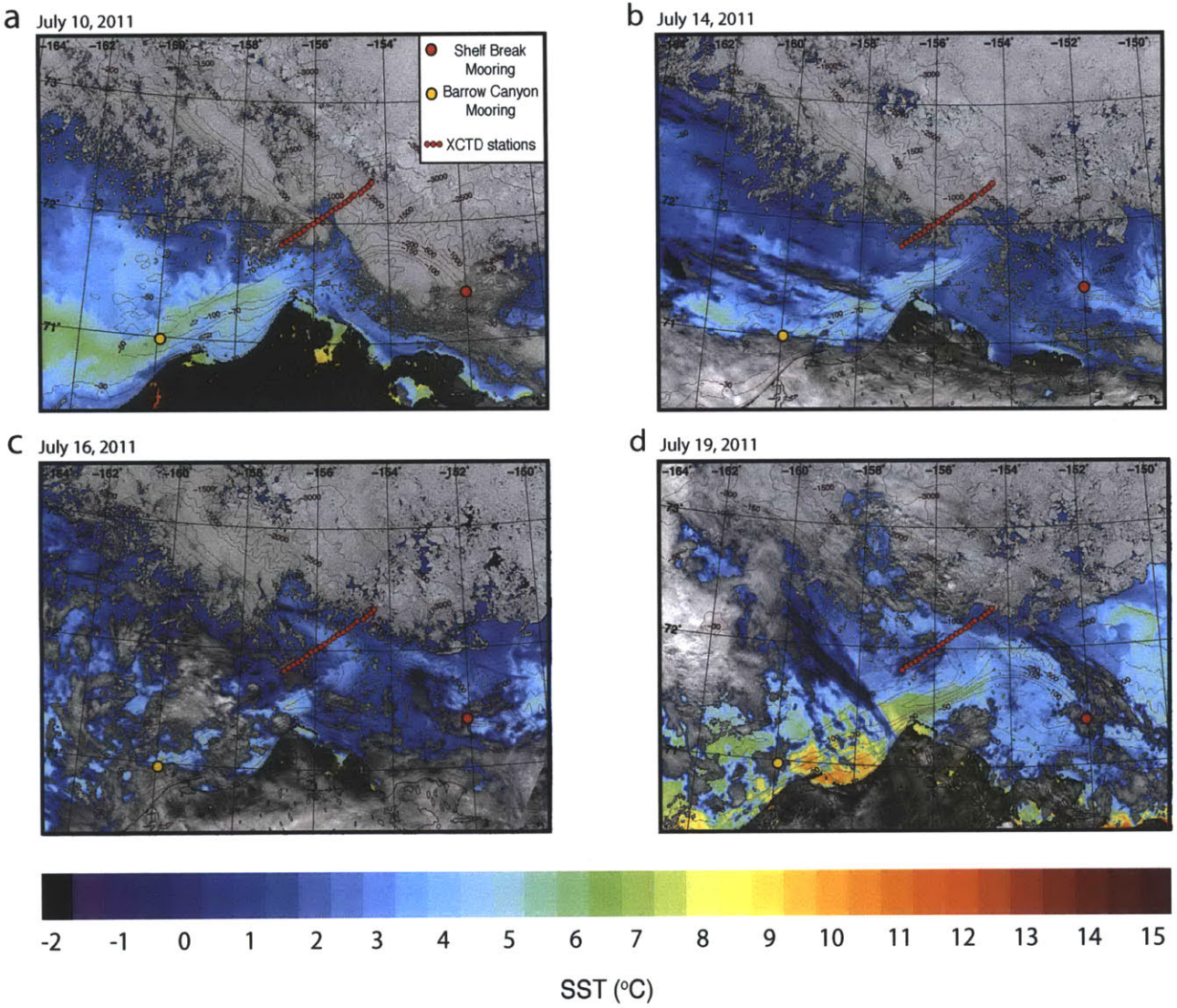

Figure 7-7: Satellite images of study region showing sea surface temperature and visible imagery for a) 10 July 2011, b) 14 July 2011, c) 16 July 2011 and d) 19 July 2011. The Beaufort shelfbreak mooring is indicated by the red circle and the Barrow Canyon mooring is indicated by the yellow circle. The locations of the USCGC Healy XCTD stations are indicated by the line of red circles.

storm). The Barrow wind record indicates that the easterly winds are still strong at this time with peaks over 10 m/s.

The third satellite image is from 16 July 2011 and, although partially obscured by clouds, it clearly shows that the tongue of warm water emanating from Barrow Canyon has turned westward and encountered the ice, appearing to cause considerable melt (although advection of the ice is likely occurring as well). Note that the warm water originating from the east in the Beaufort shelfbreak jet has now reached the mouth of Barrow Canyon. The final satellite image is from 19 July 2011. One sees that the warm water continues to progress westward and now intrudes farther into the basin and into the ice pack, enlarging the area of ice melt. The shelfbreak jet signature remains clear as well.

The Healy XCTD section was occupied on 17 July 2011, between the time of the third and fourth satellite images. The temperature and salinity profiles in conjunction with shipboard ADCP measurements allowed for the calculation of absolute geostrophic velocities as well. The vertical section of potential temperature (Figure 7-8a) reveals warm water in the upper layer (as warm as 4°C) adjacent to the ice edge. The absolute geostrophic velocity section (Figure 7-8b) indicates a reversed (westward-flowing) surface-intensified jet, located well seaward of the shelfbreak. This jet is advecting the warm summer water to the northwest at speeds up to 80 cm/s. Shoreward of the jet, and deeper in the water column, is a cyclonic eddy transporting warm water as well. This subsurface feature was likely pinched off of the main canyon outflow via a turbulent process.

Together, the satellite images and the in-situ shipboard data provide evidence that warm Pacific summer water can be diverted into the interior basin to the west of Barrow Canyon during easterly wind events. This is consistent with the above results showing that a large portion of the heat reaching Barrow Canyon does not make it

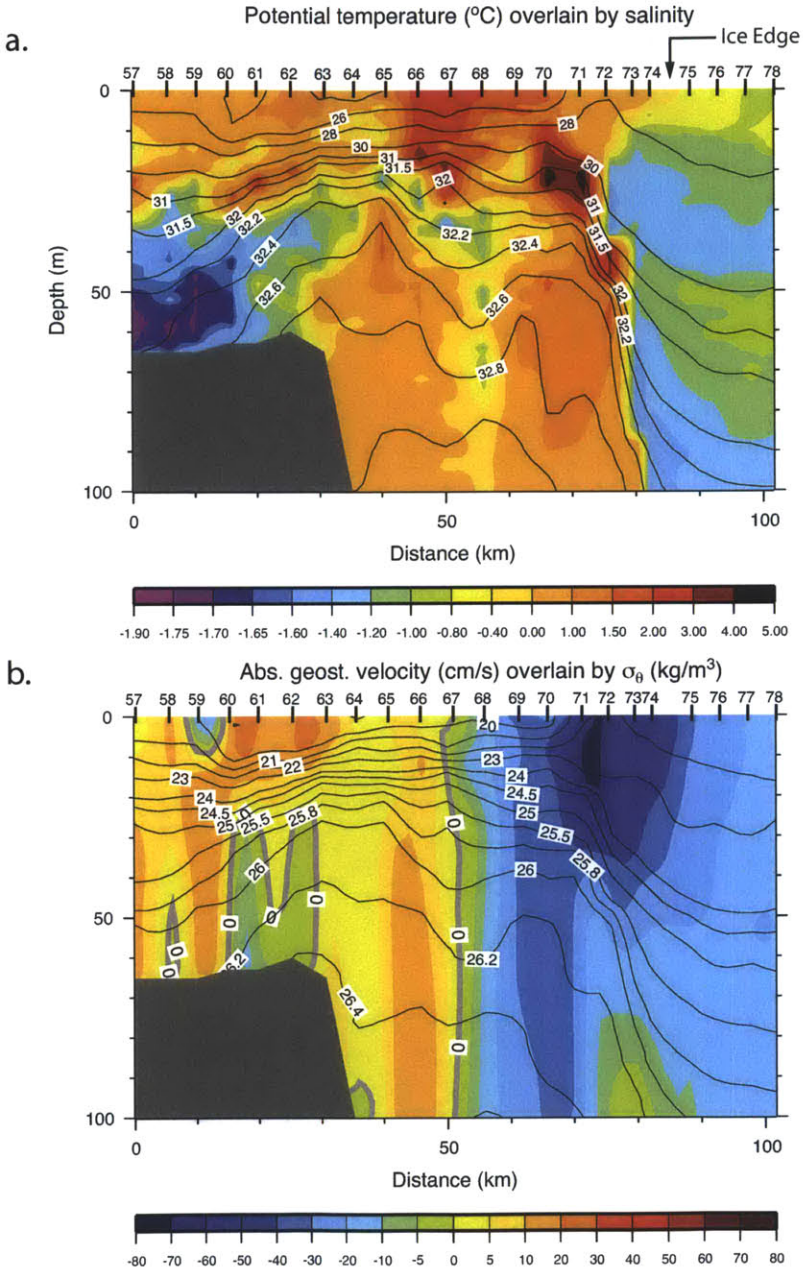

Figure 7-8: a) Vertical section of potential temperature (°C) overlain by salinity. b) Vertical section of absolute geostrophic velocity (cm/s) overlain by potential density (km/m^3). The locations the XCTD profiles are numbered along the top edge of the plot.

into the Beaufort shelfbreak jet during summers with strong easterly winds. It also supports the conclusion that a significant portion of this heat contributes to sea ice melt in the Pacific Arctic. Although not shown here, subsequent satellite images indicate that the pack-ice permanently shifted to the north following the two July wind events in summer 2011.

Chapter 8

Conclusions

This thesis has investigated the seasonal to interannual variability of the shelfbreak jet of the Alaskan Beaufort Sea, which is a primary conduit by which Pacific Water enters the Arctic Ocean north of Bering Strait. Using a 6-year mooring data set at 152°W, it was shown that, seasonally, the current has the largest volume, heat, and freshwater transport during the months of June, July, August, and September. This is the time of year when warm and fresh Pacific summer water is advected along the Beaufort slope by the current. Over the 10-year time period from 2002-2011 there has been a drastic decrease – by more than 80% – of the volume, heat and freshwater transport of the current. This decline has primarily occurred during the summer months.

In order to explain the decrease in summer transport we studied the various physical drivers of the boundary current. We find that atmospheric forcing is, to the first order, responsible for the drastic weakening of the flow. Over the decade there has been an intensification of the summer Beaufort High (BH) and a deepening of the summer Aleutian Low (AL). The resulting increase in sea level pressure gradient between the two centers of action have led to an enhancement of the the easterly winds

in the Alaskan Beaufort Sea that have opposed the boundary current.

Over this same time period the northward transport of Pacific water through Bering Strait has increased, which raises the question as to the fate of the water in recent years if it is not entering the Beaufort shelfbreak current. We find that, during years when there is strong atmospheric forcing, a large portion of the heat entering Bering Strait in summer still progresses northward to the head of Barrow Canyon, but then gets diverted away from the boundary current. The amount of heat so diverted is enough to melt approximately 50,000 km^2 of 1-meter thick sea ice.

Using satellite fields and in-situ shipboard data it was demonstrated that, during easterly wind events, warm Pacific summer water can be advected into the interior basin to the west of Barrow Canyon. This provides a plausible pathway for the large portion of the heat reaching Barrow Canyon that does not enter the Beaufort shelfbreak jet during summers with strong easterly winds along the north slope of Alaska. It also supports the conclusion that this heat contributes to significant sea ice melt in the interior Canada Basin.

Appendix A

Shelfbreak Mooring Deployments

This thesis uses data from six of the seven shelfbreak mooring deployments between 2002 and 2012. During each of these deployments, the shelfbreak mooring collected hydrographic (Temperature, Salinity) data along with velocity data for the 147 m water column. The hydrographic data gave insight into the water properties carried in the shelfbreak jet. The velocity data showed the rate at which the water passed the shelfbreak mooring and allowed for a transport estimate of the current. Below are specific details that pertain to each of the shelfbreak mooring deployments.

A.1 2002-3 Deployment

In August 2002, the shelfbreak mooring was one of eight moorings deployed as part of the western Arctic Shelf-Basin Interactions (SBI) experiment. The shelfbreak mooring was located on the Beaufort shelfbreak in 147 m of water. The mooring was equipped with a Coastal Moored Profiler (CMP), which is a conductivity, temperature and depth instrument (CTD) (Fratantoni et al., 2006). The CMP travels vertically on the mooring providing traces of temperature and salinity every 6 hours. The CMP

collected data from 50 m to 130 m depth, with 2 m vertical resolution. The instrument was set not to go above 50 m in order to avoid interference by ridging ice. There were sparse data gaps in the hydrographic record, which lasted from 01 August 2002 to 25 September 2003. The shelfbreak mooring was also equipped with a RDI Workhorse (300kHz) Acoustic Doppler Current Profiler (ADCP). This instrument was located at 135 m and provided velocity data from 130 m to the surface. The ADCP had an hourly sampling frequency and a bin size of 5 m. Overall the data coverage was good. Between November and May returns from the upper 60 m experienced some difficulties due to a lack of biological scatterers (Nikolopoulos et al., 2009). In relation to the whole record length, the temporal coverage in the upper 60 m was 85% at the shelfbreak mooring. In the lower water column the temporal coverage was greater than 95% (Nikolopoulos et al., 2009).

A.2 2003-4 Deployment

As part of the SBI experiment, the shelfbreak mooring was turned around and re-deployed in October 2003. Again, the hydrographic data was again collected by a CMP, which sampled every six hours between 45 and 130 m, having 2 m vertical resolution. On this deployment, the CMP did very well up until May 2004 and then began sampling less frequently. Overall, the CMP did 62% of the total expected profiles for the deployment, largely due to the fact the CMP began to fail in May 2004 (Fratantoni et al., 2006). A RDI Workhorse (300kHz) ADCP collected the hourly velocity data for this deployment. Due to an operator error, the ADCP was set to have only 15 bins with 5 m resolution. This gave good coverage from 130 m to 55 m depth. Unfortunately, there was no velocity information upwards of 55 m. Fortunately, the surrounding moorings in the 152°W array (BS2 and BS4) had ADCPs that sampled

the entire deployment over the upper 50 m of the water column. Consequently, the upper 55 m data gap was filled using Laplacian-spline interpolation using data from the surrounding moorings and also the shelfbreak mooring data below 55 m. The reader is referred to Fratantoni et al. (2006) for a technical report regarding the hydrographic data during the first two deployments which fell during the SBI experiment.

A.3 2005-6 Deployment

The shelfbreak mooring was next deployed in August 2005 at approximately the same location as during the SBI years. Temperature and salinity data were collected by the CMP having vertical coverage from 50 to 125 m, with 2 m vertical resolution. The CMP profiled every hour giving very high temporal coverage. There were a few large data gaps from September 2005-November 2005, but beyond that, the CMP returned good profiles up until failure on 5 April 2006. The CMP did not last the entire deployment due to battery failure due to the high sampling frequency. The 2005-06 deployment utilized an RDI LongRanger (75kHz) ADCP to measure velocity. It had 10 m bins and measured hourly velocity from 115 m to the surface. The coverage ended in mid November 2005 most likely due to poor battery performance.

A.4 2008-9 Deployment

The 2008-2009 deployment started in August 2008 and again a CMP was used to collect the hydrographic data from 50 m to 120 m depth. The CMP had 2 m vertical resolution and sampled every six hours. The CMP took good measurements for the entire deployment giving excellent temporal coverage. Similar to the prior deploy-

ment, a RDI LongRanger (75 kHz) ADCP was used to collect velocity data. The vertical coverage spanned from 111 m to the surface. The ADCP measured velocity hourly with 5 m bins. The first through fourth bin showed an increase in backscatter amplitude and were removed during processing. (F. Bahr and D. Torres, pers. comm., 2013). There was also beam interference from the mooring float, located at 40 m, leading to bins 14 and 15 being edited out as well (F. Bahr and D. Torres, pers. comm., 2013).

A.5 2009-10 Deployment

The shelfbreak mooring was turned around and deployed again from August 2009 to September 2010 at approximately the same location. The temperature and salinity were collected by a CMP, which had vertical coverage from 50 m to 130 m depth with 2 m vertical resolution. The CMP sampled every six hours and had very good temporal coverage lasting the whole deployment. Velocity data was collected using a combination of ADCPs in order to avoid the mooring float from causing data interference. An RDI Workhorse (300kHz) ADCP was set at 40 m depth (on top of the mooring float) and a RDI LongRanger (75 kHz) ADCP was set at 130 m depth. The Workhorse ADCP measured velocity from 22 m depth to the surface. Due to an operator error the bin size was set to 10 m instead of 5 m and this created a larger than normal transducer blanking range, which shortened the vertical coverage. The Workhorse ADCP stopped measuring velocity at the end of May 2010. The lower ADCP (LongRanger) measured velocity from 120 m to the surface. The LongRanger ADCP measured velocity for the entire deployment. Due to an operator error, the bin sizes were set to 5 m instead of 10 m. Overall, this did not affect data quality; it did however create a shorter transducer blanking range and in order to avoid any

transducer ringing, the bottom bin was edited out. There was also data interference by the mooring float at 40 m and the 16th bin was edited out as well. Comparing the velocity in the upper 20 m, collected by the Workhorse ADCP, and the same velocity for that vertical range collected by the LongRanger ADCP, the two time series appeared highly correlated and therefore the LongRangers velocity alone was used for the upper water column after the Workhorse stopped collecting data in May 2010.

A.6 2010-11 Deployment

For the 2010-2011 deployment, the shelfbreak mooring was again equipped with a CMP, which profiled every 6 hours measuring from 50 to 130 m. The CMP had vertical resolution of 1 m. Due to an operator error, the profiler made round trips instead of single ups or downs and therefore made twice as many profiles as expected. Consequently, the battery for the CMP ran out in late May 2011. The temporal coverage was very good during the operating timeframe since there was a higher profiling frequency. For velocity data, a similar setup to the 2009-2010 deployment was used where there was a RDI Workhorse (300 kHz) ADCP set above the mooring float at 40 m and a RDI LongRanger (75 kHz) set at the base of the mooring at 130 m depth. The Workhorse measured from 27 m to the surface with 5 m bins. The LongRanger measured from 110 m to the surface with 10 m bins. Again the mooring float interfered with the returns at the 40 m depth level and that bin was edited out.

Appendix B

Refinement of the Shelfbreak Mooring Transport Proxy

This appendix describes two procedures that were applied as part of the proxy for the transport of the Beaufort shelfbreak jet using the single shelfbreak mooring. It is important to note that these represent relatively small refinements to the original proxy described in Chapter 3. Even without these adjustments the correlation between the proxy and the full transport is quite high (r=0.88).

B.1 Alaskan Coastal Current Adjustment

Inspection of the original shelfbreak mooring proxy reveals that when the Alaskan Coastal Current (ACC) is present in the summer months, the proxy underestimates the full transport of the boundary current. Using the first year of SBI mooring array data we constructed the composite velocity section for those times when the proxy underestimated the full transport by $\geq$ 0.3 Sv (Figure B-1a). One sees that these cases correspond to times when the ACC was displaced offshore of the shelfbreak.

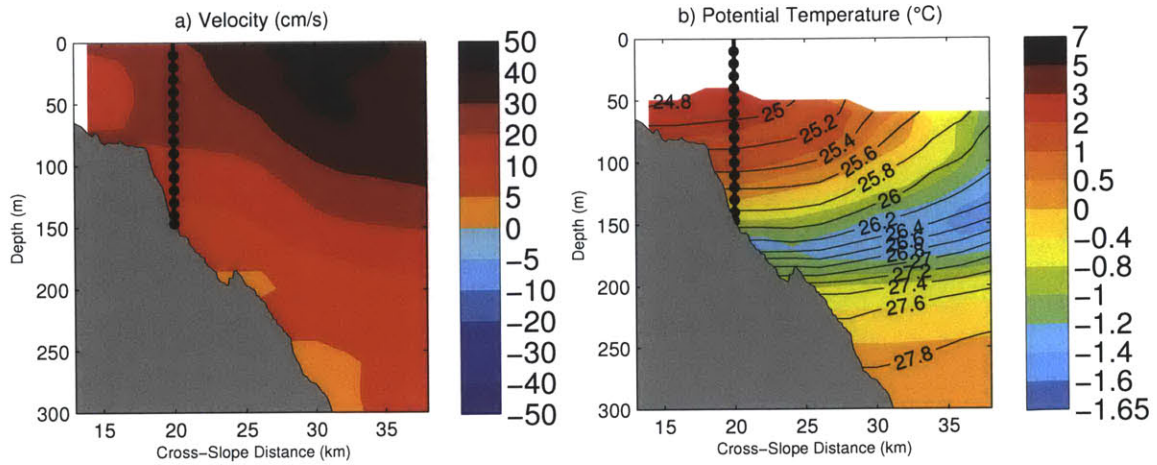

Figure B-1: a) Composite velocity section (cm/s) when the shelfbreak mooring underestimates the full transport by $\geq$ 0.3 Sv. b) Composite potential temperature section (°C) for the same time periods.

This is to be compared to those times when the proxy more accurately represented the true transport of the ACC (Figure B-2a), which occurred when the current was more closely centered on the shelfbreak.

One metric that might be used to identify instances of offshore meandering of the ACC is the temperature at the shelfbreak mooring site. As is evident by comparing Figures B-1b and B-2b, when the ACC is farther offshore the temperature in the water column at the mooring site is warmer. However, another important difference between the two cases is the vertical stratification. In particular, when the ACC is located significantly seaward of the shelfbreak the water column at the mooring site tends to be more weakly stratified than when the ACC is closer to the shelfbreak. This is shown quantitatively in Figure B-3. The reason for this is that when the temperature front of the ACC is situated farther offshore, there is more pure Alaskan Coastal Water present at the shelfbreak mooring site.

As such, we adjusted the transport proxy only when warm, weakly stratified

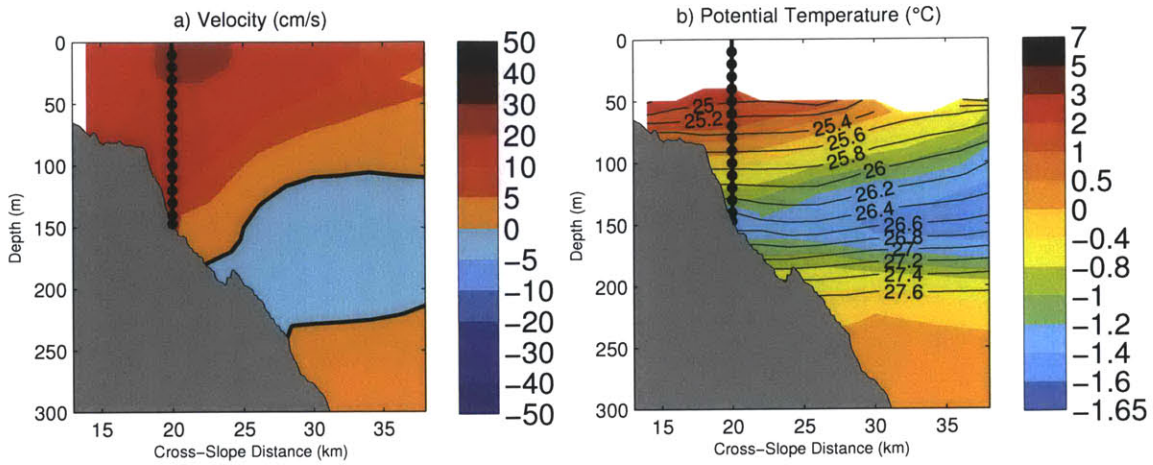

Figure B-2: a) Composite velocity section (cm/s) when the shelfbreak mooring accurately estimates the full transport during August 2002-September 2002 and July 2003-September 2003. b)Composite potential temperature section (°C) for the same time periods.

Alaskan Coastal Water was present at the mooring site. In particular, the vertically averaged potential temperature at the shelfbreak mooring had to exceed 0 °C, while the stratification in salinity had to be less than 0.009 m^{-1}. Figure B-4 shows a scatter plot of the difference between the original proxy and the transport of the full array under these conditions. The regression line in the figure was used to correct the original proxy for those time periods so identified. This same approach was used for correcting the individual water mass proxy transport timeseries for each 10 m bin.

For the summer months of August-September 2002 and July-September 2003, the transport of the boundary current was estimated to be 0.371 Sv using the data from the full array. The original proxy gives a value of 0.310 Sv, and the mean rms difference between the two is 0.295 Sv. After applying the above procedure, the mean transport of the refined proxy is 0.349 Sv and the mean rms difference is now 0.281 Sv. Hence, both in terms of the mean summer transport and the day to day variability, the refined proxy does a better job of representing the true ACC. Figure B-5 shows

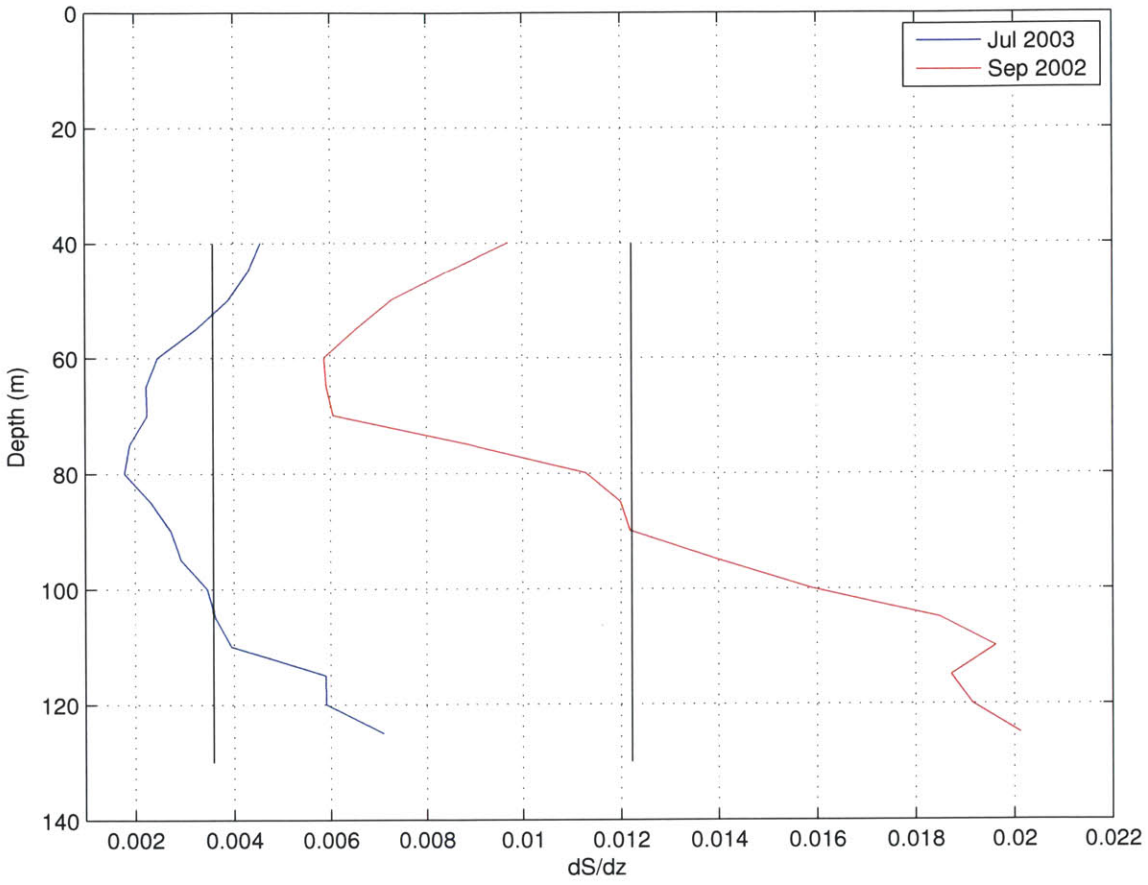

Figure B-3: Stratification at the shelfbreak mooring when the jet is situated over the mooring site (Sep 2002) versus when it is offshore of the mooring site (Jul 2003). The depth integrated stratification for each case is plotted as a black line.

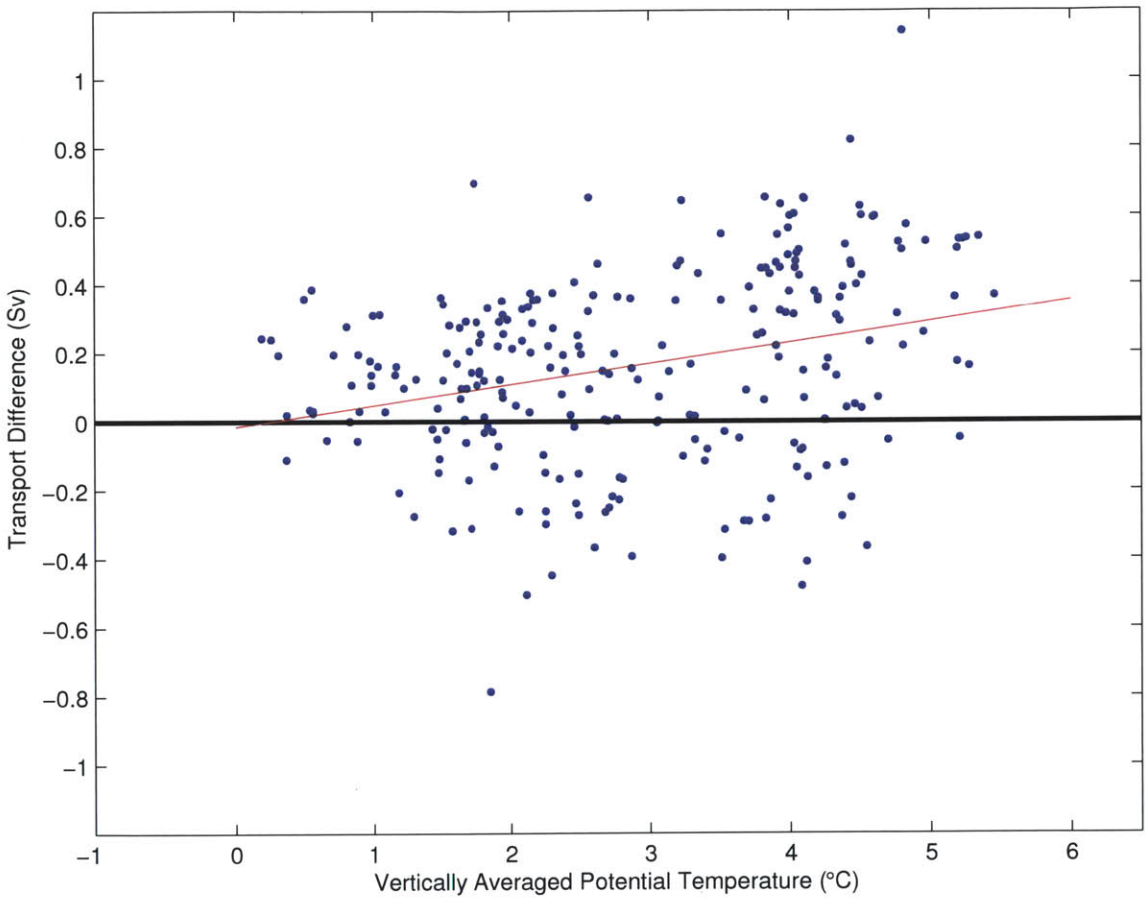

Figure B-4: Scatter plot of the difference in transport between the full array value and the shelfbreak mooring proxy for cases when warm, weakly stratified Alaskan Coastal Water is present at the shelfbreak mooring site. The best fit line is indicated (red line).

a representative example of this improvement over a three week period in summer.

B.2 Storm Adjustment

As explained in Chapter 3, the original proxy tends to overestimate the true transport of the shelfbreak jet during upwelling events, which happen most frequently during the autumn storm season. Figure B-6 shows the composite vertical section for those times when the original proxy exceeds the actual transport of the current by ≥ 0.3 Sv during the first year of SBI data. One sees that a weak signature of the eastward-flowing shelfbreak jet is present in the deepest part of the water column near the shelfbreak, while farther offshore the wind-forced flow is progressing to the west. The corresponding hydrographic composite section shows that the isopycnals are somewhat elevated due to the presence of warm and salty Atlantic water on the upper slope.

To investigate a way to compensate for this discrepancy during upwelling events, we analyzed the 26 storms during the first SBI year. In order to treat the different events in consistent fashion, their lengths were converted into percentages of the full duration of the storm. For example 0% represents the start of a storm, 50% the halfway point, and 100% the end of a storm. The start and end times are based on the onset and offset of the easterly winds. Of the 26 storms, only the strongest third result in a clear overestimate of the proxy transport. Initially the wind forcing causes a reversal in the flow in the upper water column across the section. However, the current near the base of the shelfbreak mooring takes longer to reverse because there was already a substantial eastward flow before the storm. Eventually, in most of the strong storms, there is total reversal of the flow. Then, as the storm begins to wind down, the eastward flow re-establishes itself first in the vicinity of the shelfbreak. All

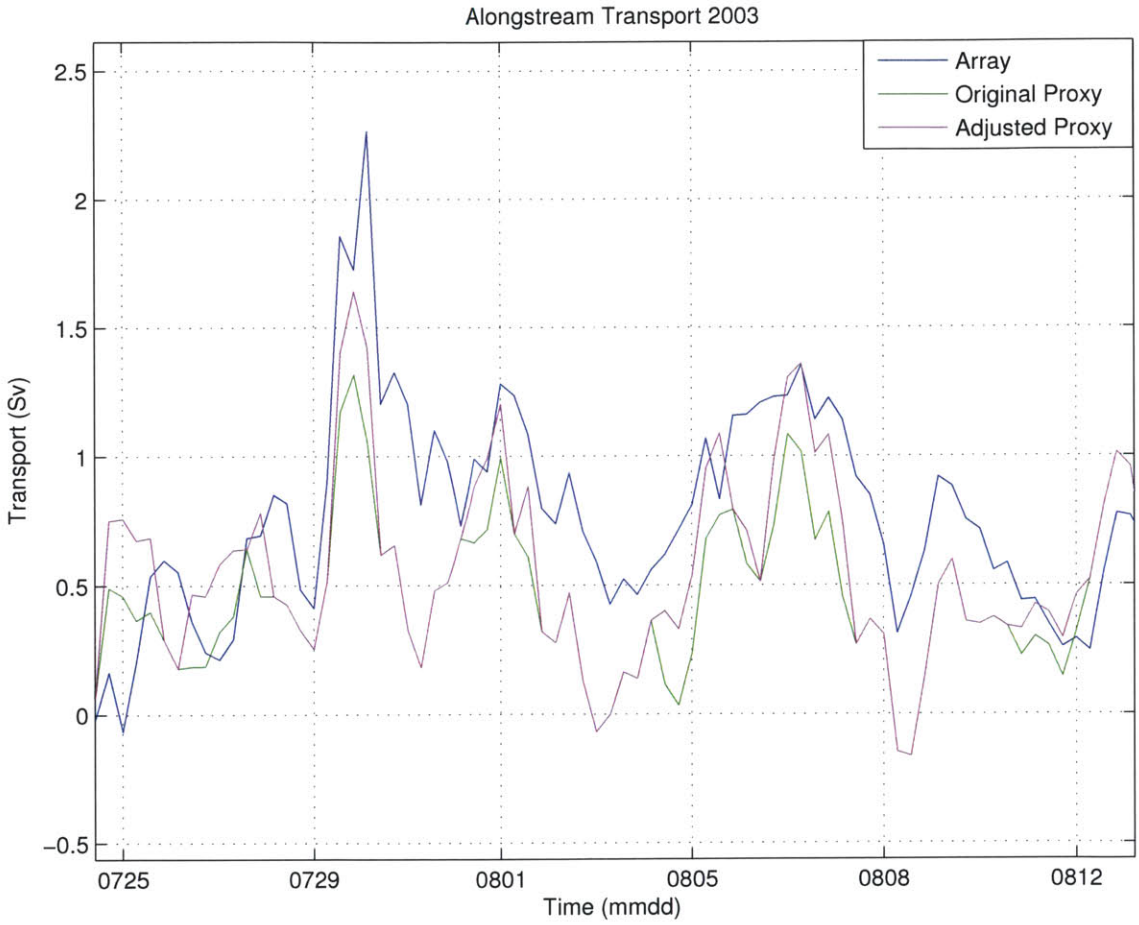

Figure B-5: Representative timeseries of the full array transport and the shelfbreak mooring proxy transport before the ACC adjustment and after the ACC adjustment.

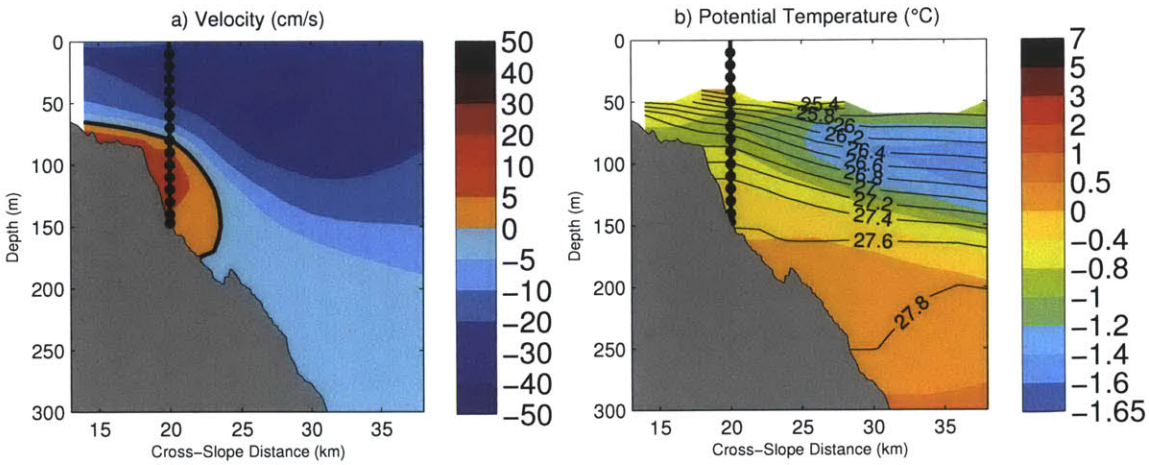

Figure B-6: a)Composite velocity section (cm/s) when the shelfbreak mooring overestimates the full transport by $\geq$ 0.3 Sv during October 2002 and November 2002. b)Composite potential temperature section (°C) for the same time periods.

told, this causes the shelfbreak mooring proxy to overestimate the current throughout the storm. Figure B-7 shows the amount of overestimation through the course of the ten strongest storms during 2002-2003, including the mean over all of these storms.

To implement a correction to the proxy for such a scenario, all of the upwelling events were identified over the 6-year shelfbreak mooring timeseries. This was done using a graphical user interface. Three main criteria were used to identify a storm (following the results of Pickart et al. (2009a), Nikolopoulos et al. (2009) and Schulze and Pickart (2012)): 1) a significant (westward) reversal in flow; 2) strong easterly winds at the Barrow weather station; and 3) a vertically averaged salinity in the lower 50 m of the shelfbreak mooring water column greater than the monthly mean salinity.

In total, 112 upwelling events of varying intensity and duration were identified. The storms have different lengths ranging from just under one day to as many as ten days. In light of the above results for the first SBI year, we assume that only the strongest third of storms cause the shelfbreak mooring proxy to significantly

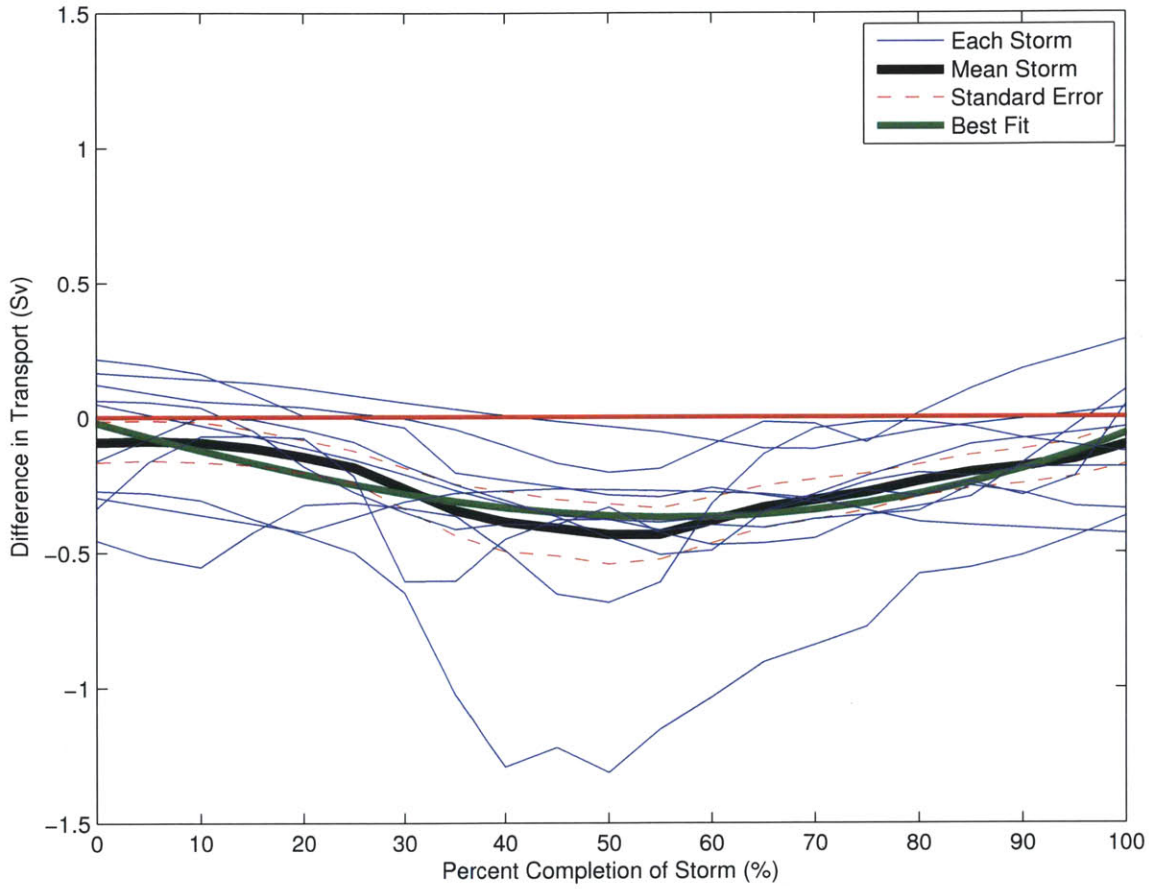

Figure B-7: Difference in transport between the full array and the original proxy over the course of the ten strongest storms from August 2002 to September 2003 (see text for details). The thick black line is the mean and the thick green line is the best fit third-order polynomial.

overestimate the transport. The strength of a given storm is based on the peak reversal (westward flow) of the current. Using the polynomial fit shown in Figure B-7, a transport correction was then applied over the course of each of the storms.

For the time period between September and November 2002, the original proxy transport is 0.044 Sv compared to the full array transport of -0.139 Sv. When the adjustments are applied for the strongest storms during this time period, the proxy transport reduces to -0.0365 Sv. Also, the mean rms difference between the proxy and the full transport decreases from 0.328 Sv to 0.251 Sv when the correction is applied. As with the ACC adjustment, the storm correction improves the comparison of both the mean transport and the variability. Figure B-8 shows a representative example of how the adjustment improved the proxy transport estimate over a five-week period during the storm season.

B.3 Impact of the Adjustments

Figure B-9 shows the comparison of the boundary current transport during the first SBI year (August 2002 to August 2003) as calculated using the data from the full array, the original proxy, and the proxy after it has been adjusted for lateral excursions of the ACC as well as the occurrence of storms. The year-long mean transport for the full array is 0.114 Sv, while that for the original proxy is 0.138 Sv. The rms difference between the two is 0.237 Sv. After applying the ACC and storm adjustments the proxy volume transport is 0.123 Sv and the rms difference is 0.203 Sv. Furthermore, the correlation between the array transport and the shelfbreak mooring proxy increases from r=.88 to r=0.92 when the adjustments are applied.

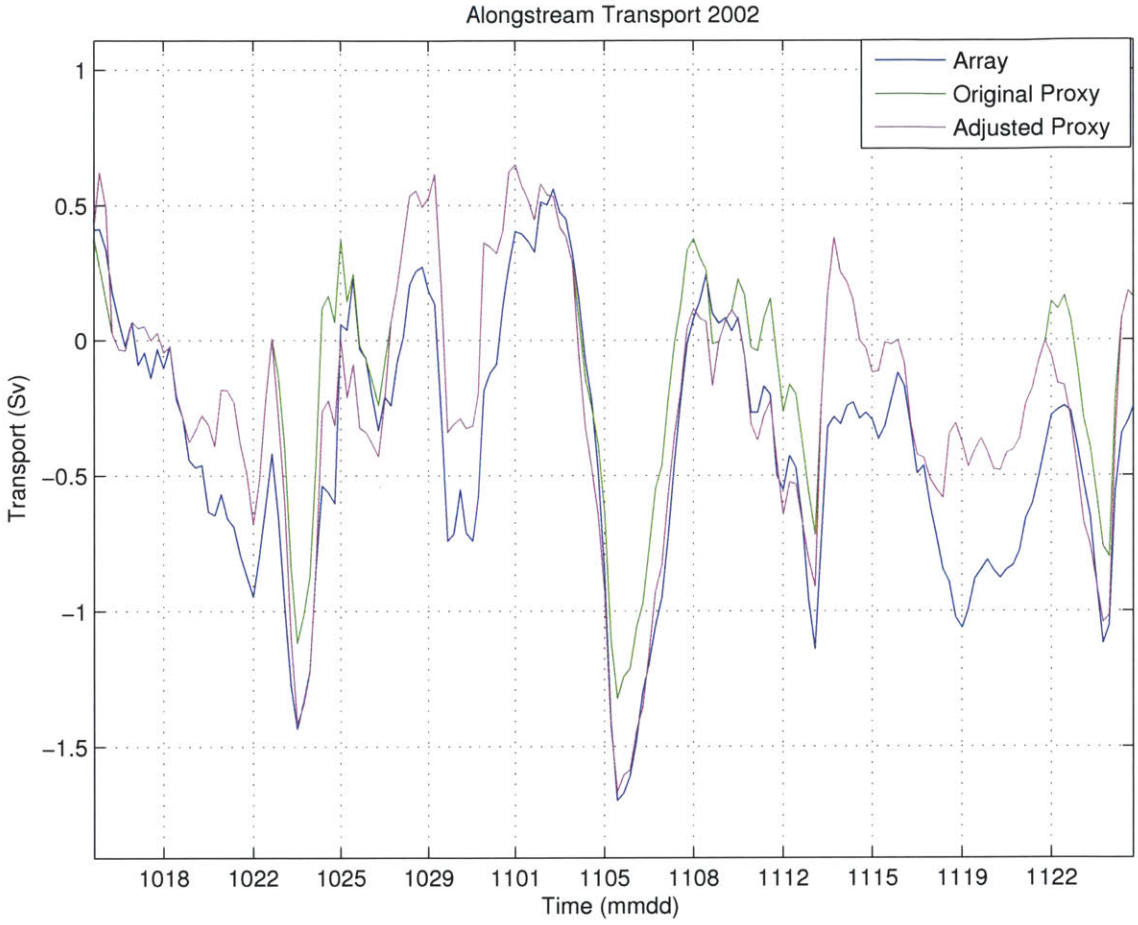

Figure B-8: Representative timeseries of the full array transport and the shelfbreak mooring proxy before the storm adjustment and after the storm adjustment.

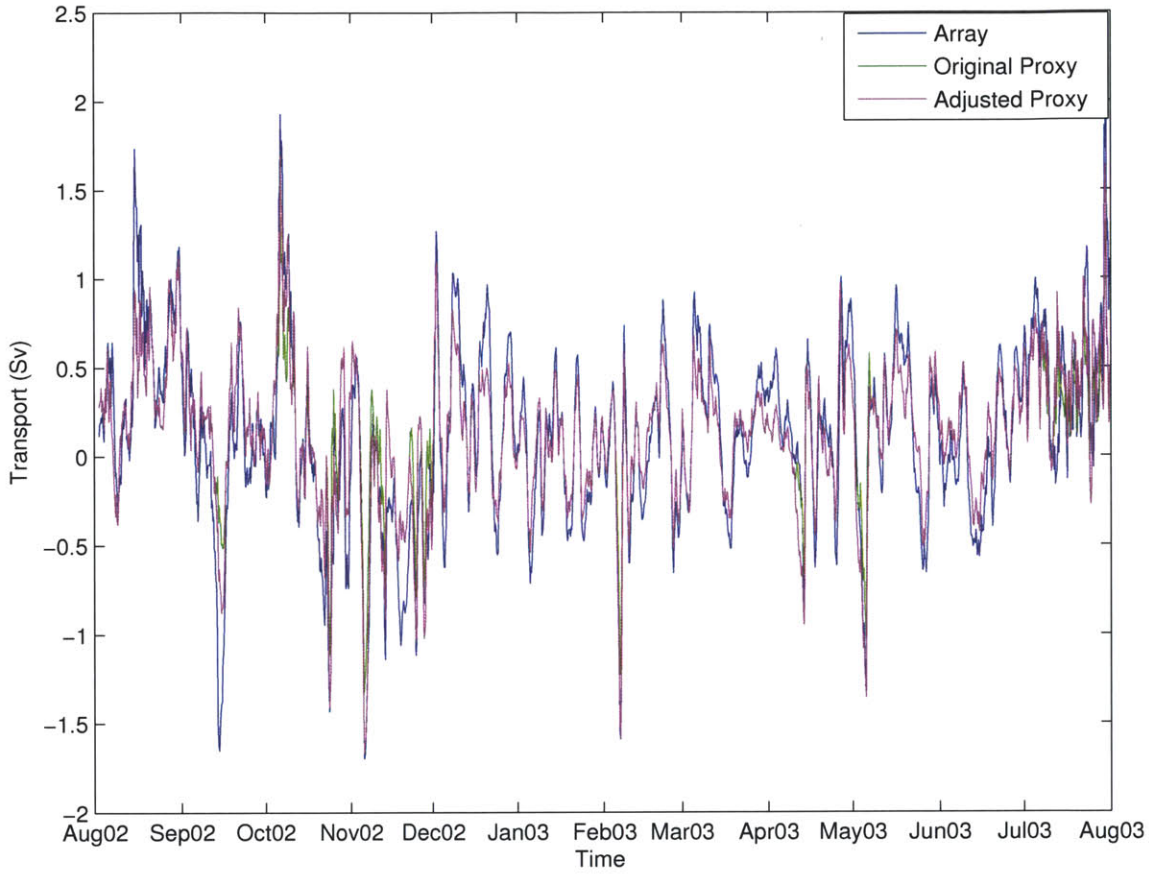

Figure B-9: Timeseries of the full array transport, the original proxy transport, and the proxy transport after the ACC adjustment and the storm adjustment.

Appendix C

NARR Validation

North American Regional Reanalysis (NARR) data are validated using in situ wind speed measurements from the weather station in Pt. Barrow, Alaska. This study uses NARR sea level pressure data and also NARR 10-meter wind speed data to study large scale atmospheric circulation for the area encompassed by the Beaufort High and Aleutian Low. We use these SLP features to explain what drives winds along the Beaufort slope. Therefore, in order to use fields from the reanalysis data set, it is important to make sure reanalysis wind speeds along the Beaufort slope correlate well with situ measurements. This will give confidence to the reanalysis data set and ensure it is doing well capturing the large scale atmospheric features, which drive local winds near the mooring site.

To assess how well the reanalysis data approximates local winds we consider the NARR 10 m winds in a box (90 km in the zonal direction and 111 km in the meridional direction) encompassing Point Barrow Alaska. The reanalysis winds are rotated to be alongcoast (105°T). In situ winds from the metrological station at Pt. Barrow, Alaska are also rotated alongcoast. We use three metrics to assess how well the reanalysis fields do approximating local winds. First, we find the average root mean

squared (rms) difference between the two data sets. The rms difference represents the equivalent of standard deviation when considering NARR data compared to in situ data. Next, annual and seasonal means are calculated for both data sets. Lastly, we calculate the correlation between the two data sets.

Table C.1: Annual metrics measuring the NARR 10 m winds to the Pt. Barrow meteorological station winds. The first metric is the root mean squared (rms) difference between the two data sets. Other metrics include the mean NARR alongcoast wind speed, the mean alongcoast Pt. Barrow wind speed and the correlation between the two timeseries.

Year	RMS Difference (m/s)	NARR (m/s)	MET (m/s)	Correlation (r)
2002	2.93	-0.92	-1.52	0.897
2003	2.52	-1.14	-1.78	0.908
2004	2.38	-2.04	-2.89	0.894
2005	2.07	-2.17	-2.75	0.913
2006	2.04	-1.09	-1.48	0.906
2007	2.16	-2.79	-3.54	0.877
2008	2.16	-1.10	-1.64	0.882
2009	2.16	-1.71	-2.15	0.905
2010	2.19	-1.61	-2.39	0.916
2011	2.05	-1.82	-2.40	0.903

Table C.1 shows the annual statistics between the reanalysis winds and in situ winds. NARR fields have an extremely high correlation with in situ winds every year, with the decade mean being about r=0.90. Only the annual correlation is shown, but seasonal correlations are very high as well. On average, the NARR data tends to underestimate in situ wind speeds between 0.39 m/s to 0.8 m/s. This underestimate of wind speed is seen in all seasons, every year. Although the NARR underestimates situ data measurements, the reanalysis data captures the interannual variations of wind speed well. The rms difference between data sets is about 2.3 m/s. This implies that at any given point in time, the majority of the NARR data is within 2.3 m/s of the in situ wind data.

Therefore, the NARR data set does a very good job at approximating local wind speed. The correlation between NARR wind and in situ wind is extremely high and the reanalysis product captures the interannual variations well. The only disadvantage is the fact that NARR tends to underestimate the in situ wind speed throughout the decade. Overall, this is not of huge concern because the interannual changes are the main focus of this study. Furthermore, when we consider local wind speed in analysis, we refer to measurements from Pt. Barrow weather station. In an effort to explain the large scale atmospheric drivers of local winds, we are confident in using NARR fields since these do a good job at approximating local wind speed and capturing interannual variability.

Bibliography

Aagaard, K., L. Coachman, and E. Carmack, 1981: On the halocline of the arctic ocean. *Deep Sea Research Part A. Oceanographic Research Papers*, **28**, 529–545.

Aagaard, K., T. J. Weingartner, S. L. Danielson, R. A. Woodgate, G. C. Johnson, and T. E. Whitledge, 2006: Some controls on flow and salinity in bering strait. *Geophysical research letters*, **33 (19)**, L19 602, doi:10.1029/2006GL026 612.

Aksenov, Y., V. Ivanov, A. Nurser, S. Bacon, I. V. Polyakov, A. C. Coward, A. C. Naveira-Garabato, and A. Beszczynska-Moeller, 2011: The arctic circumpolar boundary current. *Journal of Geophysical Research*, **116**, doi:10.1029/2010JC006 637.

Cavalieri, D., J. Crawford, M. Drinkwater, D. Eppler, L. Farmer, R. Jentz, and C. Wackerman, 1991: Aircraft active and passive microwave validation of sea ice concentration from the dmsp ssm/i. *Journal of Geophysical Research: Oceans (1978–2012)*, **96 (C12)**, 21,989–22 008.

Cavalieri, D. J., C. L. Parkinson, P. Gloersen, J. C. Comiso, and H. J. Zwally, 1999: Deriving long-term time series of sea ice cover from satellite passive-microwave multisensor data sets. *Journal of Geophysical Research: Oceans (1978–2012)*, **104 (C7)**, 15 803–15 814, doi:10.1029/1999JC900 081.

Fratantoni, P. S., S. Zimmermann, R. S. Pickart, and M. Swartz, 2006: Western arctic shelf-basin interactions experiment: processing and calibration of moored profiler data from the beaufort shelf edge mooring array. Tech. rep., Woods Hole Oceanographic Institution.

Grumbine, R. W., 1996: Automated passive microwave sea ice concentration analysis at ncep. *Unpublished manuscript avaliable from NCEP/NWS/NOAA*, **5200 Auth Road, Camp Springs, MD, 20746, USA**, 13pp.

Hansell, D. A., T. E. Whitledge, and J. J. Goering, 1993: Patterns of nitrate utilization and new production over the bering-chukchi shelf. *Continental Shelf Research*, **13 (5)**, 601–627, doi:10.1016/0278–4343(93)90 096–G.

Hill, V. and G. Cota, 2005: Spatial patterns of primary production on the shelf, slope and basin of the western arctic in 2002. *Deep Sea Research Part II: Topical Studies in Oceanography*, **52 (24)**, 3344–3354, doi:10.1016/j.dsr2.2005.10.001.

Hill, V., G. Cota, and D. Stockwell, 2005: Spring and summer phytoplankton communities in the chukchi and eastern beaufort seas. *Deep Sea Research Part II: Topical Studies in Oceanography*, **52 (24)**, 3369–3385, doi:10.1016/j.dsr2.2005.10.010.

Itoh, M., K. Shimada, T. Kamoshida, F. McLaughlin, E. Carmack, and S. Nishino, 2012: Interannual variability of pacific winter water inflow through barrow canyon from 2000 to 2006. *Journal of oceanography*, **68 (4)**, 575–592, doi:10.1007/s10 872–012–0120–1.

Kadko, D., R. S. Pickart, and J. Mathis, 2008: Age characteristics of a shelf-break eddy in the western arctic and implications for shelf-basin exchange. *Journal of Geophysical Research: Oceans (1978–2012)*, **113 (C2)**, doi: 10.1029/2007JC004 429.

Karcher, M., F. Kauker, R. Gerdes, E. Hunke, and J. Zhang, 2007: On the dynamics of atlantic water circulation in the arctic ocean. *Journal of Geophysical Research*, **112**, doi:10.1029/2006JC003630.

Mathis, J. T., R. S. Pickart, D. A. Hansell, D. Kadko, and N. R. Bates, 2007: Eddy transport of organic carbon and nutrients from the chukchi shelf: Impact on the upper halocline of the western arctic ocean. *Journal of Geophysical Research*, **112 (C5)**, C05011, doi:10.1029/2006JC003899.

Mathis, J. T., et al., 2012: Storm-induced upwelling of high pco2 waters onto the continental shelf of the western arctic ocean and implications for carbonate mineral saturation states. *Geophysical Research Letters*, **39 (7)**, L07606, doi:10.1029/2012GL051574.

McCabe, G. J., M. P. Clark, and M. C. Serreze, 2001: Trends in northern hemisphere surface cyclone frequency and intensity. *Journal of Climate*, **14**, 2763–2768.

Mesinger, D. G. K. E. M. K. S. P. e. a., F., 2006: North american regional reanalysis. *Bulletin of the American Meteorological Society*, **87**, 343–360, doi:10.1175/BAMS-87-3-343.

Mesquita, M. S., D. E. Atkinson, and K. I. Hodges, 2010: Characteristics and variability of storm tracks in the north pacific, bering sea, and alaska*. *Journal of Climate*, **23 (2)**, 294–311, doi:10.1175/2009JCLI3019.1.

Moore, G., 2012: Decadal variability and a recent amplification of the summer beaufort sea high. *Geophysical Research Letters*, **39 (10)**, L10807, doi:10.1029/2012GL051570.

Muench, R., J. Schumacher, and S. Salo, 1988: Winter currents and hydrographic

conditions on the northern central bering sea shelf. *Journal of Geophysical Research: Oceans (1978–2012)*, **93 (C1)**, 516–526.

Nikolopoulos, A., R. Pickart, P. Fratantoni, K. Shimada, D. Torres, and E. Jones, 2009: The western arctic boundary current at 152 w: Structure, variability, and transport. *Deep Sea Research Part II: Topical Studies in Oceanography*, **56 (17)**, 1164–1181, doi:10.1016/j.dsr2.2008.10.014.

Okkonen, S. R., C. J. Ashjian, R. G. Campbell, W. Maslowski, J. L. Clement-Kinney, and R. Potter, 2009: Intrusion of warm bering/chukchi waters onto the shelf in the western beaufort sea. *Journal of Geophysical Research*, **114**, C00A11, doi: 10.1029/2008JC004 870.

Overland, J. E. and A. T. Roach, 1987: Northward flow in the bering and chukchi seas. *Journal of Geophysical Research*, **92 (C7)**, 7097–7105.

Padman, L. and S. Erofeeva, 2004: A barotropic inverse tidal model for the arctic ocean. *Geophysical Research Letters*, **31 (2)**, doi: 10.1029/2003GL019 003.

Pickart, R., 2004: Shelfbreak circulation in the alaskan beaufort sea: Mean structure and variability. *Journal of Geophysical Research*, **109 (C4)**, C04 024, doi:10.1029/2003JC001 912.

Pickart, R., G. Moore, D. Torres, P. Fratantoni, R. Goldsmith, and J. Yang, 2009a: Upwelling on the continental slope of the alaskan beaufort sea: Storms, ice, and oceanographic response. *Journal of Geophysical Research*, **114 (C1)**, C00A13, doi:10.1029/2008JC005 009.

Pickart, R., M. Spall, G. Moore, T. Weingartner, R. Woodgate, K. Aagaard, and K. Shimada, 2011: Upwelling in the alaskan beaufort sea: Atmospheric forcing

and local versus non-local response. *Progress in Oceanography*, **88 (1)**, 78–100, doi:10.1016/j.pocean.2010.11.005.

Pickart, R. S., G. Moore, A. M. Macdonald, I. A. Renfrew, J. E. Walsh, and W. S. Kessler, 2009b: Seasonal evolution of aleutian low pressure systems: Implications for the north pacific subpolar circulation. *Journal of Physical Oceanography*, **39 (6)**, 1317–1339, doi:10.1175/2008JPO3891.1.

Pickart, R. S., L. M. Schulze, G. Moore, M. A. Charette, K. R. Arrigo, G. van Dijken, and S. Danielson, 2013a: Long–term trends of upwelling and impacts on primary productivity in the alaskan beaufort sea. *Deep Sea Research Part I: Oceanographic Research Papers*, doi: 10.1016/j.dsr.2013.05.003.

Pickart, R. S., M. A. Spall, and J. T. Mathis, 2013b: Dynamics of upwelling in the alaskan beaufort sea and associated shelf-basin fluxes. *Deep Sea Research Part I: Oceanographic Research Papers*, doi: 10.1016/j.dsr.2013.01.007.

Plueddemann, A. J., K. R., and E. C., 1999: Eddies in the beaufort gyre. *Ocean-Atmosphere-Ice Interactions (OAII)*, **All Hands Meeting**, 20–22 October, 1999, Virginia Beach, VA.

Reynolds, R. W., T. M. Smith, C. Liu, D. B. Chelton, K. S. Casey, and M. G. Schlax, 2007: Daily high-resolution-blended analyses for sea surface temperature. *Journal of Climate*, **20 (22)**, 5473–5496, doi:10.1175/2007JCLI1824.1.

Rudels, B., E. Jones, L. Anderson, and G. Kattner, 1994: On the intermediate depth waters of the arctic ocean. *The polar oceans and their role in shaping the global environment*, 33–46, doi:10.1029/GM085p0033.

Sambrotto, R., J. Goering, and C. McRoy, 1984: Large yearly production of phytoplankton in the western bering strait. *Science*, **225 (4667)**, 1147–1150, doi: 10.1126/science.225.4667.1147.

Schauer, U. and Beszczynska-Moeller, 2009: Problems with estimation and interpretation of oceanic heat transport-conceptual remarks for the case of fram strait in the arctic ocean. *Ocean Science*, **(5)**, 487–494.

Schulze, L. M. and R. S. Pickart, 2012: Seasonal variation of upwelling in the alaskan beaufort sea: Impact of sea ice cover. *Journal of Geophysical Research: Oceans (1978–2012)*, **117 (C6)**, doi:10.1029/2012JC007 985.

Serreze, M. C. and A. P. Barrett, 2011: Characteristics of the beaufort sea high. *Journal of Climate*, **24 (1)**, 159–182, doi:10.1175/2010JCLI3636.1.

Shimada, K., E. C. Carmack, K. Hatakeyama, and T. Takizawa, 2001: Varieties of shallow temperature maximum waters in the western canadian basin of the arctic ocean. *Geophysical Research Letters*, **28 (18)**, 3441–3444, doi:10.1029/2001GL013 168.

Shimada, K., T. Kamoshida, M. Itoh, S. Nishino, E. Carmack, F. McLaughlin, S. Zimmermann, and A. Proshutinsky, 2006: Pacific ocean inflow: Influence on catastrophic reduction of sea ice cover in the arctic ocean. *Geophysical Research Letters*, **33 (L08605)**, doi:10.1029/2005GL025 624.

Spall, M. A., R. S. Pickart, P. S. Fratantoni, and A. J. Plueddemann, 2008: Western arctic shelfbreak eddies: Formation and transport. *Journal of Physical Oceanography*, **38 (8)**, 1644–1668, doi:10.1175/2007JPO3829.1.

Steele, M., J. Morison, W. Ermold, I. Rigor, M. Ortmeyer, and K. Shimada, 2004:

Circulation of summer pacific halocline water in the arctic ocean. *Journal of Geophysical Research: Oceans (1978–2012)*, **109 (C2)**.

Steele, M., J. Zhang, and W. Ermold, 2010: Mechanisms of summertime upper arctic ocean warming and the effect on sea ice melt. *Journal of Geophysical Research*, **115 (C11)**, C11 004, doi: 10.1029/2009JC005 849.

von Appen, W. and R. Pickart, 2012: Two configurations of the western arctic shelfbreak current in summer. *Journal of Physical Oceanography*, **42 (3)**, 329–351, doi: 10.1175/JPO–D–11–026.1.

Walsh, J. E., 1978: Temporal and spatial scales of the arctic circulation. *Monthly Weather Review*, **106 (11)**, 1532–1544.

Wang, J., J. Zhang, E. Watanabe, M. Ikeda, K. Mizobata, J. E. Walsh, X. Bai, and B. Wu, 2009: Is the dipole anomaly a major driver to record lows in arctic summer sea ice extent? *Geophysical Research Letters*, **36 (5)**, doi:10.1029/2008GL036 706.

Watanabe, E., 2011: Beaufort shelf break eddies and shelf-basin exchange of pacific summer water in the western arctic ocean detected by satellite and modeling analyses. *Journal of Geophysical Research*, **116 (C8)**, C08 034, doi:10.1029/2010JC006 259.

Weingartner, T., K. Aagaard, R. Woodgate, S. Danielson, Y. Sasaki, and D. Cavalieri, 2005a: Circulation on the north central chukchi sea shelf. *Deep Sea Research Part II: Topical Studies in Oceanography*, **52 (24)**, 3150–3174, doi:10.1016/j.dsr2.2005.10.015.

Weingartner, T. J., S. L. Danielson, and T. C. Royer, 2005b: Freshwater variability

and predictability in the alaska coastal current. *Deep Sea Research Part II: Topical Studies in Oceanography*, **52 (1)**, 169–191, doi:10.1016/j.dsr2.2004.09.030.

Wilson, J. G. and J. E. Overland, 1986: *Meteorology. The Gulf of Alaska: Physical Environment and Biological Resources.* edited by D.W. Hood and S.T. Zimmerman, Alaska Office, Ocean Assessments Division, National Oceanic and Atmospheric Administration, US Department of Commerce, pp. 31-54, U.S.

Winsor, P. and D. C. Chapman, 2004: Pathways of pacific water across the chukchi sea: A numerical model study. *Journal of Geophysical Research*, **109**, C03 002, doi:10.1029/2003JC001 962.

Woodgate, R., T. Weingartner, and R. Lindsay, 2012: Observed increases in bering strait oceanic fluxes from the pacific to the arctic from 2001 to 2011 and their impacts on the arctic ocean water column. *Geophysical Research Letters*, **39 (24)**, doi:10.1029/2012GL054 092.

Woodgate, R. A. and K. Aagaard, 2005: Revising the bering strait freshwater flux into the arctic ocean. *Geophysical Research Letters*, **32**, doi:10.1029/2004GL021 747.

Woodgate, R. A., K. Aagaard, R. D. Muench, J. Gunn, G. Björk, B. Rudels, A. Roach, and U. Schauer, 2001: The arctic ocean boundary current along the eurasian slope and the adjacent lomonosov ridge: Water mass properties, transports and transformations from moored instruments. *Deep Sea Research Part I: Oceanographic Research Papers*, **48 (8)**, 1757–1792, doi:10.1016/S0967–0637(00)00 091–1.

Woodgate, R. A., K. Aagaard, and T. J. Weingartner, 2005: Monthly temperature, salinity, and transport variability of the bering strait through flow. *Geophysical Research Letters*, **32 (4)**, doi:10.1029/2004GL021 880.

Woodgate, R. A., T. Weingartner, and R. Lindsay, 2010: The 2007 bering strait oceanic heat flux and anomalous arctic sea-ice retreat. *Geophysical Research Letters*, **37**, L01 602, doi:10.1029/2009GL041 621.